VELOCITY AND POROSITY ESTIMATION OF THE UNDERTHRUSTING SEDIMENT IN THE NANKAI TROUGH ACCRETIONARY PRISM

by

Garrett Mark Kramer

Submitted in Partial Fulfillment
of the Requirements for the Degree of

Master of Science in Geophysics

New Mexico Institute of Mining and Technology
Department of Earth & Environmental Science
Socorro, NM

May, 2006

To my parents, who taught me by example.

ABSTRACT

At the Nankai subduction zone offshore SW Japan, it has been inferred that limited dewatering of underthrust sediments results in excess pore pressure, controlling the decollement strength, but this effect has not been quantitatively studied to date. 2-D PreStack Depth Migration (PSDM) was performed on seismic data collected in the seaward portion of the offshore Cape Muroto survey area to obtain robust interval velocities for the incoming sediment on the subducting plate, the prism, and the underthrust sediments. The objectives of mapping the underthrust section's velocity were porosity computation beneath and along the decollement which will ultimately lead to mapping of pore pressure distribution in future studies. PSDM interval velocities were obtained by applying several iterations of residual move-out (RMO) velocity corrections to flatten reflectors as a function of source-receiver offset on depth migrated gathers. Image quality (optimal collapse of reflectors in the stacked section) and borehole depth ties were both used as constraints to guide the velocity analysis. Careful balancing of reasonable velocity gradients was performed when strict RMO analysis produced large velocity differences between adjacent inlines. In this way, I have obtained the best constrained velocity model to date for this

accretionary prism. I have produced a fine 2-D grid of underthrust section interval velocity. Mapping of this velocity structure shows generally lower velocity in the underthrust section than in the prism sediments above, and moderately increasing velocity with depth and distance landward of the deformation front. Superimposed on this trend, localized variations within the underthrust section velocity structure do exist, suggesting possible small-scale (100's of meters) variability in porosity. I then applied an empirically derived velocity-porosity transform, permitting calculation of a quantitative distribution of porosity for the Shikoku Basin underthrust sediments. Analysis of this porosity mapping indicates inhibited dewatering of most of the underthrust section, implying superhydrostatic pore pressure persisting 15-20 km landward of the trench beneath the decollement.

ACKNOWLEDGEMENTS

This research was funded with a research assistantship provided by the National Science Foundation grant #OCE-0241375. Special thanks to my committee, Dr. Harold Tobin (research advisor), Dr. Susan Bilek, and Dr. Glenn Spinelli for their direction, instruction, and help over the past years. Thanks to collaborators Dr. Patrizia Costa-Pisani and Dr. Gregory Moore for hosting and providing computing facilities at the University of Hawaii – SOEST. Special thanks to Ms. Kathryn Fletcher and my family for their tireless support of me, in all of my endeavors.

TABLE OF CONTENTS

LIST OF FIGURES

This thesis is accepted on behalf of the
Faculty of the Institute by the following committee:

Advisor

5/19/06
Date

I release this document to the New Mexico Institute of Mining and Technology.

Student's Signature

5/19/06
Date

CHAPTER 1

INTRODUCTION

The conditions for fault slip, earthquake rupture propagation, and tsunamigenic slip in subduction zones are governed in large part by pore fluid pressure. Detecting and mapping pore pressure and effective stress anomalies along subduction thrusts is therefore an important goal of geophysical studies and drilling. Furthermore, seismic hazard mitigation has been recognized as a very important issue in recent decades. Communities dwelling near active subduction zones bear the threat of both seismogenic shaking hazards and inundation by tsunamis. In order to identify the seismic hazard associated with convergent plate boundaries, an understanding of the processes governing active seismicity must be developed. The Nankai Trough, off the west coast of Japan, offers an unparalleled opportunity to study the processes that lead to and occur during subduction zone mega-earthquakes because of its long history of documented great earthquakes, wealth of geophysical data, and relatively simple forearc geometry.

The Nankai Margin is characterized by an accretionary prism formed by the scraping off of sediments deposited on a subducting slab (Figure 1.1). Its structure is typically a complex array of imbricate thrust sheets that build up and migrate seaward

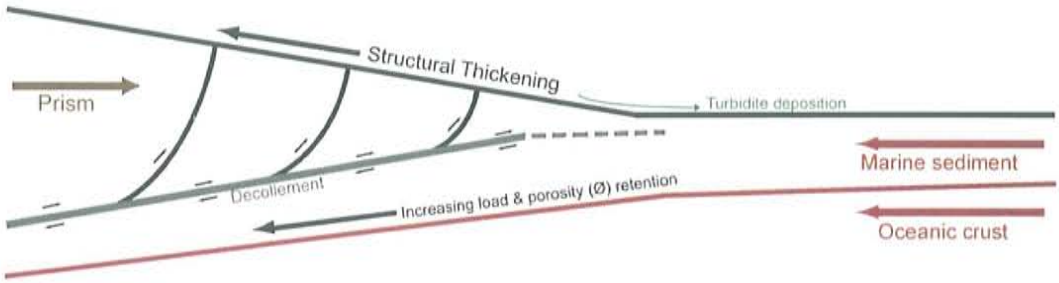

Figure 1.1: Schematic illustrating that as high porosity marine sediment enters the subduction factory it is rapidly loaded by turbidite deposition and structural thickening from offscracped sediment. In at least some cases, the permeability of marine sediments is insufficient to allow fluid escape quick enough to keep up with the loading rate resulting in excess pore pressure in the underthrust sediment sustaining porosity and influencing decollment strength.

as accretion advances. The main slip plane, or mega-thrust, develops between the two tectonic plates and is characteristically a low-angle basal thrust fault, termed the décollement. Different structural and physical processes occur in the over-riding and under-riding plates, and the décollement is the mechanical boundary that separates these domains [*Morgan and Karig*, 1995]. Sediments located above the décollement deform via horizontal shortening [*Lallemant, et al.*, 1993] while those below the décollement, the *underthrust section*, undergo primarily or entirely uniaxial compression and diagenesis [*Morgan and Karig*, 1995]; i.e., burial compaction as if it were in a basinal setting. By treating the décollement as a mechanical boundary, it can be inferred that it plays an important role in the formation and geometry of the prism. This calls for unusual properties along the décollement (i.e. pore pressure and/or lithology) to account for unique geological observations at convergent margins [*Moore, et al.*, 1990].

Elevated pore pressures potentially play a key role in the development of the décollement zone at convergent margins [*Moore*, 1989]. These elevated pore pressures are a result of rapid compaction of typically low permeability marine sediments [*Screaton and Ge*, 2000]. The nature of the incoming sediment that is underthrust rather than scraped off into the accretionary prism is therefore an important factor in predicting the properties and development of the décollement at convergent margins.

An important goal of the Ocean Drilling Program (ODP) has been to understand the role fluids play in deformation and faulting. It is commonly thought

that pore pressure is a primary control on décollement strength and the up-dip limit of seismic activity in a subduction zone [*Moore and Saffer*, 2001]. Direct measurements of pore pressures within underthrust sediments have been attempted in a number of locations via coring and down-hole instruments by the ODP, with variable success [e.g. *Davis, et al.*, 2006]. However, drill sites are isolated and restricted in depth, limiting their usefulness in predicting the spatial variability of décollement properties. Thus, there is little knowledge about variations in porosity, pore pressure, and resulting seismicity both down-dip and along strike in convergent margins [*Moore and Saffer*, 2001; *Tobin, et al.*, 1994].

Boreholes in subduction zone environments provide us with a good window into the subsurface conditions; however, combining *in situ* data with geophysical techniques can vastly expand our knowledge of subsurface conditions. Remotely sensed seismic reflection data yields information over large regions extended away from borehole locations; one "by-product" of seismic data processing is an accurate estimate of the seismic velocity structure of the imaged volume. Seismic compressional-wave velocity varies systematically with porosity, allowing partially empirical transforms to be developed between these parameters (for review, see *Marko et. al.* 2003). By combining high-quality 3D seismic reflection data with an appropriate velocity-porosity transform, a calculation of pore pressure distribution within discrete intervals, either along strike and down-dip along the décollement, can be made. If the fluids retained within the underthrust sediments maintain higher

porosity conditions than those in equilibrium with compaction under hydrostatic (drained) conditions, it implies that excess fluid pressure persists and permeability is insufficient to allow fluids to escape [*Screaton, et al.*, 2000]. Fluid overpressure will equalize via migration when the décollement steps down into them, faults reach the décollement zone allowing fluid expulsion, or excess pressure reaches conditions sufficient for hydrofracturing [*Screaton, et al.*, 2002].

In this study, high-quality seismic reflection data collected in the Nankai subduction zone off Cape Muroto, Japan (Figures 1.2 & 1.3) is processed utilizing 2-D Kirchoff pre-stack depth migration (PSDM). The use of PSDM processing yields robust velocity estimates of the underthrust section for this dataset [*Pisani, et al.*, 2005]. By applying an empirically derived porosity transform [*Hoffman and Tobin*, 2005], a high resolution estimate of porosity variability in Shikoku Basin underthrust sediments is produced. The inferred porosity distribution within the underthrust sediment is mapped along strike and downdip and shows inhibited compaction relative to the predicted hydrostatic condition for the underthrusting sediments, implying super-hydrostatic pore pressure, a possible main control on the updip limit of seismicity. Later studies will utilize this inferred porosity distribution within the underthrust sediments to quantitatively predict pore pressure and décollement strength [*Saffer, et al.*, 2000].

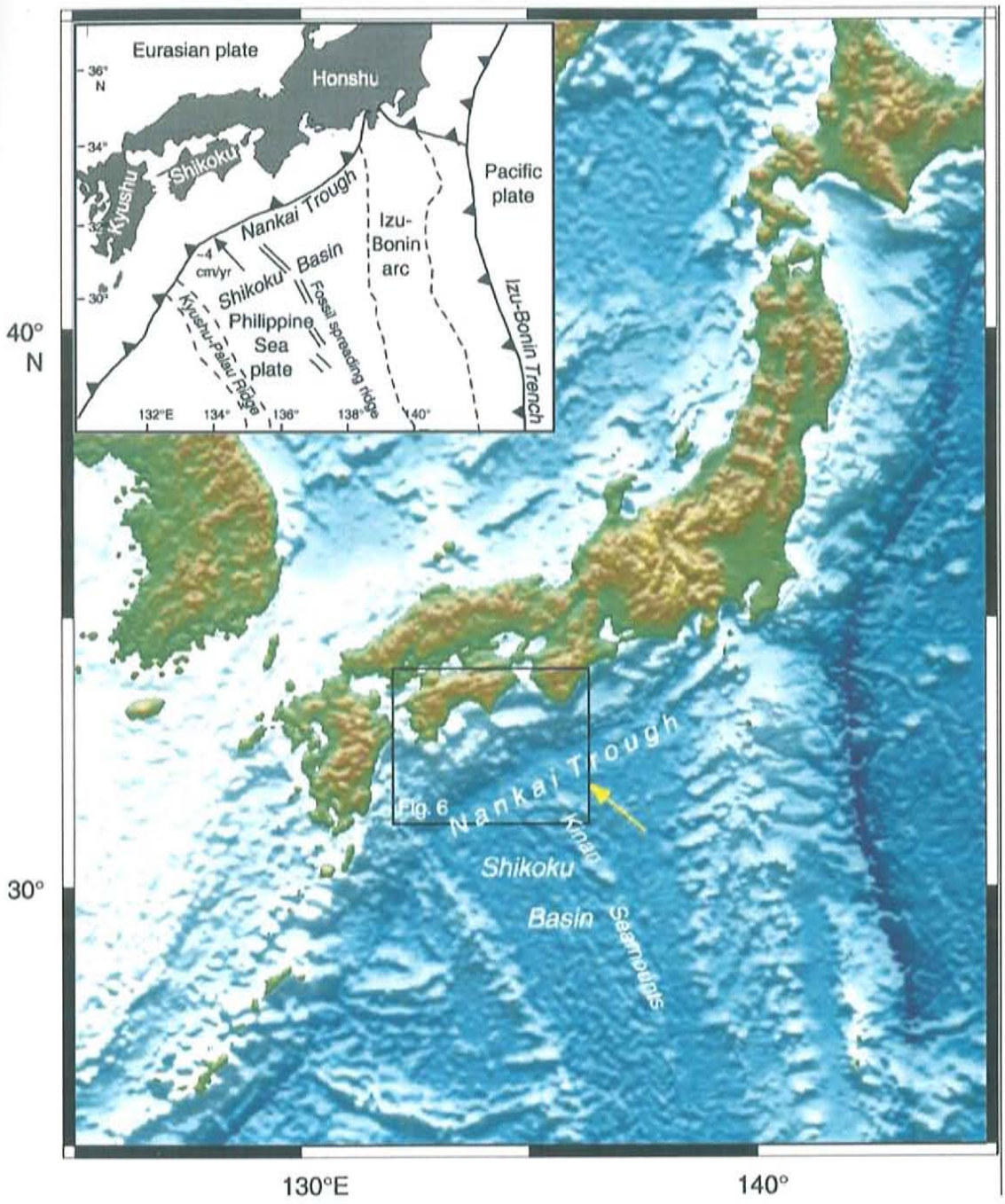

Figure 1.2: Map showing the location of the Nankai Trough. The black box outlines the enlarged section shown in Figure 1.3. The convergence direction is indicated by the yellow arrow. The inset (upper left) illustrates the tectonics associated with the Nankai Trough. [*Shipboard Scientific Party,* 2001].

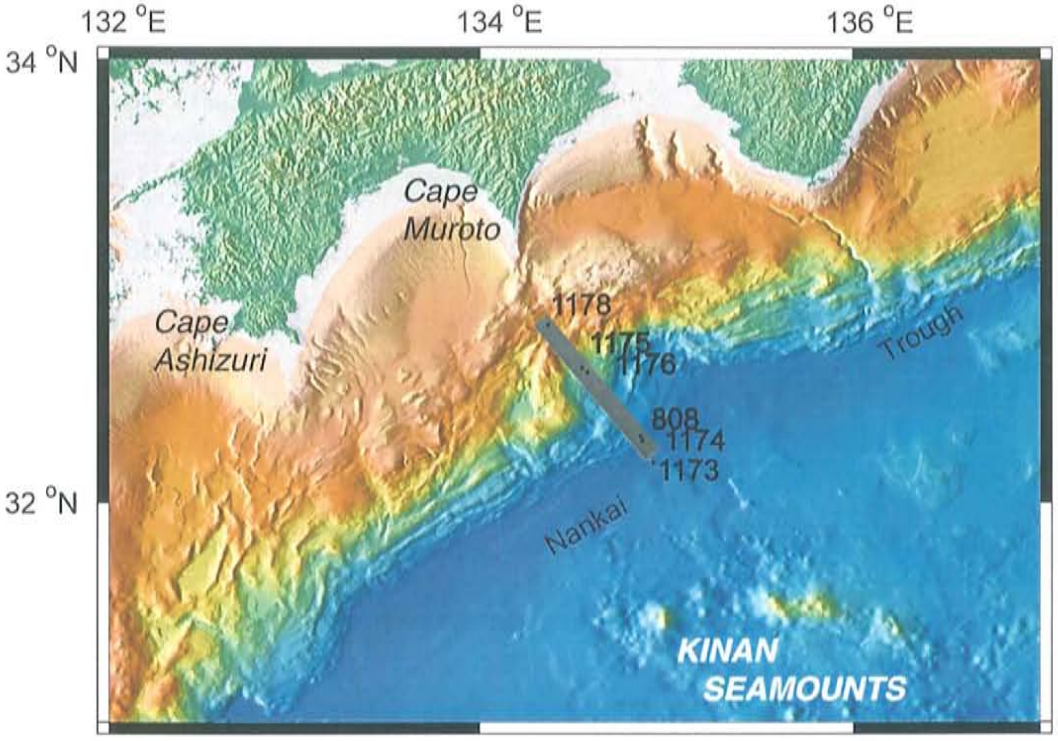

Figure 1.3: Map showing the location of Muroto 3D seismic survey (grey box) and ODP drill Sites 1173, 1174, and 808 for Legs 190 and 196 within the Nankai Trough offshore Cape Muroto, Japan [*Shipboard Scientific Party,* 2002].

CHAPTER 2

BACKGROUND

2.1 Geologic Overview

The Nankai accretionary prism is located on the plate boundary formed by the Philippine Sea Plate subducting beneath the Eurasian Plate at a convergence rate of 2-4 $^{cm}/_{yr}$ (see Fig. 1.1) [*Seno, et al.*, 1993]. Great earthquakes (magnitude > 8) at the Nankai Trough have an average recurrence interval of ~180 yrs historically [*Ando*, 1975; *Hori, et al.*, 2004]. Shikoku Basin sediments, a thick hemipelagic to terrigeneous section on the incoming Philippine Sea Plate, are actively accreting into the prism or are underthrust beneath the margin. The record of accretion from the Cretaceous through the Miocene is exposed on the islands of Japan northwest of the Nankai Trough in the Shimanto Belt rocks [*Moore, et al.*, 2001b]; the young post-Pliocene prism forms the continental slope offshore.

Accretionary prisms are composed of imbricate thrust sheets that include material offscraped from the subducting plate [*Morgan and Karig*, 1995]. A fundamental component of the subduction system is a low angle thrust boundary or décollement separating the overlying prism from subducting material which typically

localizes within the incoming seafloor sediment section [*Byrne and Fisher*, 1990]. The strength of the décollement has been shown to influence the seafloor slope of the prism; a weak décollement yields a shallow taper angle as exhibited in the seaward portion of the Nankai accretionary complex [*Davis, et al.*, 1983; *Maltman, et al.*, 1993].

2.2 Previous Studies

Numerous studies have shown that subduction megathrusts are weak [*Davis, et al.*, 1983] and fluid rich [*Bangs, et al.*, 1999] above their updip limit of seismicity. At the Nankai subduction zone offshore SW Japan, it has been inferred that limited permeability of the underthrusting sediments and rapid loading from turbidite deposition cause fluid overpressures at the décollement. This has been suggested for the décollement where it has been drilled at the trench [*Screaton, et al.*, 2002]; fluid overpressures along the décollement may persist beneath the prism.

The Nankai accretionary complex has been studied extensively through ODP Legs 131, 190, and 196 [*Bangs, et al.*, 2004; *Gulick, et al.*, 2004; *Moore, et al.*, 2005]. The R/V *Joides Resolution* was able to drill through the décollement and penetrate the underthrusting sediments at sites 808 & 1174 obtaining valuable *in situ* measurements of physical properties at the onset of deformation (Figure 2.1) [*Shipboard Scientific Party*, 2001]. Through this data combined with core experiments, an empirical velocity-to-porosity transform has been developed for the Shikoku Basin underthrust

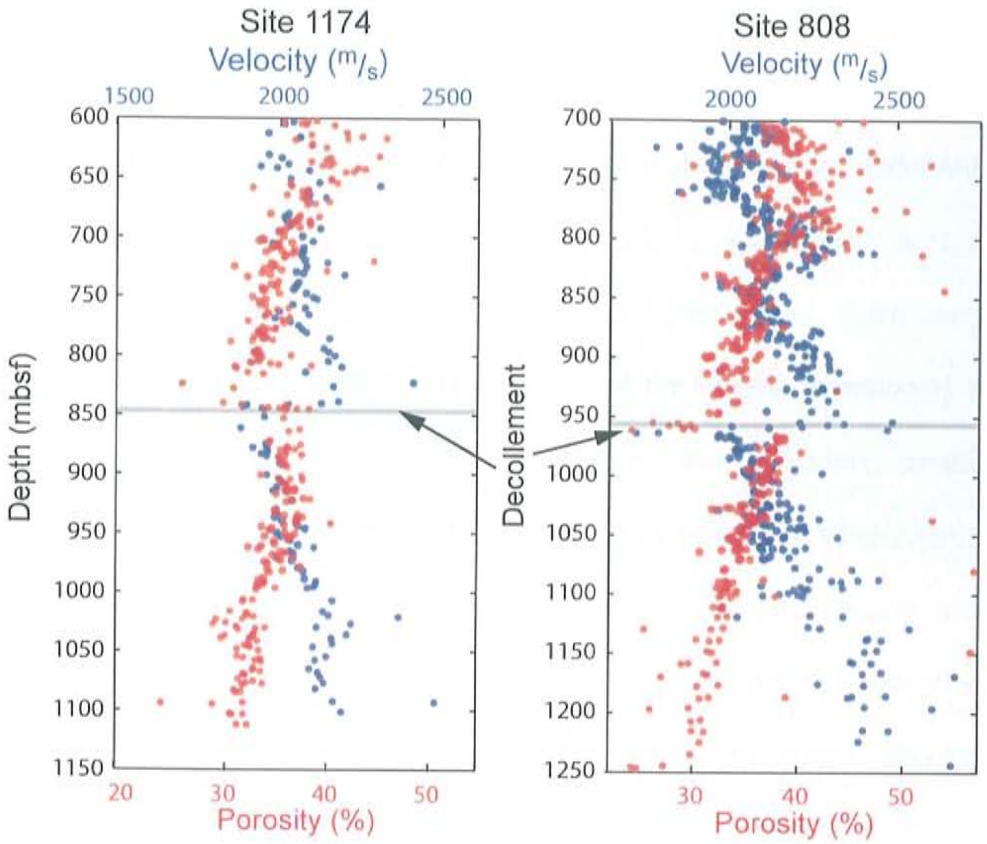

Figure 2.1: ODP Sites 1174 & 808 physical property data plotted near the decollement zone. The vertical gradient for both velocity and porosity is offset at the decollement boundary [*Shipboard Scientific Party*, 2002].

sediments to be used for inferred porosity calculation away from the boreholes [*Hoffman and Tobin*, 2005] (see section 3.3 below).

Several studies have used seismic survey data to estimate porosity in sediments at depth. *Von Huene* et al. [1998] applied an empirical site specific velocity-porosity relation, determined from local cores obtained during the Deep Sea Drilling Project, using seismic data of the Alaskan margin and its underthrusting sediments, finding porosity reduction patterns beneath the accretionary wedge that mapped to the varying structural styles within the overlying prism. *Cochrane* et al. [1994] presented good quality MCS data at the toe of the Oregon accretionary prism which allowed detailed stacking velocity analysis on 'flat' reflectors, detailing a velocity inversion across the décollement reverse polarity reflection; when *Hamiton et al.'s* [1978] velocity – density mudstone curve was applied, a porosity increase relative to the overlying sediments was observed beneath the proto-décollement. *Bangs et al.* [1999] used modeled reflection amplitudes of the imaged décollement from the Barbados prism to infer porosity and found large scale fluid channeling processes at this plate boundary (Figure 2.2). Another study applied a similar reflection amplitude technique to infer the qualitative fluid pressures and how they changed downdip within the décollement boundary of the Nankai subduction zone (Figure 2.3) [*Bangs, et al.*, 2004]. They found that a strong décollement reflection developed from a porosity contrast between the overlying rapidly loaded prism material and the subdued consolidation of the underthrust sediments, but the reflection

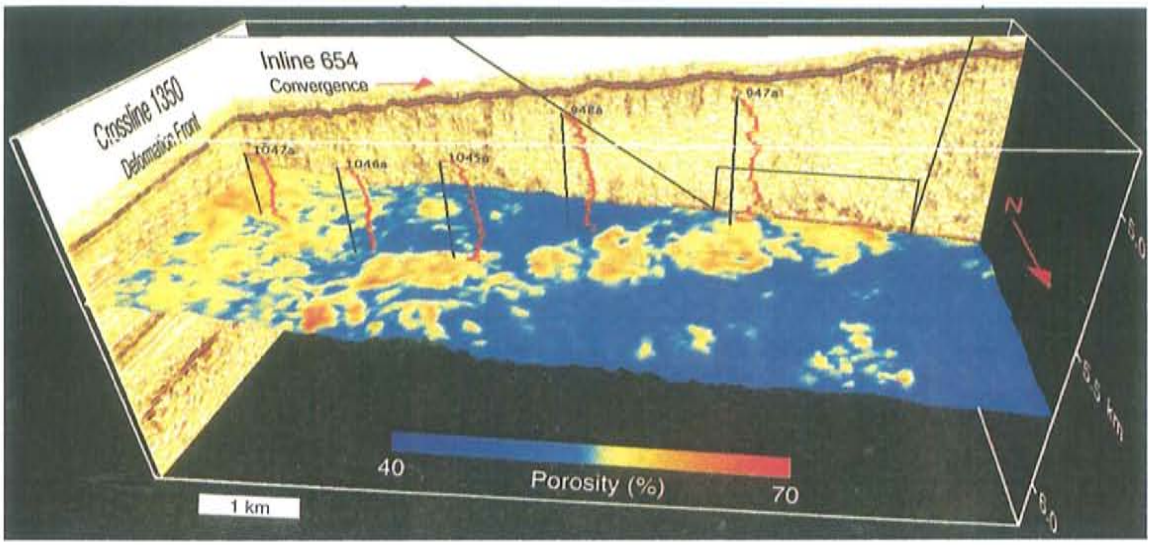

Figure 2.2: A 3-D perspective view of seismic data collected within the Barbados accretionary prism. The decollement surface is shown with contoured porosity derived from reflection amplitude. ODP drill site locations and corresponding density logs are plotted [from *Bangs et. al.*, 2001].

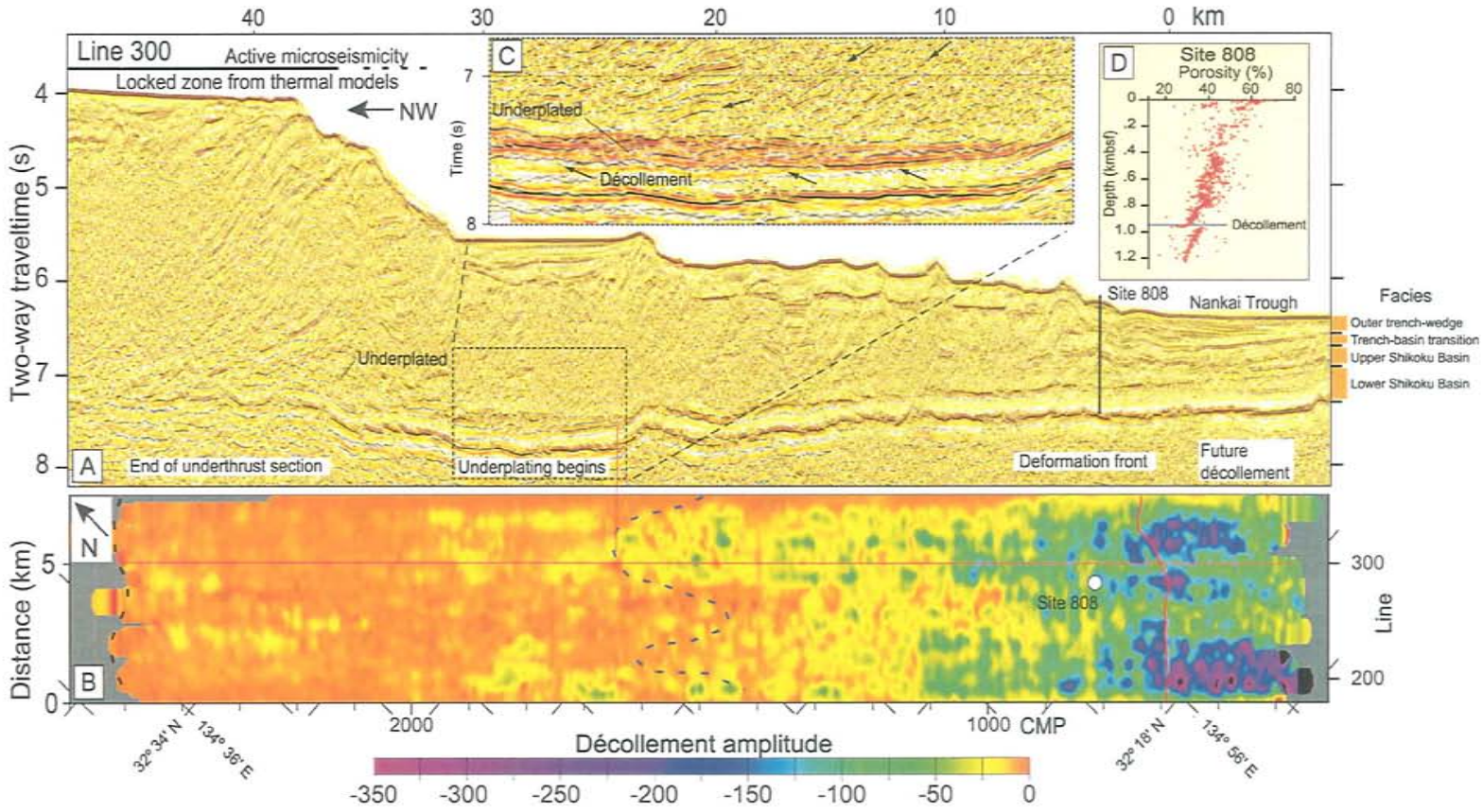

Figure 2.3: Map of decollement reflection amplitude within the Nankai Trough. Red line is the deformation front. Blue dashed line marks updip edge of underplating. Black dashed line is downdip edge of underthrust section [from *Bangs et. al.*, 2004].

amplitude diminishes with progress landward/downdip [*Bangs, et al.*, 2004]. At the Costa Rica subduction zone, the entire incoming sediment package is underthrust [*Saffer, et al.*, 2000; *Saito and Goldberg*, 2001] allowing a direct estimate of fluid production and permeability below the décollement by observation of the decrease in volume as the underthrust sediment are progressively loaded [*Saffer, et al.*, 2000].

All of these studies have suggested that at subduction zones the décollement is a mechanical discontinuity that separates drained, horizontally shortened, offscraped prism sediments from relatively undrained underthrust sediment in which excess pore pressure is transiently sustained [*Saffer*, 2003; *Screaton, et al.*, 2002], little relative tectonic deformation takes place [*Byrne and Fisher*, 1990; *Maltman, et al.*, 1993; *Moore, et al.*, 2005], and vertical compaction dominates [*Bray and Karig*, 1985]. Fluid overpressure at the décollement and in the underthrust sediment weakens décollement strength and is thought to possibly be a main control determining the updip limit of seismicity [*Moore and Saffer*, 2001].

2.3 Structural Description

Based on seismic reflection data from the 1999 Muroto Transect the Nankai accretionary prism has been classified into several structural/tectonic zones (Figure 2.4) [*Moore, et al.*, 2001a]: Nankai Trough Trench axial zone, protothrust zone (PTZ), imbricate thrust zone (ITZ), out-of-sequence thrust (OOST) zone, large thrust-slice (LTS) zone, and landward-dipping reflector (LDR) zone. Only the trench,

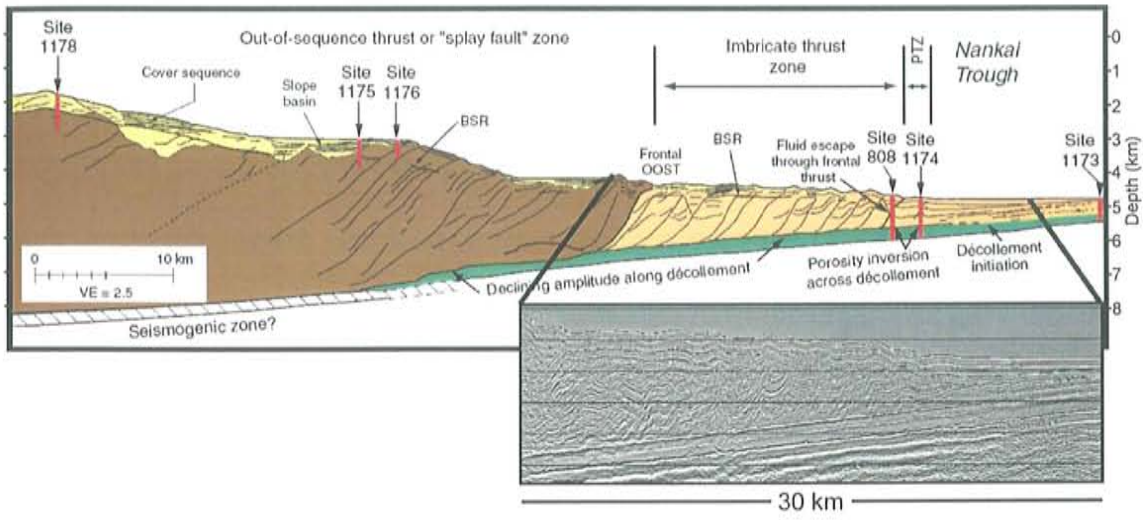

Figure 2.4: Schematic interpretation of inline seismic data from the Muroto Transect showing tectonic domains and locations of ODP Leg 190 drill sites. Seismic data inset location shows the inline boundary of the survey data used for this study [from *Moore, et. al.*, 2001].

protothrust, imbricate thrust and out-of-sequence thrust zones will be described in detail here as those regions encompass the limits of the seismic data for this study.

The Nankai Trough trench domain is composed of a unit of seaward thinning turbidites that overly the Shikoku Basin hemipelagic sediments. In the Shikoku Basin seaward of the Nankai Trough, sediments are composed of <100 m of turbidites with hemipelagic strata below [*Moore, et al.*, 2001a]. ODP Site 1173 cored the Shikoku Basin sediments seaward of the trench as a reference prior to deformation and rapid loading.

The protothrust zone is bounded by the onset of deformation seaward and the first landward frontal thrust; it is characterized by diffuse structural thickening [*Gulick, et al.*, 2004; *Moore, et al.*, 2001a]. Within this domain, trench turbidites and upper hemipelagic units from the Shikoku Basin are accreted to the upper plate while the décollement starts to form within the Lower Shikoku Basin stratigraphic unit [*Moore, et al.*, 2001a]. ODP site 1174 is located within this domain and cored through the décollement, the subducting sediments, and into the basement.

Further landward, past the onset of deformation, is the imbricate thrust zone which is composed of roughly 12 seaward-vergent continuous thrust packages [*Moore, et al.*, 2001a]. The thrusts sole into a well defined basal décollement. *Gulick et. al.* [2004] have demonstrated that northeastward-oriented, landward-stepping thrust packages within the ITZ was the prism's rebuilding response to a subducting seamount leaving the Tosa Bae embayment of the prism. ODP site 808 was drilled

and cored near the seaward boundary of the ITZ where it penetrated the frontal thrust, décollement, underthrust section and into the basement. At Site 808, borehole resistivity images indicate that deformation of the incoming sediment within the prism is a result of a tectonically controlled stress field that is influenced by lithology [*McNeill, et al.*, 2004]. However, within the décollement, fracture orientation is variable suggesting stress heterogeneities, rotation, and transient fluid migration [*Bourlange, et al.*, 2003; *McNeill, et al.*, 2004].

The out-of-sequence thrust (OOST) zone is approximately 30 km landward of the frontal thrust and is characterized by imbricate thrusts that are cut by a younger lower-angled thrust fault system [*Moore, et al.*, 2001a]. A small portion of this region is narrowly imaged in the downdip/landward portion of this study. ODP Sites 1175, 1176, and 1178 were drilled in this region but did not penetrate the underthrust section.

CHAPTER 3

SEISMIC PROCESSING & INFERRED POROSITY

An integrated approach, combining *in situ* borehole information, seismic reflection data, and a velocity-porosity transform is required to quantify porosity distribution in the subsurface. Boreholes into subduction zone environments provide detailed information on subsurface conditions; however they are isolated and limited in depth, and provide only 1-D information. Because P-wave velocity can be linked to other physical properties of interest, velocity from seismic reflection and refraction surveys provides the best available information for shedding light on rock properties away from borehole locations. In order to quantify the porosity distribution of the underthrust sediments from the Muroto 3D seismic volume off the coast of Japan, Kirchoff pre-stack depth migration (PSDM) processing was utilized to both image structure accurately and obtain robust velocity estimates. These PSDM-defined velocities were used to compute porosity via an empirically-derived P-wave velocity-to-porosity transform specific to the Nankai subduction zone underthrust sediments [*Hoffman and Tobin*, 2005].

3.1 Kirchoff Pre-Stack Depth Migration

Seismic data collection requires a controlled seismic wave energy source to be input into the earth, recorded, and later processed to form an image. This seismic energy travels as elastic compressional waves (P-wave) whose velocity is a function of the material rigidity and density. The product of the material density and the compressional-wave velocity is a physical property of the rock that is defined as the acoustic impedance. Contrasts in acoustic impedance values cause reflections of the spherically spreading elastic wave energy propagating in the subsurface. Because of subsurface scattering, diffraction, and 3-D raypath effects, reflected energy is not necessarily recorded at its proper 3-D time/depth location by the seismic traces plotted at common midpoint locations. The nature of seismic energy propagation and complex subsurface geology require the data to be processed, or migrated, to its actual subsurface position [*Sheriff*, 1995]. Seismic data migration therefore involves repositioning of data elements to make their imaged location more representative to their true reflection location in the subsurface.

In this study, the Kirchoff PSDM method was used to process seismic data. Kirchoff PSDM is an algorithm that solves the wave equation in integral form and operates on seismic data elements prior to trace stacking of the section [*Sheriff*, 1995]. Because of this, it is highly sensitive to velocity changes and is widely accepted as the most appropriate migration algorithm to apply in areas where high velocity gradients and complex subsurface structures exist [*Reshef*, 1997]. Its results are believed to

most accurately represent the subsurface structure and *in situ* velocity, of all available methods. The generation of robust velocity estimates from PSDM iterations is therefore the most appropriate input to a compressional-wave velocity-to-porosity transform allowing accurate mapping of porosity in the underthrust section.

In practice, Kirchoff PSDM is an iterative process that requires a starting input velocity field that is used for the pre-stack migration (Figure 3.1). The outputs of a migration are depth gathers for each common depth point (CDP) that are used to empirically assess the improvement and decide if further velocity updates are required. Depth gathers are plots of individual seismic traces sorted by source-receiver offset vs. depth for each CDP location. Near (zero) offset traces are plotted near the Y-axis and increase in source-receiver offset down the X-axis, i.e. far offset (Figure 3.2). These depth gathers are stacked together to produce the seismic section. When stacked, planes of reflectors that occur at a common depth on each individual trace stack more coherently than others that don't have the reflector at a common depth. An ideal depth gather would have the same reflection wavelet at the same depth for all source-receiver offsets. Updating the velocity field is achieved by analyzing the depth gathers and picking a residual moveout (RMO) correction. RMO is calculated from the semblance for a horizon or reflector in the depth gathers. The RMO is used as an input to a global tomographic inversion to correct the velocity model in a way to appropriately flatten the reflector in the depth gathers. The RMO was calculated and picked along high amplitude reflective horizons so that the

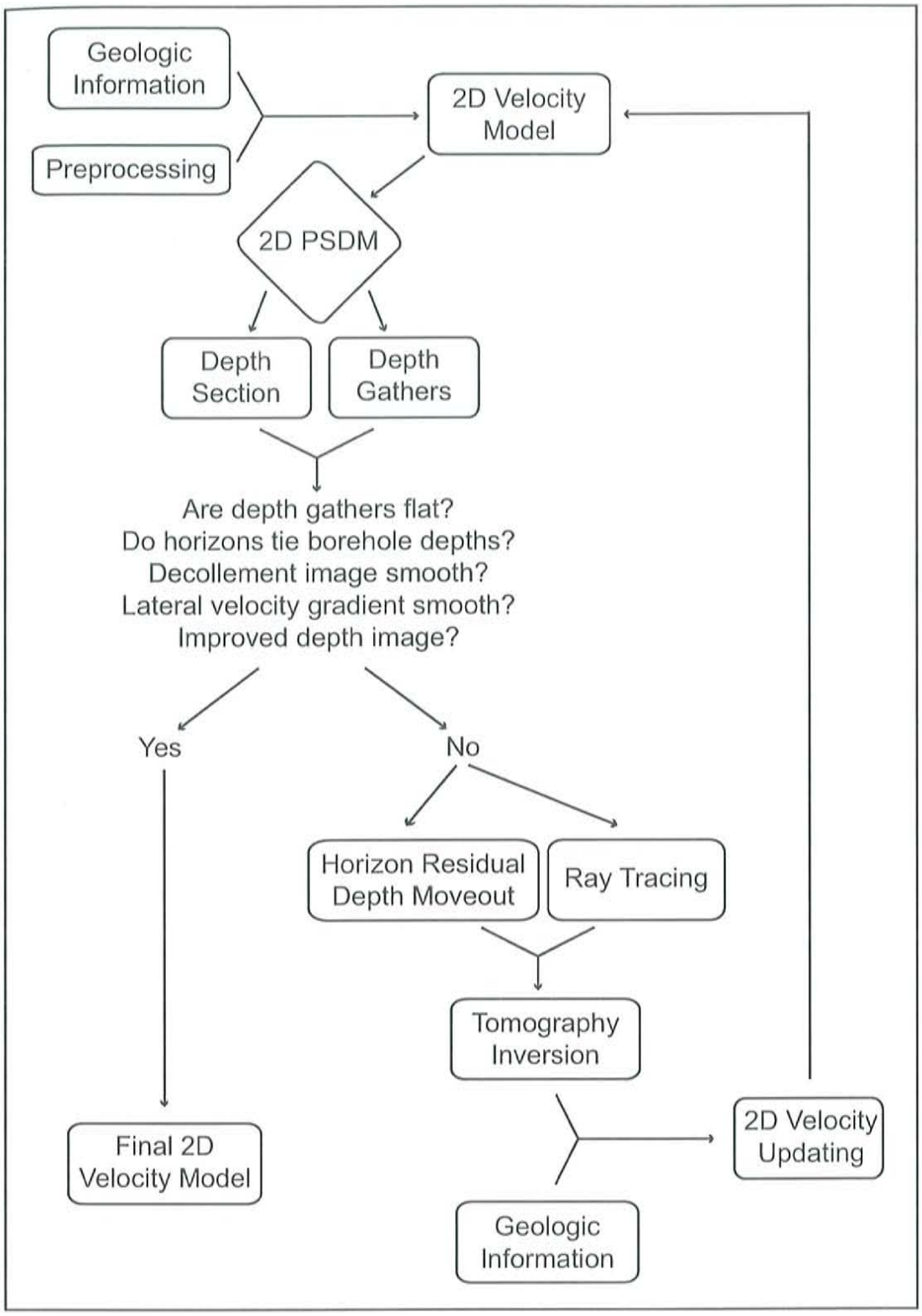

Figure 3.1: Schematic illustrating the PSDM flow: inputs, outputs, and iterative nature of 2D pre-stack depth migration.

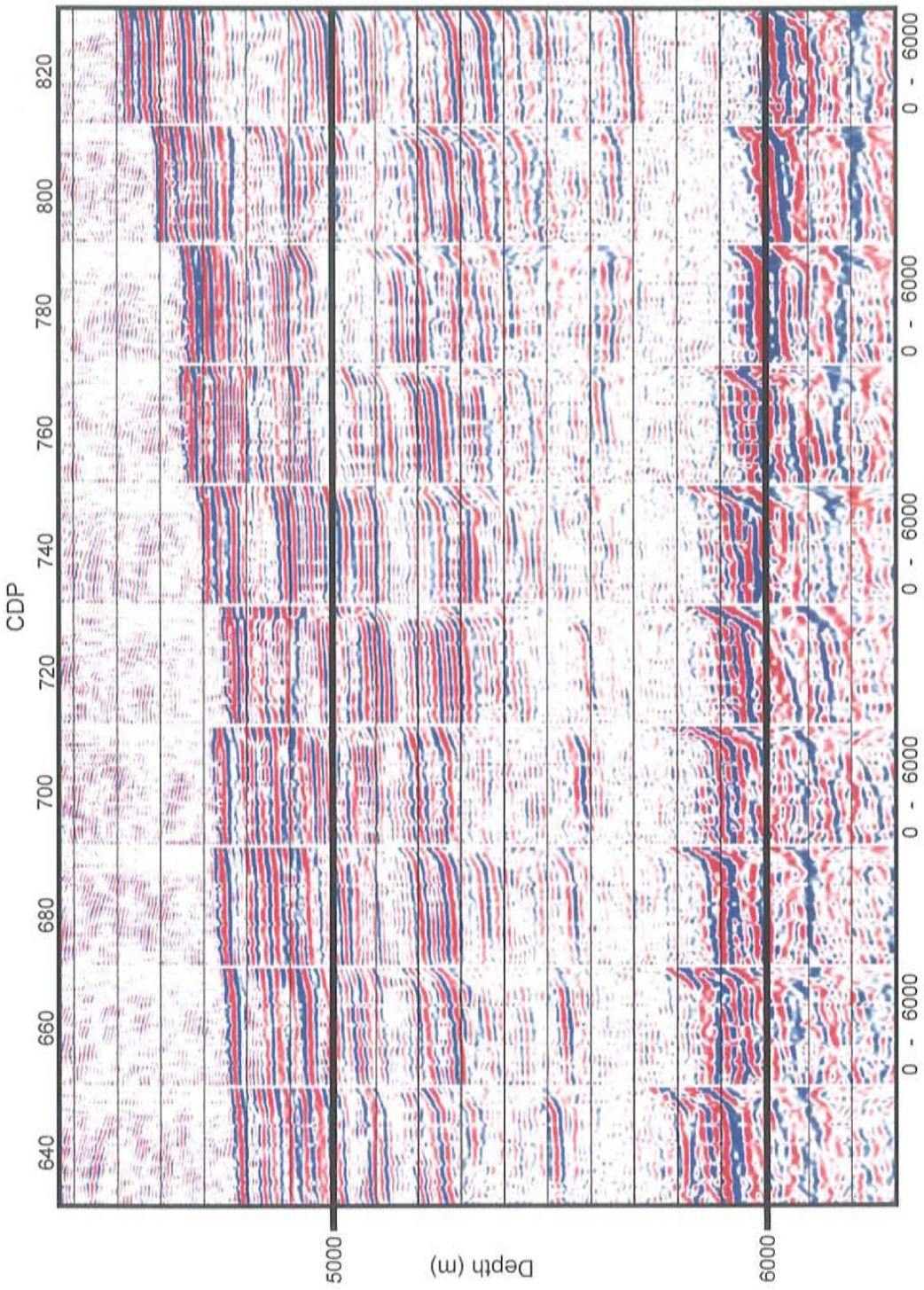

Figure 3.2: Example of depth gathers from the trench area along inline 290 of the Muroto 3-D survey

migration results can be seen on the depth gathers, i.e. on the non-stacked seismic data (Fig 3.3). In essence, PSDM iteratively refines the input velocity field to produce the migration which best collapses the reflectors in the stacked section, or optimizes coherence on reflectors in depth gathers before stacking (Figure 3.4).

3.2 Migration on the Nankai Seismic Dataset

Kirchoff pre-stack depth migration was carried out using commercial seismic processing software. For most of this study, Landmark ProMax was used to carry out the PSDM processing; Paradigm's GeoDepth software package was also used for some processing steps including checking results from Promax. ProMax proved advantageous because of the capability to run as multi-processing jobs, as well as allowing additional control and constraints over corrections and updates made to the velocity field and horizon depths as the PSDM iterations progressed.

As stated before, seismic data migration is undertaken to improve the image quality. However, a very important output for this study from the PSDM processing is an accurate velocity field. In order to obtain a robust estimate of P-wave velocity for the Muroto seismic volume, several iterations of 2D PSDM were completed every 5 inlines, for 31 total processed lines, spaced 250 m apart. The initial velocity model input for the 2D migration was an adjacent inline velocity model that had already been processed, seeded by results of inlines 215 & 284 of *Pisani et al.* [2005].

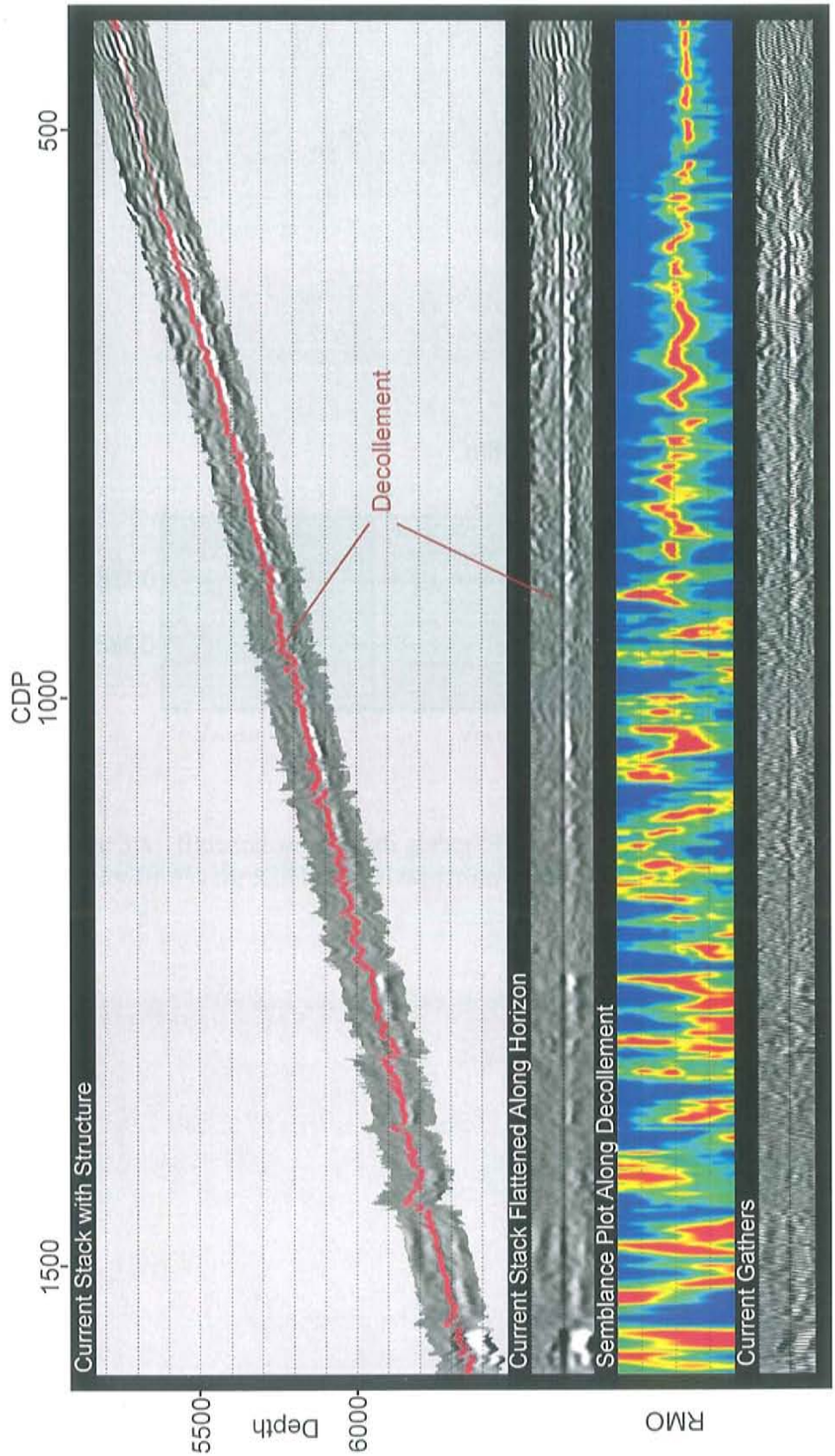

Figure 3.3: Example velocity analysis panel showing the residual moveout correction, semblance of velocity to flatten depth gathers, for the decollement horizon. The RMO gradually gets smaller after several iterations of pre-stack depth migration.

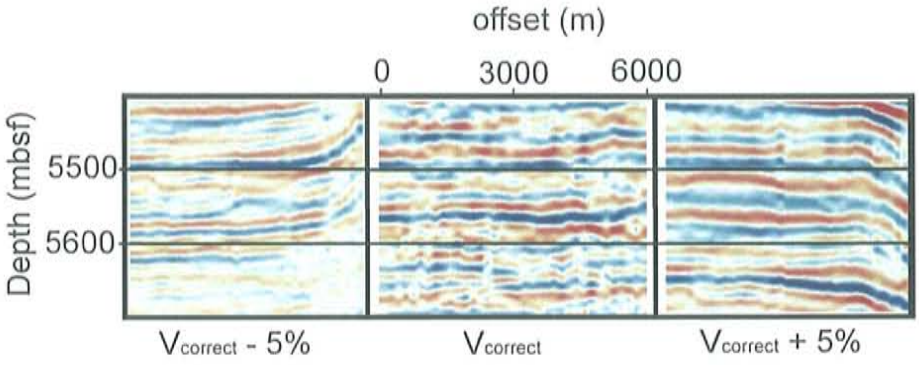

Figure 3.4: Illustration of depth gather "flatness" and sensitivity by varying the velocity by 5% for Kirchoff PSDM [from *Pisani et al.*, 2005].

Reflectors in depth gathers, as illustrated previously, are ideally migrated to the same depth for the entire shot-receiver offset spectrum. This allows maximum coherent stacking. Unfortunately, this method alone generally produced an inaccurate velocity field for 2D processing of the seismic data, so additional constraints for velocity updating were employed. The criteria used to evaluate velocity field accuracy included: (1) flatness of reflectors in depth gathers (see Figure 3.4); (2) correlation between imaged horizon depth and borehole horizon depth; (3) enhancement of continuity and smoothness of reflectors; (4) realistic borehole based estimation of the thickness of the underthrust sediment package; and (5) improvement of velocity field smoothness. For example, we assumed that near-borehole seismic lines with imaged horizons such as the décollement should have a velocity field that migrates the reflection to the true depth as measured in the borehole, and that reflected horizons should be relatively smooth and continuous. We sought to avoid sharp short-distance steps down or up in the décollement image. The thickness of the underthrust section is thought be relatively continuous along strike and decrease downdip given the geometry of the survey area [*Moore, et al.,* 2005] (see Figure 1.2). Combined, these criteria constrained the depth and continuity of the décollement and basement horizons for the PSDM iterations, generating an accurate velocity field for the prism and underthrust sediments.

Errors in 2-D inline velocity models and discrepancies between migration velocity and that required to tie at the boreholes were attributed to the very complex

streamer navigation associated with the acquisition, out of plane reflected energy, complex subsurface geometry, and possibly high velocity gradients. In addition to the complexity of the survey, internal reflectivity in the underthrusting section was limited, which precluded precise determination of interval variations in velocity of the underthrusting sediments. To minimize error in the updated velocity model associated with the inversion step within the PSDM workflow, the inversion was constrained by forcing the décollement and the top of basement horizons to be nearly planar horizons. Iterations proceeded until all these factors were optimally balanced and no additional improvement to imaging was seen with further velocity adjustment.

3.3 Velocity to Porosity Transform

In order to quantify the porosity and ultimately pore pressure distribution within the underthrust sediments at the Nankai Trough by using compressional wave velocity, the empirical transform of *Hoffman and Tobin* [2004] was used. This transform was based on the approach of *Erickson and Jarrard* [1998], who set out to design a global velocity-porosity transform using sediments from the Amazon Fan. They found the limiting curves can be plotted for a compressional wave velocity vs. porosity relationship for siliclastic sediments in a global sense, determined only by the variables porosity, shale fraction, and consolidation history. They generated two boundary curves that represent the normal-consolidation conditions typically found in a sedimentary basin versus an analogous high-consolidation environment such as in an

accretionary prism (Figure 3.5). *Hyndman* [1993] fit a smooth polynomial to ODP Site 808 for the Nankai sediments, obtaining an empirical velocity porosity relation, based on *Hon et al.* [1986], *Hamilton* [1978], and *Jarrard et al.* [1989]. However, *Hoffman and Tobin* [2004] found that *Erickson and Jarrard's* normal-consolidation model better fit the core data from the underthrusting Shikoku Basin section at the Muroto Transect. Utilizing this normal-consolidation P-wave velocity–to–porosity model as a starting point, additional fitting parameters were computed to better fit the borehole data for ODP drill sites 1173, 1174, and 808 (Figure 3.5) which was used to compute porosity for this study with the following function.

$$V_p = A + B\phi + \frac{0.305}{(\phi + C)^2 + \frac{0.305}{1.51 - A - B} - C^2 - 2C - 1} + 0.61(\upsilon_{sh} - 1.123)[X_m]$$

Where:

$X_m = \tanh(40(\phi - \phi_c)) - |\tanh(40(\phi - \phi_c))|$
V_p = compressional wave velocity
ϕ = fractional porosity
υ_{sh} = shale fraction
A, B, C = empirical coefficients
ϕ_c = critical prosity

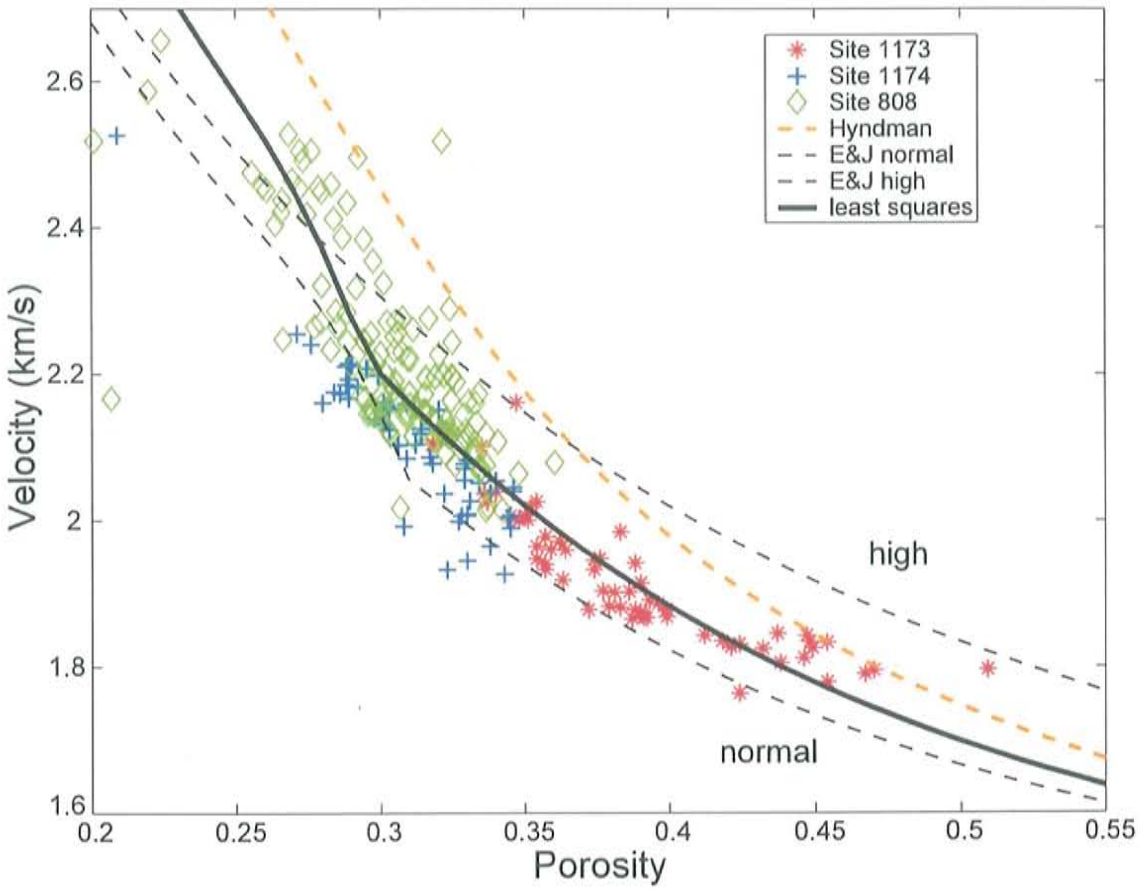

Figure 3.5: Empirical velocity-porosity formulations for the underthrust sediments for Sites 1173, 1174 and 808. The least squares best fit (solid black line) is plotted for a shale fraction of 1 [*Hoffman & Tobin*, 2004]. The formulations for normal- and high-consolidation [*Erickson and Jarrard*, 1998] and plotted for shale fractions of 1 as well as the formulation from Hyndman et al. [1993]. Data points are ultrasonic P-wave velocity and porosity measured on core samples of the underthrust section and its lateral equivalent in the trench, corrected for rebound from in situ pressure [after *Hoffman & Tobin*, 2004].

3.4 Décollement Referenced Planes

For each of the 32 inlines in the Muroto seismic volume processed with PSDM, we generated a stacked section and associated velocity model which were used to extract the appropriate velocity data for porosity computation of the underthrust sediments. The seafloor and décollement horizons were manually picked and depth information for each CDP was extracted. Several horizons were created at constant depths below the décollement in the underthrust sediments, and the PSDM velocity values along these horizons were extracted and porosity was calculated for each velocity value. Results were exported to a spreadsheet file (see Appendix C).

CHAPTER 4

RESULTS

4.1 Seismic Image Results

I present results first on the 2-D structural imaging in the PSDM, then on the evolution of velocity and porosity in the underthrust sediments. This new pre-stack depth migration processing of the Muroto transect has greatly improved the depth image of the toe on the Nankai accretionary prism. An example depth section stack (inline 290) and the corresponding velocity model used for the pre-stack depth migration is plotted in Figure 4.1. All 31 processed inlines are shown in Appendix A. Projected ODP borehole locations 808 & 1174, which penetrated the underthrust section, are shown for location reference.

The prism structure and stratigraphic assemblage are imaged clearly across all lines, showing numerous imbricate thrusts terminating into a well defined décollement zone. A gas-hydrate reflector is present in many areas ~500 m below the seafloor. The décollement image is characterized by a strong reverse polarity reflection wavelet indicating a negative reflection coefficient, or decrease in velocity and/or density at the base of the accretionary prism. Our PSDM processing clearly refined, sharpened, and improved the décollement image in this area of the prism, relative to previous

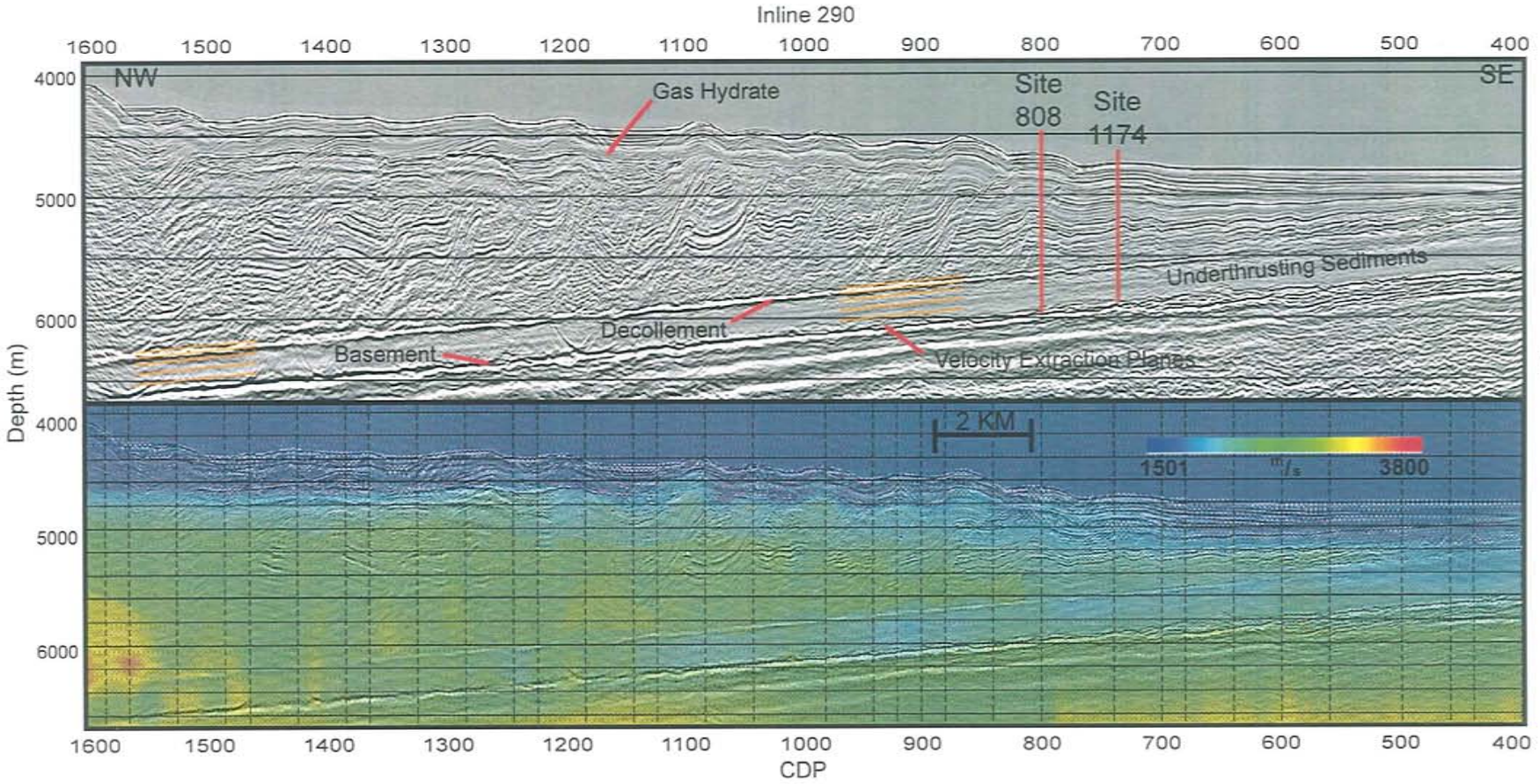

Figure 4.1: Inline 290 migrated seismic stack and corresponding velocity model with projected ODP borehole locations

post-stack and time migrations [*Bangs, et al.*, 2000; *Gulick, et al.*, 2004; *Moore, et al.*, 1990]. The top of basement is characterized by a strong normal polarity reflection wavelet, indicative of a large increase in P-wave velocity. The horizon was processed to remain relatively flat, although actual basement topography is unknown. Its continuity and reflective character is somewhat noisy at points, although it is a vast improvement from post stack versions. Much effort would be required to refine the top of basement image further and is not critical for this study.

Between the décollement and top of basement are the underthrusting sediments, whose internal reflectivity has become more coherently imaged and improved somewhat, but has not developed sufficient continuity to permit definition of internal intervals for PSDM processing. The underthrust sediment package is approximately 300 meters thick and decreases approximately 25 m in thickness as it progresses to the landward/downdip extent of the survey (30 km). Treating this as a single interval, with a gradient in velocity (somewhat variable from place to place) from bottom to top, defines the average PSDM migration velocity for the underthrust package.

4.2 Velocity Results

Contoured 2D inline velocity results can be found in Figure 4.1 and in Appendix A. We used a constant water velocity of 1501 $^{m}/_{s}$ for the velocity model building. Velocity in the sediment package within the trench area (~CDP 400 – 600)

has a stronger vertical gradient than lateral as normal compaction conditions exist here [*P. Pisani,* personal communication, 2005]. Progressing landward into the prism, the lateral velocity gradient increases, and a clearly defined décollement reflection develops beyond CDP ~650. Across the décollement zone, a strong vertical velocity inversion of approximately 50 – 150 $^{m}/_{s}$ is prominent throughout the data volume at the top of the underthrust section.

We extracted interval velocity at a constant 75 meters below the picked décollement horizon every 5 inlines and every CDP (400-1600) from the seismic data volume, and color contoured them in a perspective image (CDP (or X-line) number vs. Inline number vs. Depth) (Figure 4.2). Because the PSDM contains vertical gradients in velocity, but no discrete intervals within the underthrust package, we chose this constant 75 m depth as representative of the velocity structure approximately one full wavelength below the décollement zone discontinuity, and hence not contaminated by overlying velocity structure. This probably overestimates the true velocity immediately below the décollement (see for example, Figure 2.1), translating into a conservative estimate of inhibited consolidation and overpressure. Velocity planes depth referenced at 0, 25, 150 and 250 meters below the décollement were also extracted and are plotted in a similar fashion (Figure 4.3). The PSDM-generated interval velocity for the underthrust sediments ranges from ~1700 - 3200 $^{m}/_{s}$. Along-strike, patchy variability in the underthrust velocity structure is thought to be real at least in part, but it is unclear how much basement topography on the order of 10's of

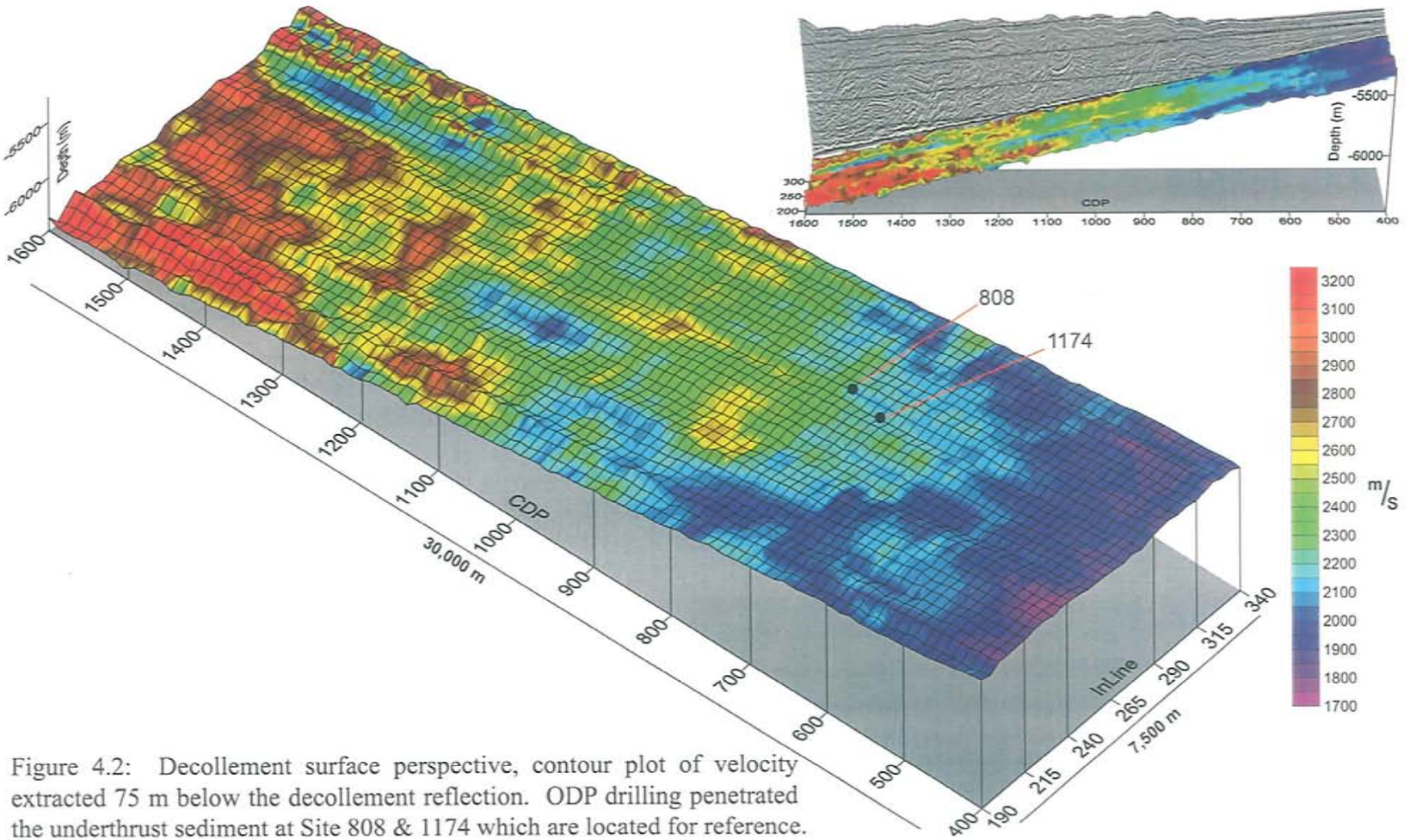

Figure 4.2: Decollement surface perspective, contour plot of velocity extracted 75 m below the decollement reflection. ODP drilling penetrated the underthrust sediment at Site 808 & 1174 which are located for reference.

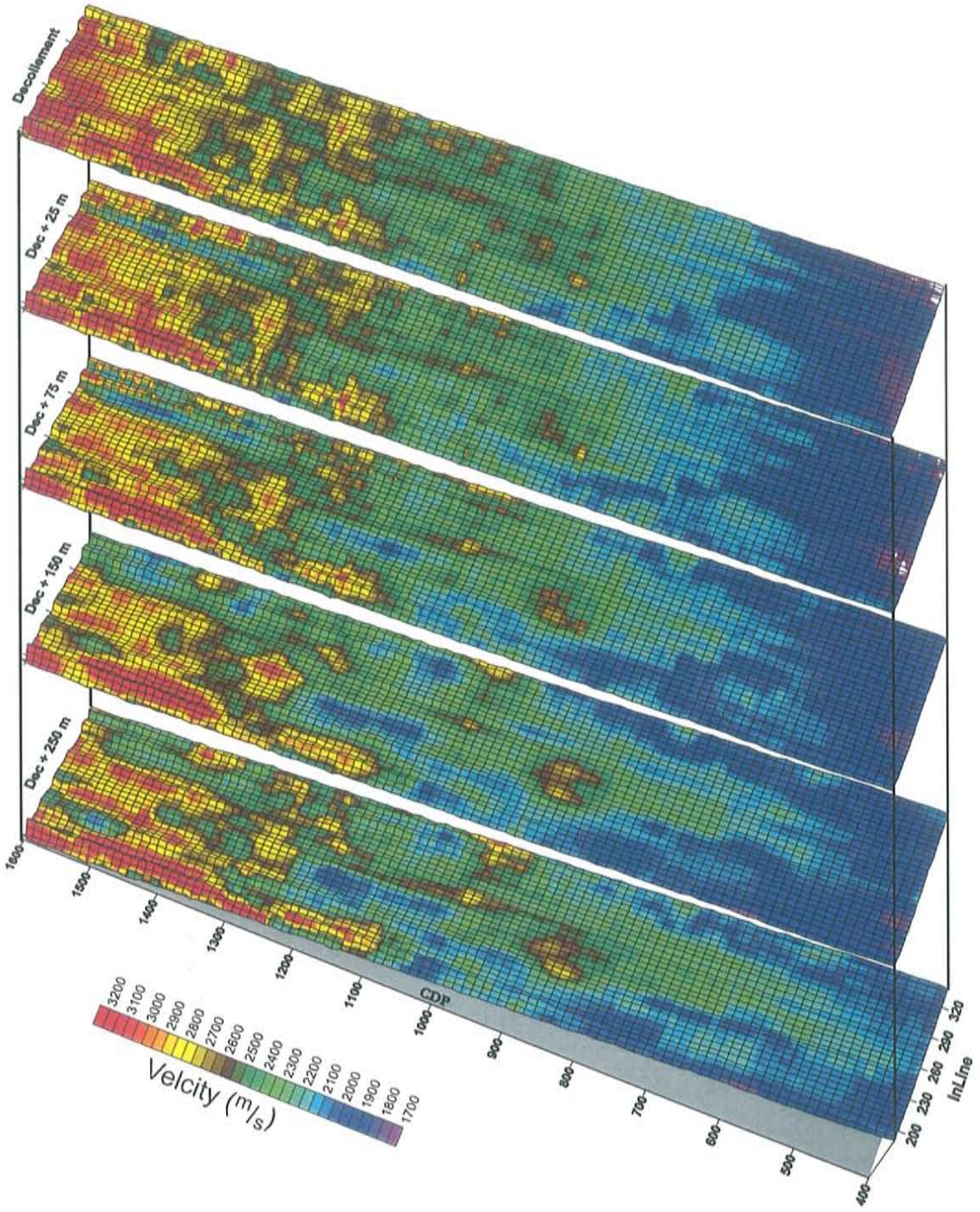

Figure 4.3: Decollement surface perspective, contoured plots of velocity within the underthrust sediments at the Nankai Trough.

meters would affect the 2-D velocity updating iterations and along strike variability. Fast or slow features that plot along one single 2-D inline are thought to be anomalous, such as the high velocity feature downdip of CDP 1250 on inline 320, 75 meters below the décollement plane. 3-D target oriented PSDM has been applied near Sites 808 and 1174 showing little change in velocity values, trends in gradient have not changed overall [*Pisani, et al.,* 2005; *P. Pisani,* personal communication, 2005]. The velocities generated for the final 2-D PSDM processing are input into the velocity - porosity transform for the Nankai sediments of Hoffman and Tobin [2004].

4.3 Porosity Results

Inferred porosity distribution within the underthrust sediments calculated from the empirical transform is plotted in a similar fashion as the extracted velocity and ranges from ~50% to ~10% (Figures 4.4 & 4.5). The underthrust sediments at the trench-ward end of the transect (crossline 400) contain approximately 40% porosity and decrease by 8% to 12% as they progress landward 10 km to ODP Site 808 (crossline 800). Downdip of Site 808, porosity values remain relatively constant to crossline 1100, after which the porosity decreases to as little as 10% within the underthrust sediments.

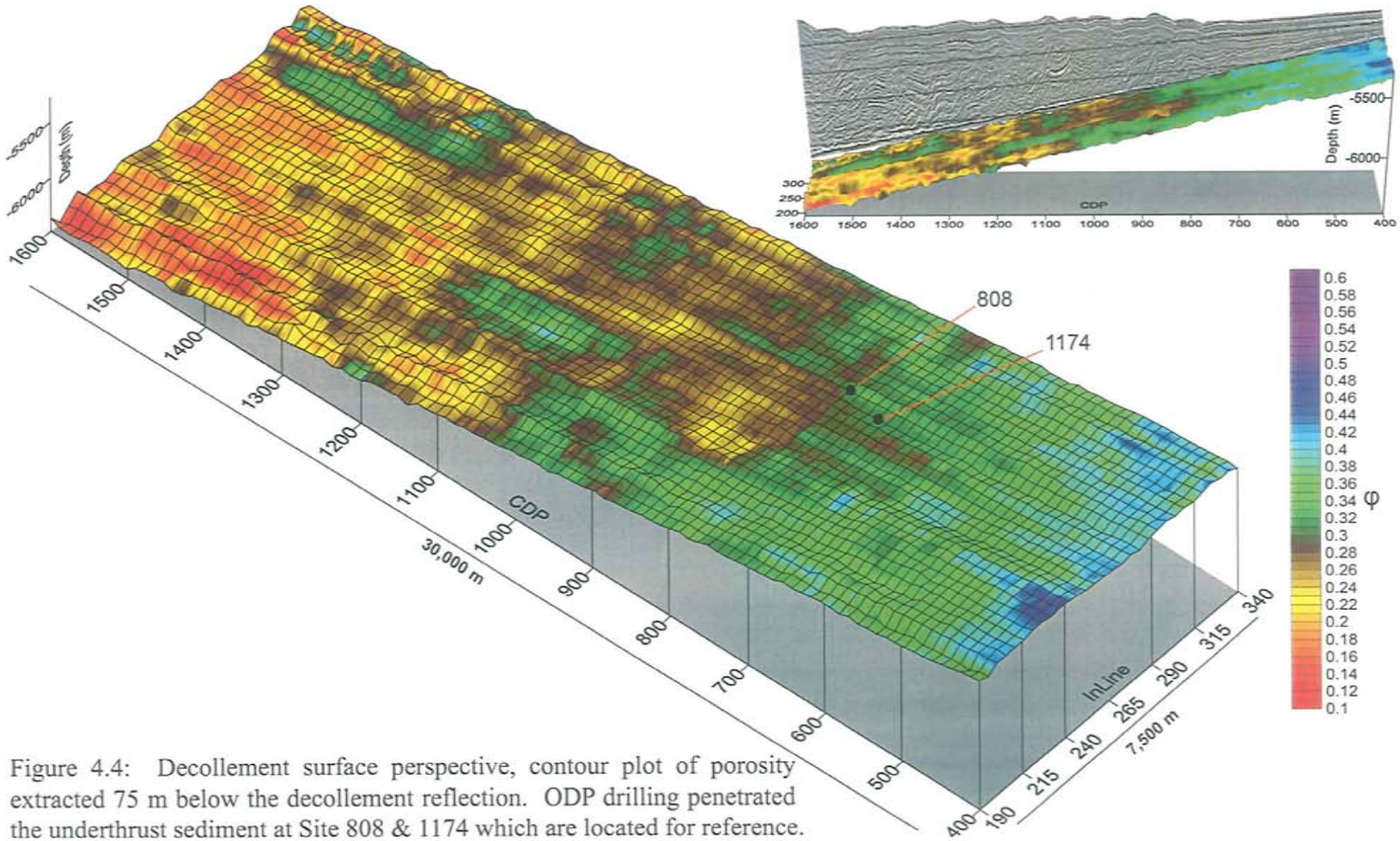

Figure 4.4: Decollement surface perspective, contour plot of porosity extracted 75 m below the decollement reflection. ODP drilling penetrated the underthrust sediment at Site 808 & 1174 which are located for reference.

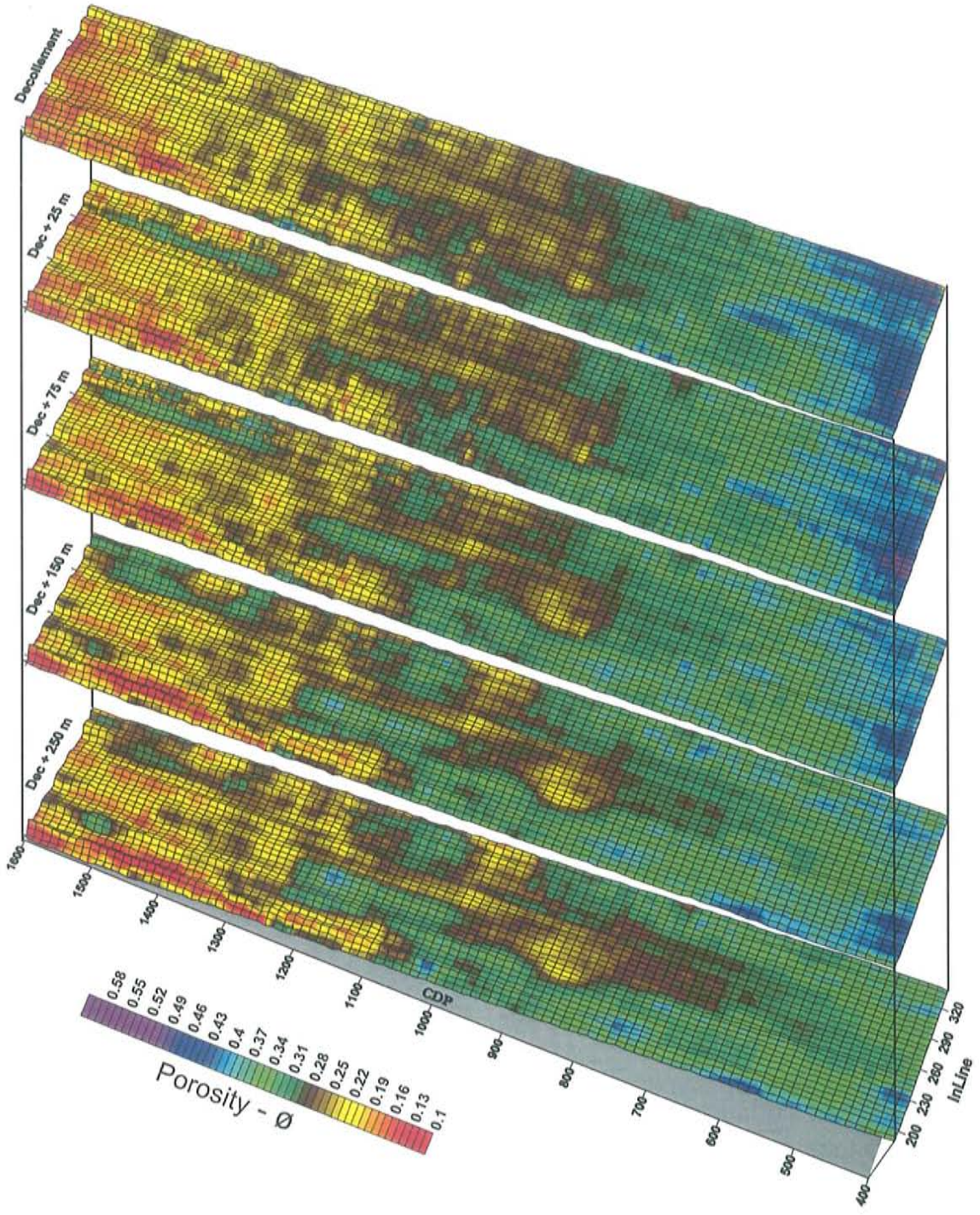

Figure 4.5: Decollement surface perspectives, contoured plots of inferred porosity within the underthrust sediments at the Nankai Trough.

CHAPTER 5

DISCUSSION

5.1 Depth Image Discussion

PSDM processing has greatly improved the seismic depth image of the Muroto Transect for structural interpretation and attribute studies, although migration artifacts are still present in isolated areas in the depth sections after processing. Correcting these areas proved difficult and would have required very non-realistic velocities to obtain further improvements in imaging. These migration artifacts can be attributed to possible acquisition & initial binning errors, seismic anisotropy and/or noise within the dataset. For instance, the reflectivity of the décollement varies within the data volume (see seismic images in Appendix A & Figure 4.1). It becomes a strong recognizable reverse polarity reflection around CDP 600. The reflection remains high amplitude and consistent for 15 km downdip (CDP 1100 - 1200) then its image drops in amplitude and becomes non-continuous. We attribute this degradation to noise, in addition to difficulties associated with imaging through complex structure, as opposed to a real effect caused by a lower impedance contrast. The lower amplitude non-continuous reflection would signify a decreasing porosity contrast between the underthrust sediments and overlying prism. However, the décollement

reflection regains its amplitude landward from this area; regaining a porosity contrast downdip is unlikely, favoring the hypothesis that this non-continuous nature is an imaging artifact.

Depths to critical reflection horizons (décollement & top of basement) in the 2-D seismic depth sections tie to depths projected from the drill sites. This was an important constraint and compromised the depth gather flatness, generally requiring them to be under-migrated in order to correlate reflections to known depths. Simply updating the velocity model to flatten the depth gathers produced inaccurate depth ties at the boreholes. We chose compromised values that preserve good depth ties at known locations (Site 808 & 1174) and relaxed the depth tie requirement as distance increased away from the boreholes. Quantifying uncertainty in the depth of the décollement and top of basement away from the boreholes is impossible; I relied upon balancing image quality and realistic velocity gradients (i.e. smoothness of the velocity model) in the PSDM processing.

5.2 Seismic Velocity & Inferred Porosity of the Underthrust Sediment

Comparison of LWD ISONIC, core, wireline and PSDM velocities at Site 808, 1174 and 1173 show that the PSDM seismic velocities correlate well with the *in situ* velocity data (Figure 5.1) [*Pisani, et al.*, 2005]. A key horizon, the décollement, is associated with a seismic velocity inversion typically of 50-150 ^{m}/s across the zone.

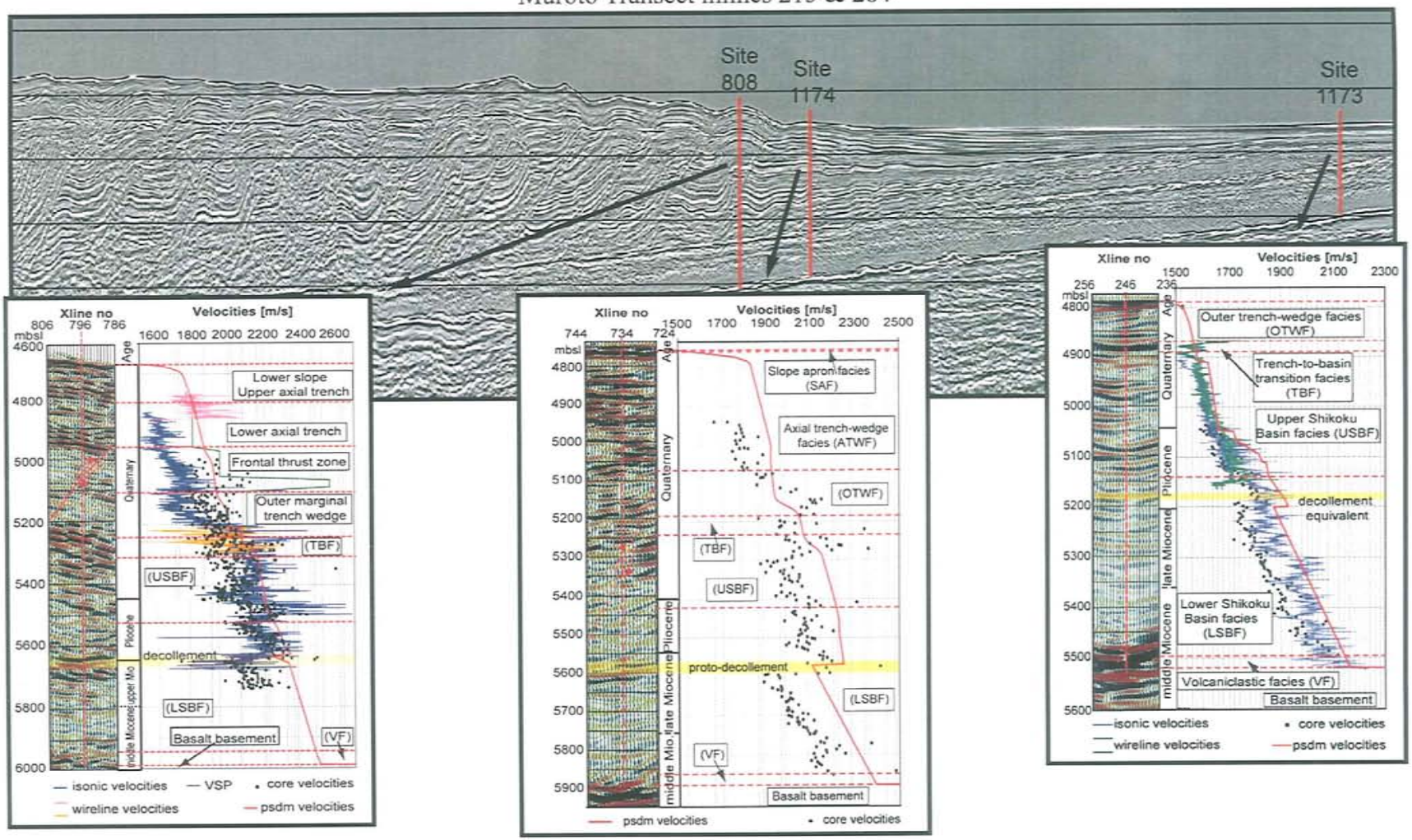

Figure 5.1: ODP Site 1173, 1174, & 808 wireline, core, isonic, and PSDM velocity [from *Pisani et al.*, 2005].

Deviation of *in situ* velocity measurements from the PSDM velocity field within the prism can be attributed to rock properties, such as anisotropy [*Pisani, et al.*, 2005].

The underthrust sediment interval below the décollement did not contain sufficient reflectivity and 'pickable' horizons to subdivide into velocity intervals and perform internal detailed velocity analysis via PSDM methods. Therefore, the 300 m thick underthrust section (thinning landward) was treated as one interval allowing vertical and lateral velocity gradients. Along strike variability within the underthrust sediments is thought to be somewhat related to the 2-D nature of processing 3-D images, in addition to possible basement topography. Error estimation of the velocity values are difficult to quantify given the empirical nature of PSDM processing. Depth gather flatness, although important, was generally under-migrated using geologically reasonable velocities.

Velocity sensitivity of the final velocity models from the 2-D PSDM processing are thought to be within ± 5%. Image quality, depth to known horizons at Sites 808 & 1174, and depth gather flatness, which were some of the main criteria used to guide the velocity updating, are all noticeably affected by varying the velocity ± 5% below the seafloor (Figure 5.2). Although the velocity values differ significantly from core measurements above and below the décollement, the local velocity gradient and depth of the horizon are modeled quite well. Differences can be attributed in part to elastic rebound of core samples from *in situ* conditions; *in situ* velocity will be approximately 43 $^{m}/_{s}$ higher than core data at atmospheric pressure

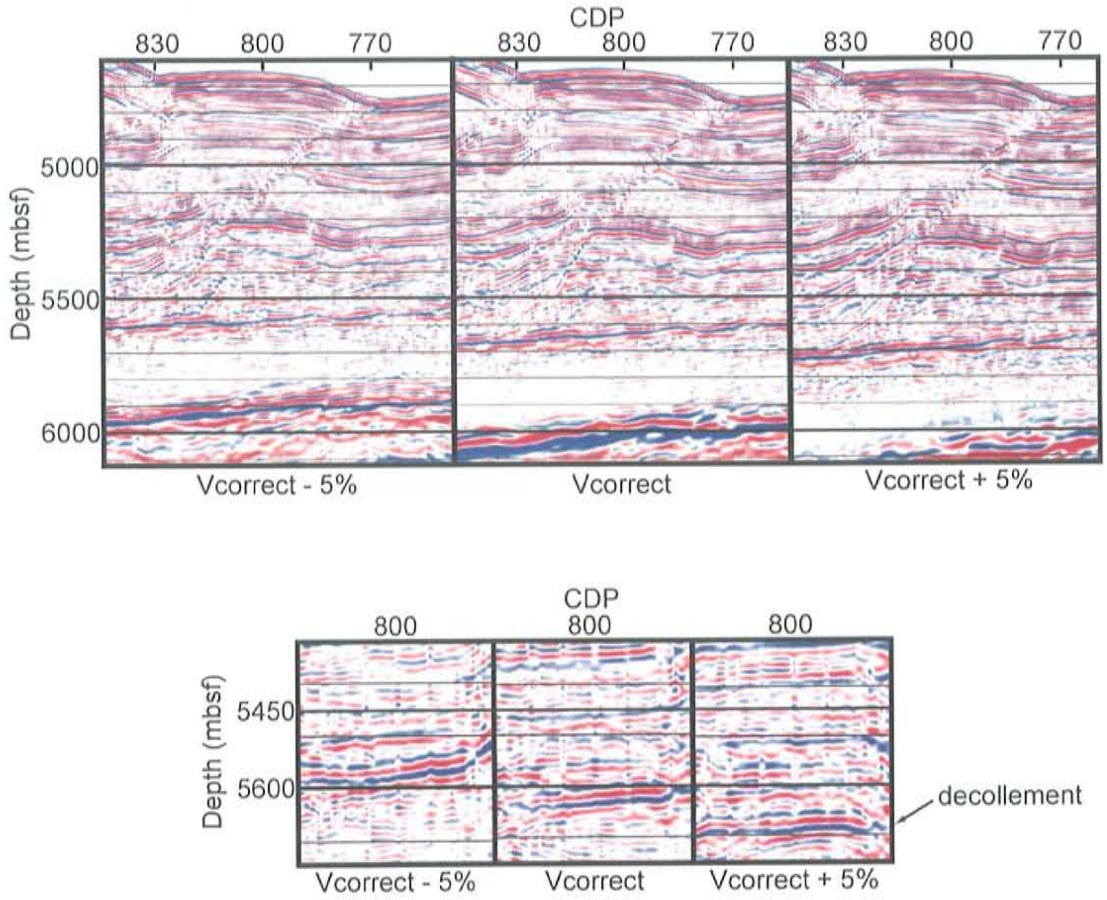

Figure 5.2: Area of depth section for inline 290 near Site 808 illustrating the image quality, underthrusting sediment thickness, and depth to decollement reflection for the correct velocity and +/- 5% (top). In addition, the depth gathers of CDP 800 (Site 808 corresponds to CDP 796 along inline 284, ~250 meters away) for inline 290 illustrating depth gather flatness and migrated depth for the correct velocity and +/- 5% (bottom).

[*Hoffman and Tobin*, 2005]. Hence, the PSDM velocity field is representative of *in situ* velocity and can be considered an accurate seismic attribute for further studies [e.g. *Pisani, et al.*, 2005].

The underthrust sediment *in situ* velocity corresponds to strongly elevated porosity conditions sustained by inhibited dewatering [*Screaton, et al.*, 2002; *Screaton, et al.*, 2000]. Comparison of core measurement velocity and seismic velocity from PSDM iterations show some deviation above and below the décollement at Site 808 and 1174 (Figure 5.3). At Site 808, a velocity decrease across the décollement was preserved; however, the velocity values and gradient is higher than the values measured *in situ* within the underthrust package. One possible explanation for differing velocity gradient can be attributed to the requirement of tying the top of basement horizon depth in the velocity updating. By contrast, at Site 1174 the seismic velocity gradient below the décollement matches the *in situ* velocity gradient quite well. The final depth sections with corresponding velocity models (see Figure 4.1 & Appendix A) and velocity extraction planes (Figures 4.2, 4.3) show that most of the underthrust sediments contain a lower velocity than the overlying prism, indicating the vertical velocity gradient at Site 1174 is a more representative trend of the underthrusting sediments and the gradient at Site 808 is unusual in our velocity field.

Considering that the empirical velocity-porosity transform is rather insensitive to error in velocity compared to the PSDM sensitivity to velocity changes [*Hoffman and Tobin*, 2005], error for inferred porosity differing from *in situ* measurements is a

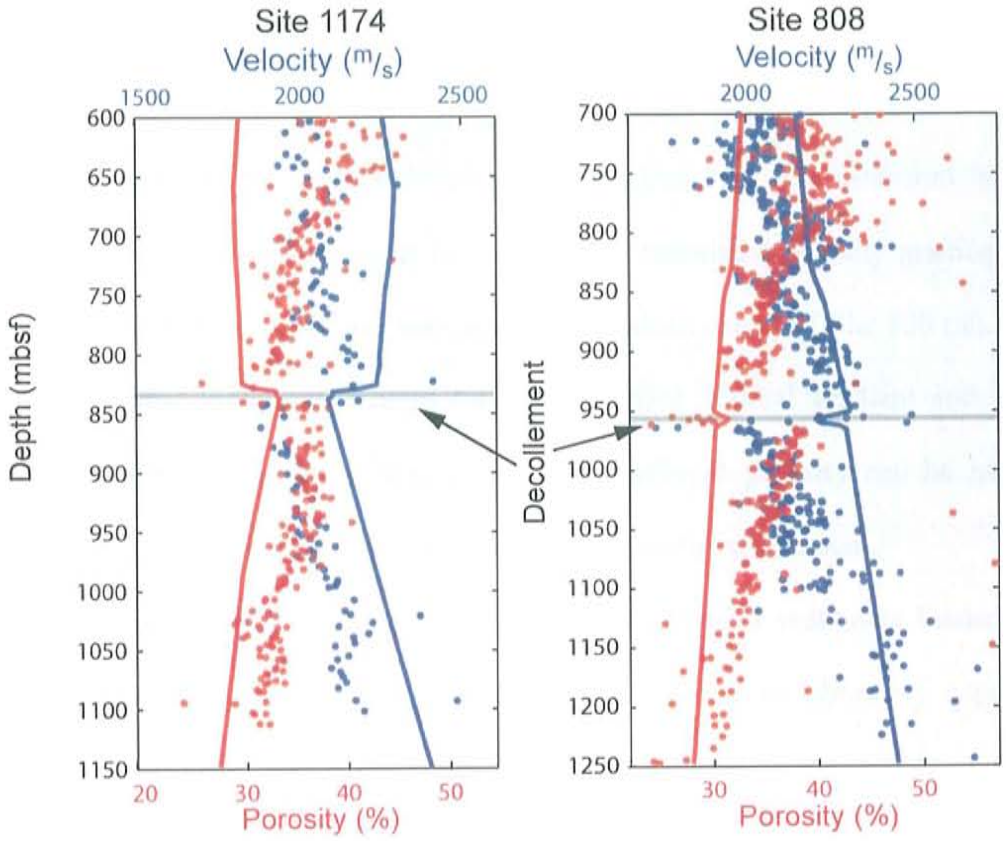

Figure 5.3: ODP Sites 1174 & 808 physical property data plotted near the decollement zone. The vertical gradient for both velocity and porosity is offset at the decollement boundary [*Shipboard Scientific Party*, 2002]. - & - are PSDM velocity and inferred porosity respectively.

function of velocity modeling as well as the empirical transform. Comparison of core measurement porosity and inferred porosity from PSDM velocity shows similar trends, but also shows some deviation in absolute porosity values above and below the décollement at Site 808 and 1174 (see Figure 5.3). At Site 1174, the inferred porosity and *in situ* porosity gradients correlate but the values differ by approximately 3 - 8 porosity units. At Site 808, inferred porosity is less than that measured *in situ* by almost 10 porosity units in areas; in addition, the calculated porosity gradient differs significantly (but see previous paragraph on anomalous nature of Site 808 tie). Thus, the underthrust sediments contain the representative vertical gradient and absolute velocity difference trends at Site 1174, PSDM-inferred porosity can be used as a conservative estimate of porosity values for the underthrust sediment.

I computed the expected porosity for fully drained sediments loaded by the overlying wedge, using a compaction function derived from laboratory experiments [*D. Saffer,* personal communication, 2005]. This represents the porosity we would expect if pore pressure was hydrostatic in the underthrust section everywhere. A porosity greater than this value at a given location implies inhibited drainage and elevated pore pressure (undercompacted). PSDM–derived porosity is above this drained value in most of the underthrust section, indicating that porosity is retained and strongly elevated, relative to normal compaction conditions for the Shikoku Basin sediments (Figure 5.4). Porosity of the underthrust sediment starts (CDP 400 – seaward of the trench) at or close to normal compaction conditions but, after

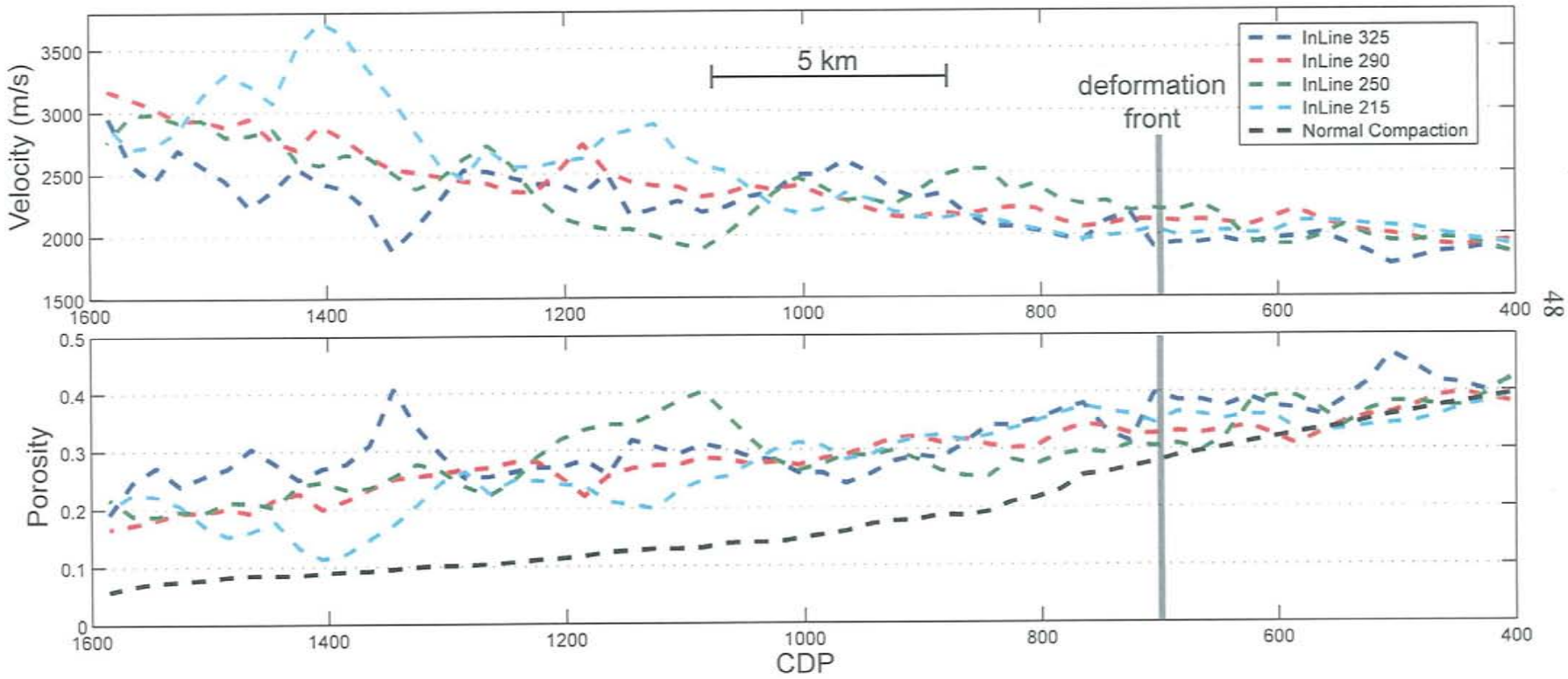

Figure 5.4: Velocity and porosity plotted vs. CDP for 4 processed inlines. The normal compaction curve computed for Shikoku Basin sediments lies below the porosities of the 4 inlines, implying inhibited dewatering of the underthrusting sediments.

becoming loaded by trench turbidites, structural thickening, and the onset of deformation [e.g. *Screaton, et al.*, 2000], predicted porosity becomes elevated (~CDP 700). Moving landward, calculated porosity values diverge at ~CDP 1100 because of poorer control in the PSDM velocity iterations; nevertheless the underthrust sediment maintains its elevated porosity framework to the landward boundary of the seismic survey area (30 km). This suggests that the permeability of the underthrust package and décollement are not sufficient to allow pore fluids to readily escape, resulting in development of excess pore pressure.

Excess pore pressure in the underthrust sediments, which are in hydrologic communication with the décollement [*Screaton, et al.*, 2002], has implications as it could be a main control [*Moore, et al.*, 1990] for décollement strength and the updip limit of seismicity. The updip seismogenic limit is thought to depend on a suite of factors including (1) declining fluid production, (2) cementation, (3) and/or the thermal gradient controlling low-grade metamorphism [*Moore and Saffer*, 2001; *Spinelli and Saffer*, 2004] all of which act in combination to increase effective stress across the décollement boundary. Fluid production in particular is due to the loss of intrinsically retained porosity as directly imaged here; *Saffer and Bekins* [1998] show that this retained pore fluid increasingly builds overpressure back to 30 km landward of the deformation front when an underthrust sediment slow consolidation condition is applied (Figure 5.5). This study corroborates their model result that this fluid contained within underthrusting sediment is strongly retained during initial

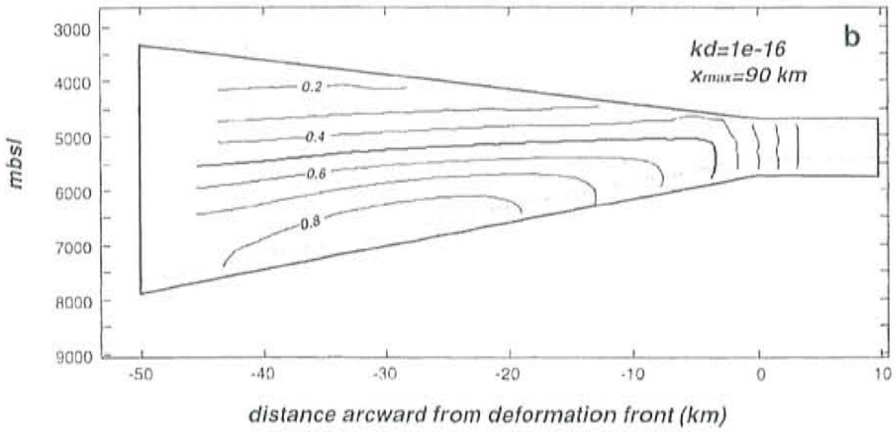

Figure 5.5: Contour plot of modeled steady state normalized pore pressure (λ^*) within the Nankai Trough with 20% smectite for slow underthrust sediment consolidation. Delayed consolidation leads to evenly distributed pore pressure increasing up and maximizing ~ 30 km landward of the deformation front [from *Saffer and Bekins*, 1998].

underthrusting; in essence, maintaining elevated porosity conditions beneath the décollement. With robust porosity estimates of underthrusting sediment at the Nankai Trough, quantifying effective stress through permeability and pore pressure estimates can now be achieved for this transect.

CHAPTER 6

CONCLUSION

High-quality seismic reflection data collected in the forearc of the Nankai subduction zone off Cape Muroto, Japan was processed with 2-D Kirchoff pre-stack depth migration, generating robust interval velocity estimates for the underthrust sediment. Porosity inferred via an empirical transform from velocity indicates that compaction is strongly inhibited relative to the predicted hydrostatic condition for the outer accretionary wedge, even though the velocity is probably somewhat higher, and computed porosity lower, than true *in situ* values. Hence, this is a conservative (lower bound) estimate of excess porosity. This suggests that the permeability of the underthrust package and décollement are not sufficient to allow pore fluids to readily escape during rapid loading by the advancing wedge, resulting in excess pore pressure persisting 20 to 30 km landward of the deformation front and onset of underthrusting. Excess pore pressure in the underthrust sediments, which are in hydrologic communication with the décollement [*Screaton et. al.,* 2002], has implications for wedge and megathrust mechanics, as it could be a main control [*Moore, et al.*, 1990] for décollement strength and the updip limit of seismicity.

REFERENCES

Adatia, R. H., and A. J. Maltman (2005), Initial permeability determinations on sediments from the Nankai Trough accretionary prism, ODP Sites 1173 and 1174, *Proceedings of the Ocean Drilling Program; scientific results; deformation and fluid flow processes in the Nankai Trough accretionary prism; coring, logging while drilling and advanced CORKs covering Legs 190 to 196 of the cruises of the drilling vessel JOIDES Resolution; Sydney, Australia, to Yokohama, Japan, Sites 1173-1178, 23 May-16 July 2000; and Keelung, Taiwan, to Kochi, Japan, Sites 808-1173, 2 May-1 July 2001*, *190/196*, 12.

Ando, M. (1975), Source Mechanisms and Tectonic Significance of Historical Earthquakes Along Nankai Trough, Japan, *Tectonophysics*, *27*, 119-140.

Bangs, N. L., et al. (2004), Evolution of the Nankai Trough decollement from the trench into the seismogenic zone; inferences from three-dimensional seismic reflection imaging, *Geology (Boulder)*, *32*, 273-276.

Bangs, N. L., et al. (1996), Elevated fluid pressure and fault zone dilation inferred from seismic models of the northern Barbados Ridge decollement, *Journal of Geophysical Research-Solid Earth*, *101*, 627-642.

Bangs, N. L., et al. (2000), Character of the central Nankai Trough subduction thrust; preliminary results from 3-D seismic reflection imaging, *Conference: American Geophysical Union 2000 fall meeting, San Francisco, CA, United States, Dec. 15-19, 2000*, *81*, 1097-1098.

Bangs, N. L. B., and S. P. S. Gulick (2005), Physical properties along the developing decollement in the Nankai Trough; inferences from 3-D seismic reflection data inversion and Leg 190 and 196 drilling data, *Proceedings of the Ocean Drilling Program; scientific results; deformation and fluid flow processes in the Nankai Trough accretionary prism; coring, logging while drilling and advanced CORKs covering Legs 190 to 196 of the cruises of the drilling vessel JOIDES Resolution; Sydney, Australia, to Yokohama, Japan, Sites 1173-1178, 23 May-16 July 2000; and Keelung, Taiwan, to Kochi, Japan, Sites 808-1173, 2 May-1 July 2001*, *190/196*, 18.

Bangs, N. L. B., et al. (1999), Fluid accumulation and channeling along the northern Barbados Ridge decollement thrust, *Journal of Geophysical Research-Solid Earth, 104*, 20399-20414.

Bangs, N. L. B., et al. (1990), Seismic velocites from the Barbados Ridge complex - Indicators of high pore fluid pressures in an accretionary complex, *Journal of Geophysical Research-Solid Earth and Planets, 95*, 8767-8782.

Bekins, B. A., et al. (1995), Episodic and constant flow models for the origin of low-chloride waters in a modern accretionary complex, *Water Resources Research, 31*, 3205-3215.

Bilek, S. L., and T. Lay (1998), Variation of interplate fault zone properties with depth in the Japan subduction zone, *Science, 281*, 1175-1178.

Bourlange, S., et al. (2003), Fracture porosity in the decollement zone of Nankai accretionary wedge using logging while drilling resistivity data, *Earth and Planetary Science Letters, 209*, 103-112.

Bray, C. J., and D. E. Karig (1985), Porosity of sediments in accretionary prisms and some implications for dewatering processes, *Journal of Geophysical Research-Solid Earth and Planets, 90*, 768-778.

Brown, K. M., et al. (2001), Smectite diagenesis, pore-water freshening, and fluid flow at the toe of the Nankai wedge, *Earth and Planetary Science Letters, 194*, 97-109.

Byrne, T., and D. Fisher (1990), Evidence for a weak and overpressured decollement beneath sediment-dominated accretionary prisms, *Journal of Geophysical Research-Solid Earth and Planets, 95*, 9081-9097.

Carson, B., and E. J. Screaton (1998), Fluid flow in accretionary prisms: Evidence for focused, time-variable discharge, *Reviews of Geophysics, 36*, 329-351.

Chambers, R. L., et al. (2000), Petroleum geostatistics for nongeostatisticians; part 1, *The Leading Edge (Tulsa, OK), 19*, 474-479.

Chang, H., et al. (1998), 3-D prestack Kirchhoff depth migration; from prototype to production in massively parallel processor environment, *Geophysics, 63*, 546-556.

Chlieh, M., et al. (2004), Crustal deformation fault slip during the seismic cycle in the North Chile subduction zone, from GPS and InSAR observations, *Geophysical Journal International*, *158*, 695-711.

Cochrane, G. R., et al. (1994), Velocity and inferred porosity model of the Oregon accretionary prism from multichannel seismic-reflection data - Implications on sediment dewarering and overpressure, *Journal of Geophysical Research-Solid Earth*, *99*, 7033-7043.

Conrad, C. P., et al. (2003), Great earthquakes and slab pull; interaction between seismic coupling and plate-slab coupling, *Earth and Planetary Science Letters*, *218*, 109-122.

Davis, D., et al. (1983), Mechanics of fold-and-thrust belts and accretionary wedges, *Journal of Geophysical Research*, *88*, 1153-1172.

Davis, E. E., et al. (2006), A discrete episode of seismic and aseismic deformation of the Nankai trough subduction zone accretionary prism and incoming Philippine Sea plate, *Earth and Planetary Science Letters*, *242*, 73-84.

Demets, C., et al. (1990), Current Plate Motions, *Geophysical Journal International*, *101*, 425-478.

Dvorkin, J., and A. Nur (1996), Elasticity of high-porosity sandstones: Theory for two North Sea data sets, *Geophysics*, *61*, 1363-1370.

Erickson, S. N., and R. D. Jarrard (1998), Velocity-porosity relationships for water-saturated siliciclastic sediments, *Journal of Geophysical Research-Solid Earth*, *103*, 30385-30406.

Farmer, P., et al. (1996), Exploring the subsalt, *Oilfield Review*, *8*.

Fowler, S. R., et al. (1985), Sediment dewatering in the Makran accretionary prism, *Earth and Planetary Science Letters*, *75*, 427-438.

Gamage, K., and E. J. Screaton (2005), Permeabilities of Nankai accretionary prism sediments, *Proceedings of the Ocean Drilling Program; scientific results; deformation and fluid flow processes in the Nankai Trough accretionary prism; coring, logging while drilling and advanced CORKs covering Legs 190 to 196 of the cruises of the drilling vessel JOIDES Resolution; Sydney, Australia, to Yokohama, Japan, Sites*

1173-1178, 23 May-16 July 2000; and Keelung, Taiwan, to Kochi, Japan, Sites 808-1173, 2 May-1 July 2001, 190/196, 22.

Gettemy, G. L., and H. J. Tobin (2003), Tectonic signatures in centimeter-scale velocity-porosity relationships of Costa Rica convergent margin sediments, *Journal of Geophysical Research-Solid Earth*, *108*, 2494.

Gettemy, G. L., et al. (2004), Multi-scale compressional wave velocity structure of the San Gregorio Fault zone, *Geophysical Research Letters*, *31*, L06601.

Gulick, S. P. S., et al. (2004), Three-dimensional architecture of the Nankai accretionary prism's imbricate thrust zone off Cape Muroto, Japan; prism reconstruction via en echelon thrust propagation, *Journal of Geophysical Research*, *109*.

Hamilton, E. L. (1976), Shear-Wave Velocity Versus Depth in Marine Sediments - Review, *Geophysics*, *41*, 985-996.

Hamilton, E. L. (1978), Sound velocity-density relations in sea-floor sediments and rocks, *Journal of the Acoustical Society of America*, *63*, 366-377.

Han, D., et al. (1986), Effects of porosity and clay content on wave velocities in sandstones, *Geophysics*, *51*, 2093-2107.

Han, D., et al. (1987), Effects of porosity and clay content on wave velocities in sandstones - reply, *Geophysics*, *52*, 1439-1441.

Hoffman, N. W., and H. J. Tobin (2005), An empirical relationship between velocity and porosity for underthrust sediments in the Nankai Trough accretionary prism, *Proceedings of the Ocean Drilling Program; scientific results; deformation and fluid flow processes in the Nankai Trough accretionary prism; coring, logging while drilling and advanced CORKs covering Legs 190 to 196 of the cruises of the drilling vessel JOIDES Resolution; Sydney, Australia, to Yokohama, Japan, Sites 1173-1178, 23 May-16 July 2000; and Keelung, Taiwan, to Kochi, Japan, Sites 808-1173, 2 May-1 July 2001, 190/196*, 23.

Hori, T., et al. (2004), A numerical simulation of earthquake cycles along the Nankai Trough in southwest Japan: lateral variation in fictional property due to the slab geometry controls the nucleation position, *Earth and Planetary Science Letters*, *228*, 215-226.

Housen, B. A., et al. (1996), Strain decoupling across the decollement of the Barbados accretionary prism, *Geology*, *24*, 127-130.

Hyndman, R. D., et al. (1993), Velocity, porosity, and pore-fluid loss from the Nankai subduction zone accretionary prism, *Affiliation (analytic): Ecol*, *131*, 211-220.

Jarrard, R. D. (1997), Origins of porosity and velocity variations at Cascadia accretionary prism, *Geophysical Research Letters*, *24*, 325-328.

Jarrard, R. D. (2003), Subduction fluxes of water, carbon dioxide, chlorine, and potassium, *Geochemistry Geophysics Geosystems*, *4*, 8905.

Jarrard, R. D., et al. (1989), Velocity and density of sediments of Eirik Ridge, Labrador Sea; control by porosity and mineralogy, *Affiliatio*, *105*, 811-835.

Lallemant, S. J., et al. (1993), Stress tensors at the toe of the Nankai accretionary prism; an application of inverse methods to slickenlined faults, *Proceedings of the Ocean Drilling Program; scientific results; Nankai Trough; covering Leg 131 of the cruises of the drilling vessel JOIDES Resolution, Apra Harbor, Guam, to Pusan, South Korea, Site 808, 26 March- June 1990 131*, 103-122.

Le Pichon, X., et al. (1993), Accretion and erosion in subduction zones - The role of fluids, *Annual Review of Earth and Planetary Sciences*, *21*, 307-331.

Lohrmann, J., et al. (2003), The impact of analogue material properties on the geometry, kinematics, and dynamics of convergent sand wedges, *Journal of Structural Geology*, *25*, 1691-1711.

Mackay, M. E., et al. (1995), The case against porosity change: seismic velocity decrease at the toe of the Oregon accretionary prism, *Geology*, *23*, 827-830.

Maltman, A. J., et al. (1993), Deformation at the toe of an active accretionary prism; synopsis of results from ODP Leg 131, Nankai, SW Japan, *Journal of Structural Geology*, *15*, 949-964.

Mavko, G., et al. (2003), The Rock Physics Handbook: Tools for Seismic Ananlysis in Pourous Media.

McIntosh, K. D., and M. K. Sen (2000), Geophysical evidence for dewatering and deformation processes in the ODP Leg 170 area offshore Costa Rica, *Earth and Planetary Science Letters*, *178*, 125-138.

McNeill, L. C., et al. (2004), Deformation and in situ stress in the Nankai Accretionary Prism from resistivity-at-bit images, ODP Leg 196, *Geophysical Research Letters*, *31*, L02602.

Mikada, H., et al. (2001), Proceedings of the Ocean Drilling Program, initial reports, deformation and fluid flow processes in the Nankai Trough accretionary prism, logging while drilling and advanced CORKs; covering Leg 196 of the cruises of the drilling vessel JOIDES Resolution, Keelung, Chinese Taipei, to Kochi, Japan, sites 808 and 1173, 2 May-1 July 2001, *Source Note: CD-ROM format, ISSN 1096-2522; WWW format, ISSN 1096-2158*, *196*, (variously paginated).

Miyazaki, S., and K. Heki (2001), Crustal velocity field of southwest Japan: Subduction and arc-arc collision, *Journal of Geophysical Research-Solid Earth*, *106*, 4305-4326.

Moore, G. F., et al. (2005a), Legs 190 and 196 synthesis; deformation and fluid flow processes in the Nankai Trough accretionary prism, *Proceedings of the Ocean Drilling Program; scientific results; deformation and fluid flow processes in the Nankai Trough accretionary prism; coring, logging while drilling and advanced CORKs covering Legs 190 to 196 of the cruises of the drilling vessel JOIDES Resolution; Sydney, Australia, to Yokohama, Japan, Sites 1173-1178, 23 May-16 July 2000; and Keelung, Taiwan, to Kochi, Japan, Sites 808-1173, 2 May-1 July 2001*, *190/196*, 26.

Moore, G. F., et al. (1990), Structure of the Nankai Trough Accretionary Zone from Multichannel Seismic Reflection Data, *Journal of Geophysical Research-Solid Earth and Planets*, *95*, 8753-8765.

Moore, G. F., et al. (2001a), Structural setting of the Leg 190 Muroto Transect, *Proceedings of the Ocean Drilling Program, initial reports, deformation and fluid flow processes in the Nankai Trough accretionary prism; covering Leg 190 of the cruises of the drilling vessel JOIDES Resolution, Sydney, Australia, to Yokohama, Japan; sites 1173-1178, 6 May-16 July 2000*, *190*, 14.

Moore, G. F., et al. (2005b), Scientific Results (CD-ROM), *Proceedings of the Ocean Drilling Program, deformation and fluid flow processes in the Nankai Trough accretionary prism; coring, logging while drilling and advanced CORKs covering*

Legs 190 to 196 of the cruises of the drilling vessel JOIDES Resolution; Sydney, Australia, to Yokohama, Japan, Sites 1173-1178, 23 May-16 July 2000; and Keelung, Taiwan, to Kochi, Japan, Sites 808-1173, 2 May-1 July 2001, *190/196*, (variously paginated).

Moore, G. F., et al. (2001b), New insights into deformation and fluid flow processes in the Nankai Trough accretionary prism: Results of Ocean Drilling Program Leg 190, *Geochemistry Geophysics Geosystems*, *2*, 2001GC000166.

Moore, J. C. (1989), Tectonics and Hydrogeology of Accretionary Prisms - Role of the Decollement Zone, *Journal of Structural Geology*, *11*, 95-106.

Moore, J. C., and D. Saffer (2001), Updip limit of the seismogenic zone beneath the accretionary prism of southwest Japan: An effect of diagenetic to low-grade metamorphic processes and increasing effective stress, *Geology*, *29*, 183-186.

Morgan, J., and D. E. Karig (1995), Decollement processes at the Nankai accretionary margin, Southeast Japan; propagation, deformation and dewatering, *Journal of Geophysical Research*, *100*, 15,221-215,231.

Neuzil, C. E. (1994), How permeable are clays and shales, *Water Resources Research*, *30*, 145-150.

Park, J.-O., et al. (2003), A subducted oceanic ridge influencing the Nankai megathrust earthquake rupture, *Earth and Planetary Science Letters*, *217*, 77-84.

Park, J. O., et al. (2002), A deep strong reflector in the Nankai accretionary wedge from multichannel seismic data: Implications for underplating and interseismic shear stress release - art. no. 2061, *Journal of Geophysical Research-Solid Earth*, *107*, 2061-2061.

Pisani, P. C., et al. (2005), Targeted 3-D prestack depth imaging at Legs 190-196 ODP drill sites (Nankai Trough, Japan), *Geophysical Research Letters*, *32*, L20309.

Reshef, M. (1997), The use of 3-D prestack depth imaging to estimate layer velocities and reflector positions, *Geophysics*, *62*, 206-210.

Reshef, M. (2001), Some aspects of interval velocity analysis using 3-D depth-migrated gathers, *Geophysics*, *66*, 261-266.

Roden, R., et al. (2002), PSDM 2, the sequel, *The Leading Edge (Tulsa, OK)*, *21*, 1204-1246.

Rupke, L. H., et al. (2004), Serpentine and the subduction zone water cycle, *Earth and Planetary Science Letters*, *223*, 17-34.

Saffer, D. M. (2003), Pore pressure development and progressive dewatering in underthrust sediments at the Costa Rican subduction margin: Comparison with northern Barbados and Nankai, *Journal of Geophysical Research-Solid Earth*, *108*, 2261.

Saffer, D. M., and B. A. Bekins (1998), Episodic fluid flow in the Nankai accretionary complex: Timescale, geochemistry, flow rates, and fluid budget, *Journal of Geophysical Research-Solid Earth*, *103*, 30351-30370.

Saffer, D. M., and B. A. Bekins (1999), Fluid budgets at convergent plate margins: Implications for the extent and duration of fault-zone dilation, *Geology*, *27*, 1095-1098.

Saffer, D. M., and B. A. Bekins (2002), Hydrologic controls on the morphology and mechanics of accretionary wedges, *Geology*, *30*, 271-274.

Saffer, D. M., and A. W. McKiernan (2005), Permeability of underthrust sediments at the Costa Rican subduction zone: Scale dependence and implications for dewatering, *Geophysical Research Letters*, *32*, L02302.

Saffer, D. M., et al. (2000), Inferred pore pressures at the Costa Rica subduction zone: implications for dewatering processes, *Earth and Planetary Science Letters*, *177*, 193-207.

Saito, S., and D. Goldberg (2001), Compaction and dewatering processes of the oceanic sediments in the Costa Rica and Barbados subduction zones: estimates from in situ physical property measurements, *Earth and Planetary Science Letters*, *191*, 283-293.

Scholz, C. H. (1998), Earthquakes and friction laws, *Nature*, *391*, 37-42.

Screaton, E., and S. M. Ge (1997), An assessment of along-strike fluid and heat transport within the Barbados Ridge accretionary complex: Results of preliminary modeling, *Geophysical Research Letters*, *24*, 3085-3088.

Screaton, E., and S. M. Ge (2000), Anomalously high porosities in the proto-decollement zone of the Barbados accretionary complex: Do they indicate overpressures?, *Geophysical Research Letters*, *27*, 1993-1996.

Screaton, E., et al. (2002), Porosity loss within the underthrust sediments of the Nankai accretionary complex: Implications for overpressures, *Geology*, *30*, 19-22.

Screaton, E. J., and D. M. Saffer (2005), Fluid expulsion and overpressure development during initial subduction at the Costa Rica convergent margin, *Earth and Planetary Science Letters*, *233*, 361-374.

Screaton, E. J., et al. (2000), Dewatering of underthrust sediments in the Nankai accretionary complex; results from Ocean Drilling Program Leg 190, *Conference: American Geophysical Union 2000 fall meeting, San Francisco, CA, United States, Dec. 15-19, 2000*, *81*, 1065.

Screaton, E. J., et al. (1990), Permeabilities, fluid pressures, and flow-rates in the Barbados Ridge complex, *Journal of Geophysical Research-Solid Earth and Planets*, *95*, 8997-9007.

Sheriff, R. E., and Geldart, L. P. (1995), Exploration Seismology, *Cambridge Univ. Press*.

Shipboard Scientific Party (2001), Leg 190 summary, *In Moore, G.F., Taira, A., Klaus, A., et al., Proc. ODP, Init. Repts., 190: College Station TX (Ocean Drilling Program)*, 1-87.

Shipley, T. H., et al. (1994), Siesmically inferred dilatancy distribution, northern Barbados Ridge decollement - implications for fluid migration and fault strength, *Geology*, *22*, 411-414.

Shipley, T. H., et al. (1990), Underthrust sediments, fluid migration paths, and mud volcanos associated with the accretionary wedge off Costa Rica - Middle America trench, *Journal of Geophysical Research-Solid Earth and Planets*, *95*, 8743-8752.

Spinelli, G. A., and D. M. Saffer (2004), Along-strike variations in underthrust sediment dewatering on the Nicoya margin, Costa Rica related to the updip limit of seismicity, *Geophysical Research Letters*, *31*, L04613.

Stern, R. J. (2002), Subduction zones - art. no. 1012, *Reviews of Geophysics*, *40*, 1012-1012.

Szeliga, W., et al. (2004), Southern Cascadia episodic slow earthquakes, *Geophysical Research Letters*, *31*, L16602.

Takahashi, N., et al. (2002), Seismic structure of western end of the Nankai trough seismogenic zone - art. no. 2212, *Journal of Geophysical Research-Solid Earth*, *107*, 2212-2212.

Takahashi, N., et al. (2003), Heterogeneous structure of western Nankai seismogenic zone deduced by multichannel reflection data and wide-angle seismic data, *Tectonophysics*, *364*, 167-190.

Taylor, B., and A. M. Goodliffe (2004), The West Philippine Basin and the initiation of subduction, revisited, *Geophysical Research Letters*, *31*, L12602.

Tobin, H., et al. (2001), Structure, inferred mechanical properties, and implications for fluid transport in the decollement zone, Costa Rica convergent margin, *Geology*, *29*, 907-910.

Tobin, H. J., et al. (1993), Fluid-flow along a strike-slip-fault at the toe of the oregon accretionary prism - implications for the geometry of frontal accretion, *Geological Society of America Bulletin*, *105*, 569-582.

Tobin, H. J., et al. (1994), Fluid pressure in the frontal thrust of the Oregon accretionary prism - experimental constraints, *Geology*, *22*, 979-982.

Torres, M. E., et al. (2004), Relationship of pore water freshening to accretionary processes in the Cascadia margin: Fluid sources and gas hydrate abundance, *Geophysical Research Letters*, *31*, L22305.

Vannucchi, P., et al. (2004), Long-term subduction-erosion along the Guatemalan margin of the Middle America Trench, *Geology (Boulder)*, *32*, 617-620.

von Huene, R., et al. (1998), Mass and fluid flux during accretion at the Alaskan margin, *Geological Society of America Bulletin*, *110*, 468-482.

von Huene, R., et al. (2004), Generic model of subduction erosion, *Geology (Boulder)*, *32*, 913-916.

Wang, C. Y., et al. (1994), Tectonic dewatereing and mechanics of protorthrust zones - example from the Cascadia Accretionary Margin, *Journal of Geophysical Research-Solid Earth*, *99*, 20043-20050.

Wang, K. L., et al. (1995), Case for very-low coupling stress on the Cascadia subduction fault, *Journal of Geophysical Research-Solid Earth*, *100*, 12907-12918.

Zhao, Z. Y., et al. (1998), Deformation and dewatering of the subducting plate beneath the lower slope of the northern Barbados accretionary prism, *Journal of Geophysical Research-Solid Earth*, *103*, 30431-30449.

Appendix A

The following figures detail the 2D inline PSDM results. The data volume was processed every 5 inlines from 190 to 340. The resultant seismic depth sections and associated velocity model used for the migration are displayed.

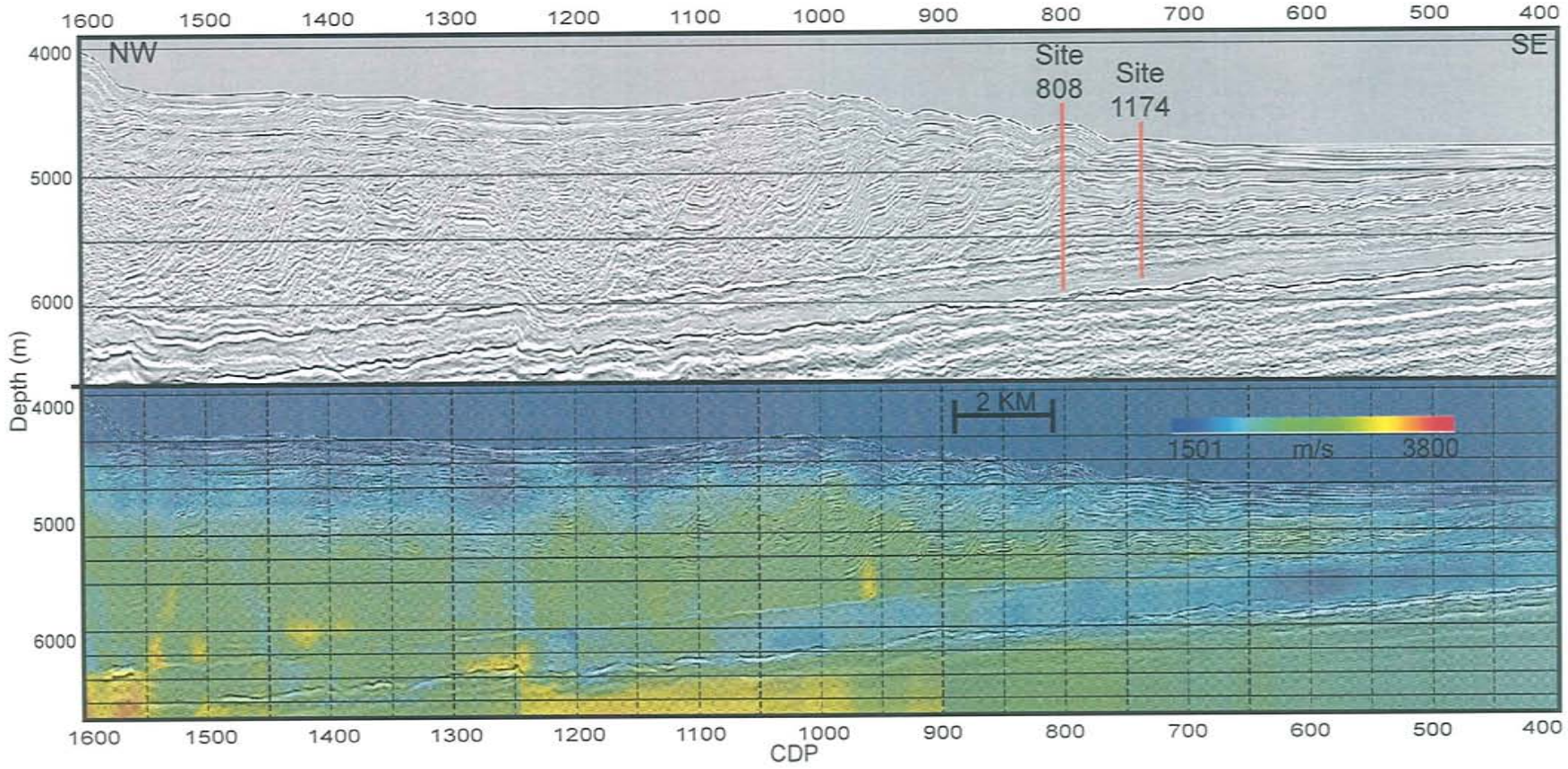

Figure A.1: Inline 190 migrated seismic stack and corresponding velocity model with projected ODP borehole locations

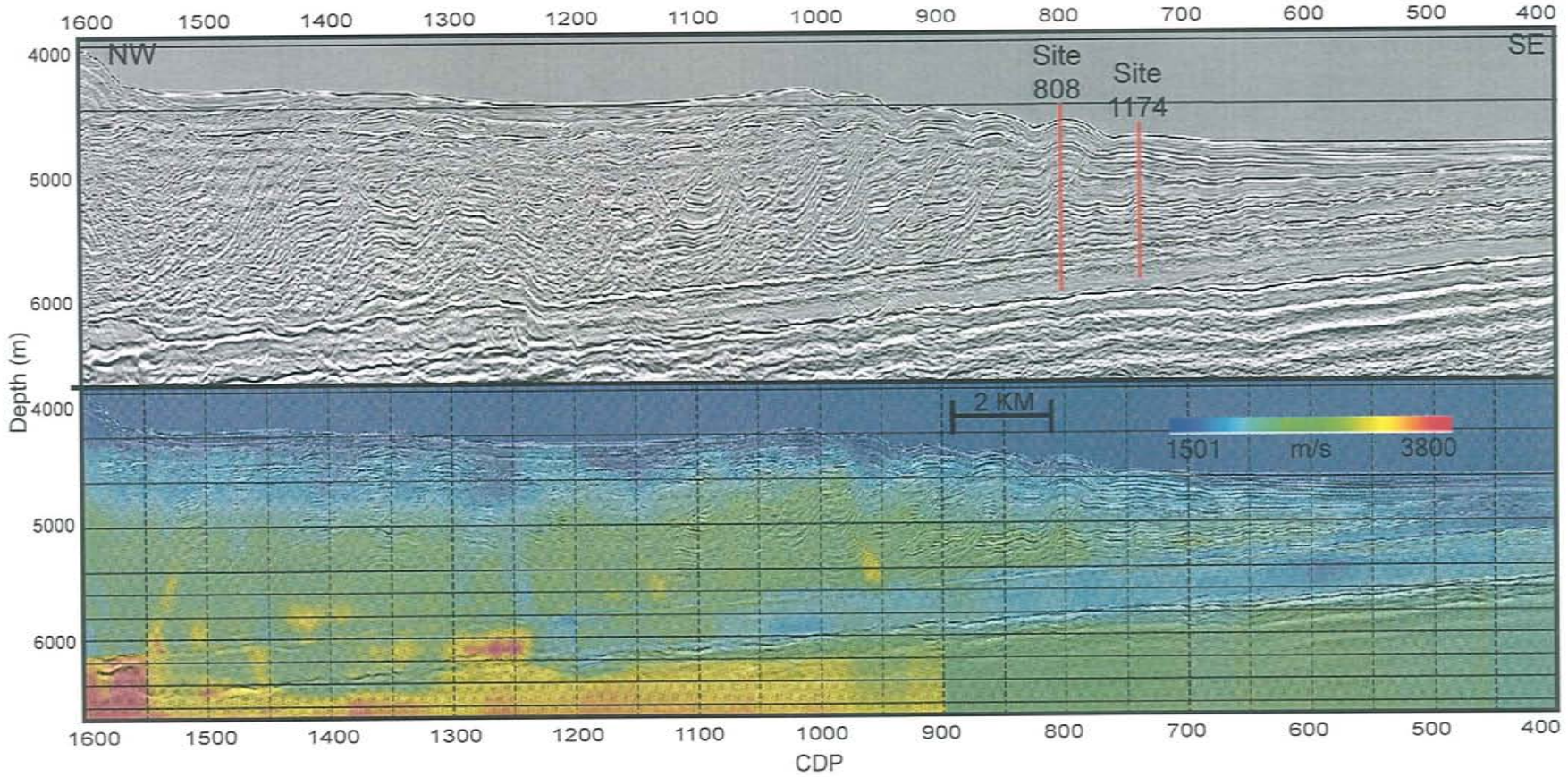

Figure A.2: Inline 195 migrated seismic stack and corresponding velocity model sith projected ODP borehole locations

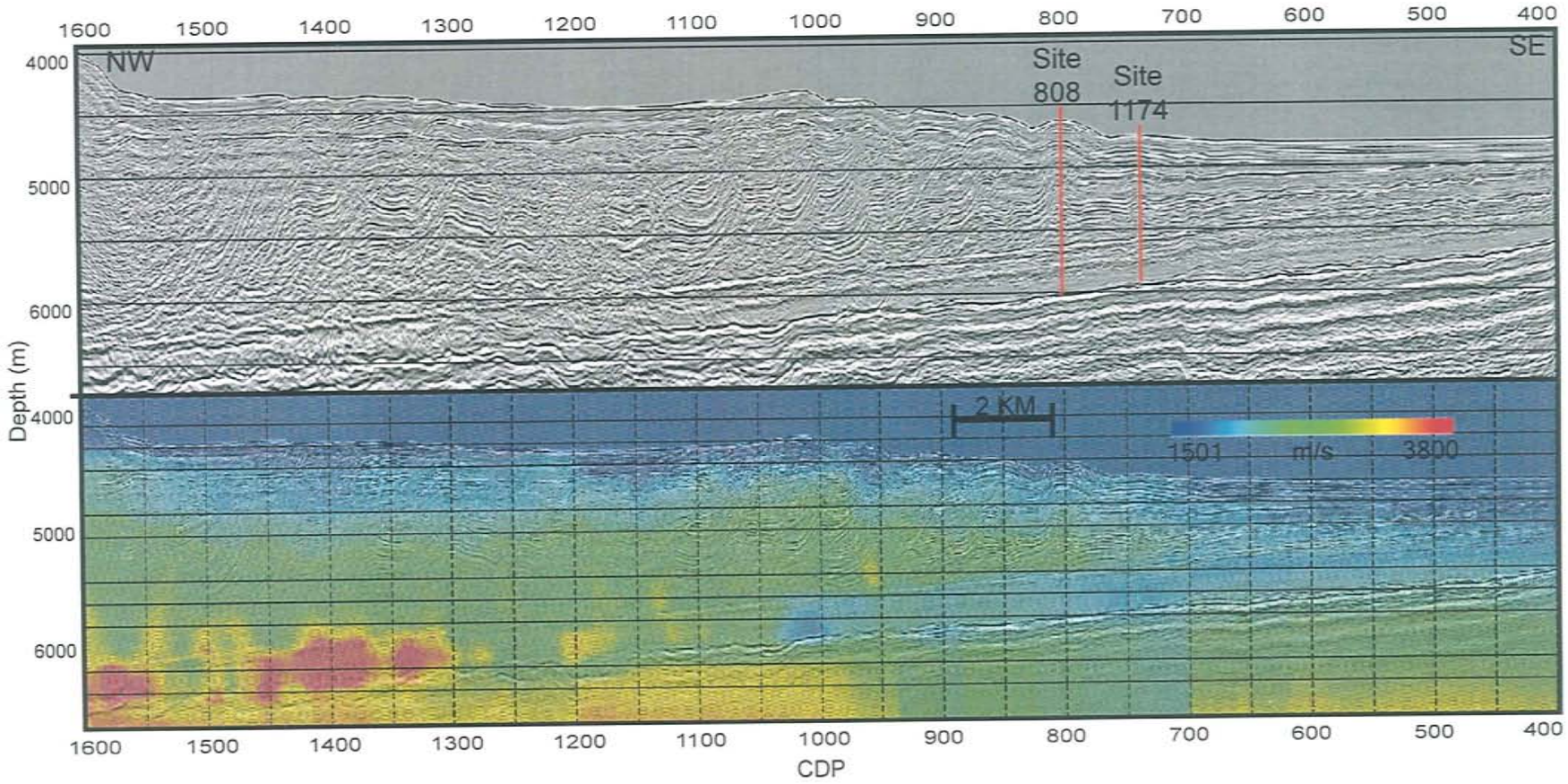

Figure A.3: Inline 200 migrated seismic stack and corresponding velocity model with projected ODP borehole locations

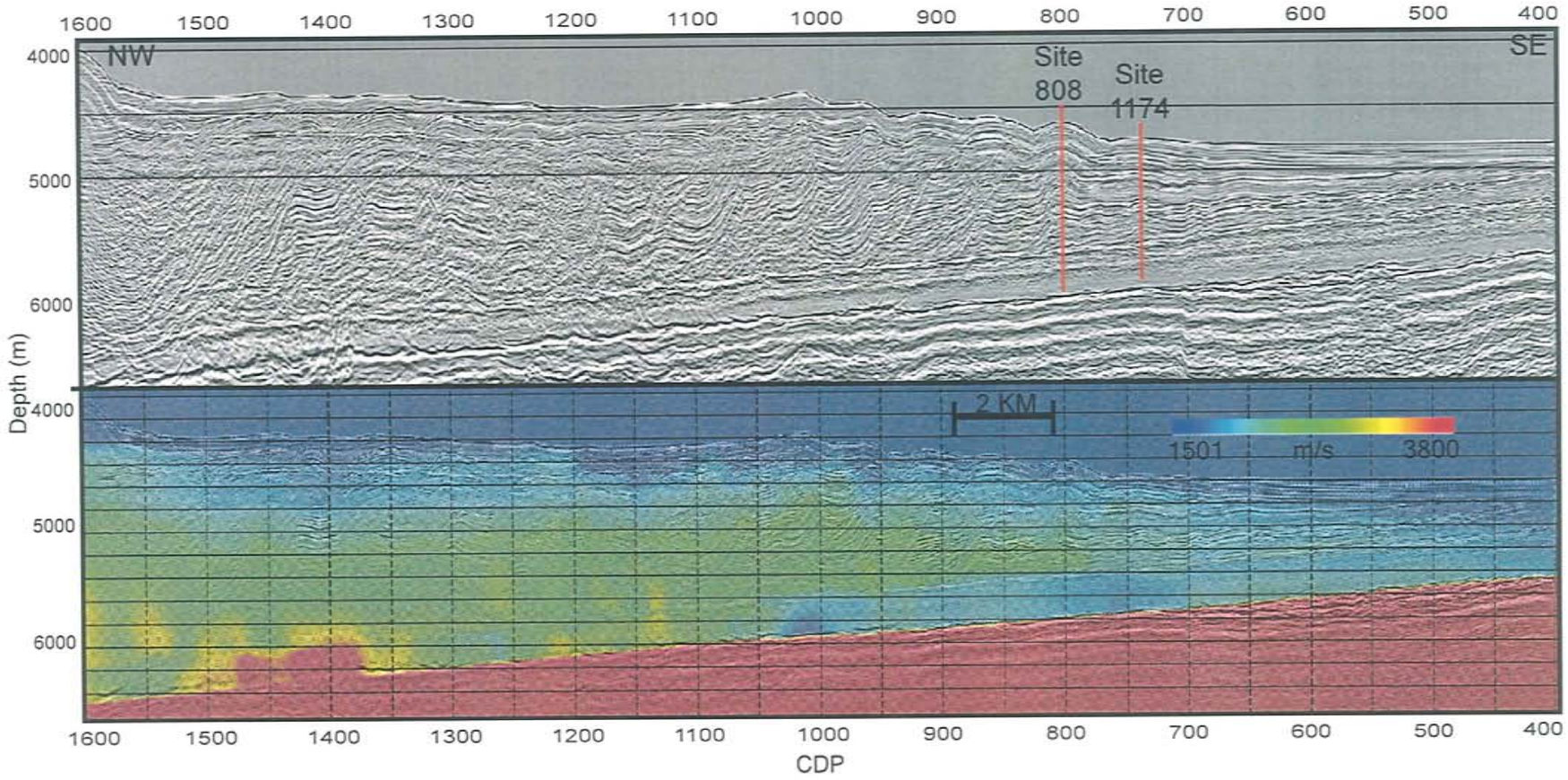

Figure A.4: Inline 205 migrated seismic stack and corresponding velocity model with projected ODP borehole locations

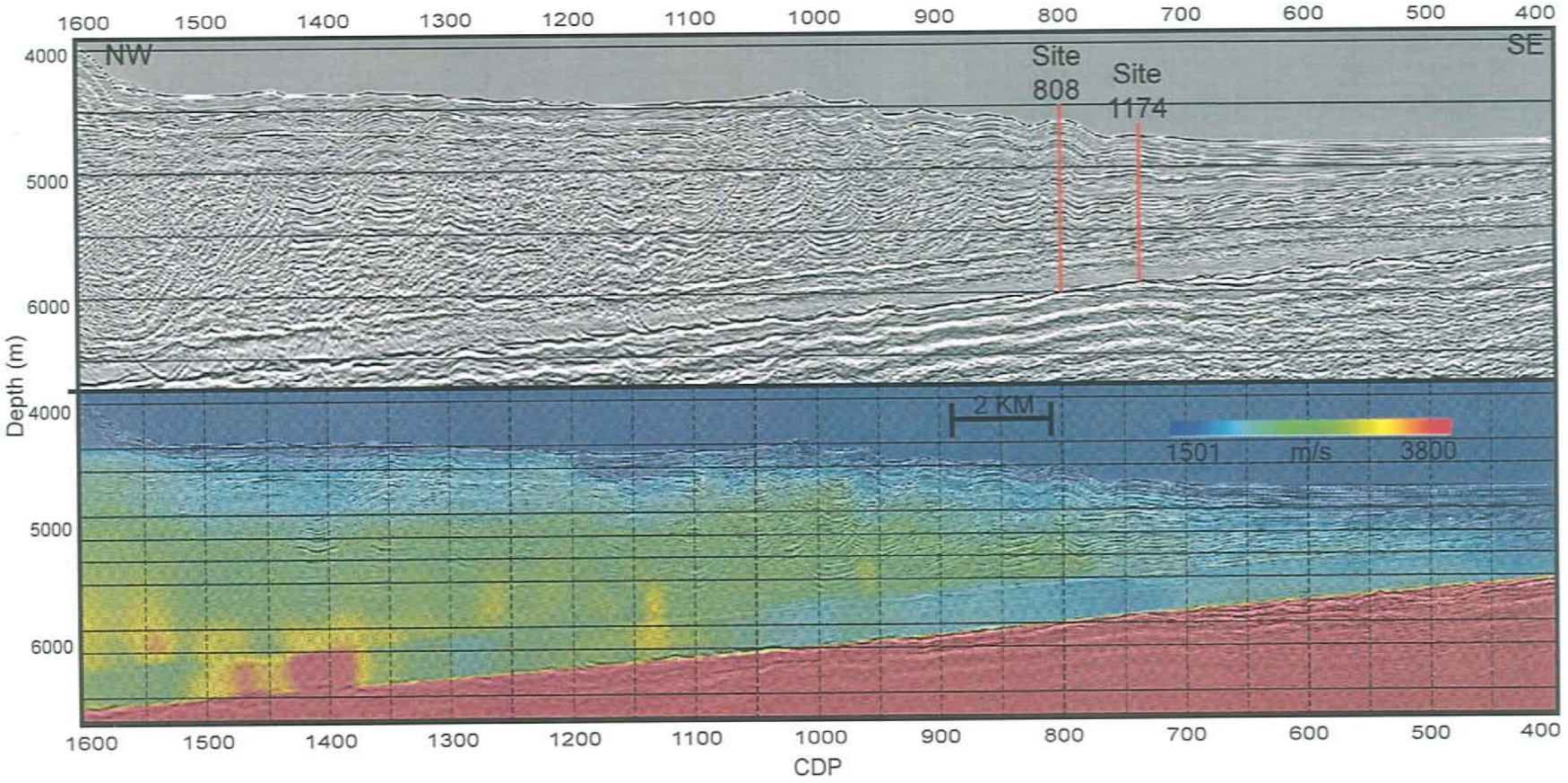

Figure A.5: Inline 210 migrated seismic stack and corresponding velocity model with projected ODP borehole locations

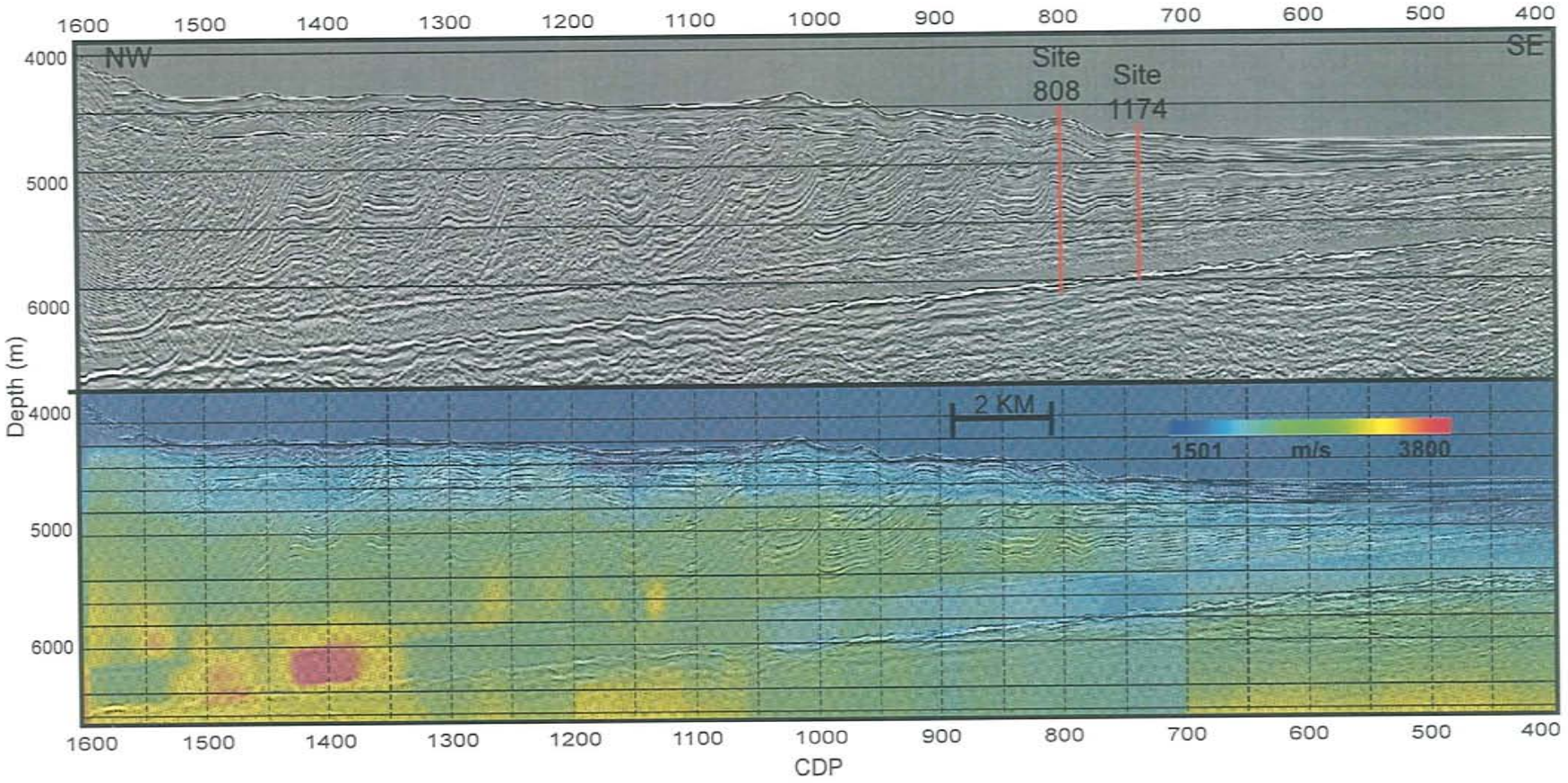

Figure A.6: Inline 215 migrated seismic stack and corresponding velocity model with projected ODP borehole locations

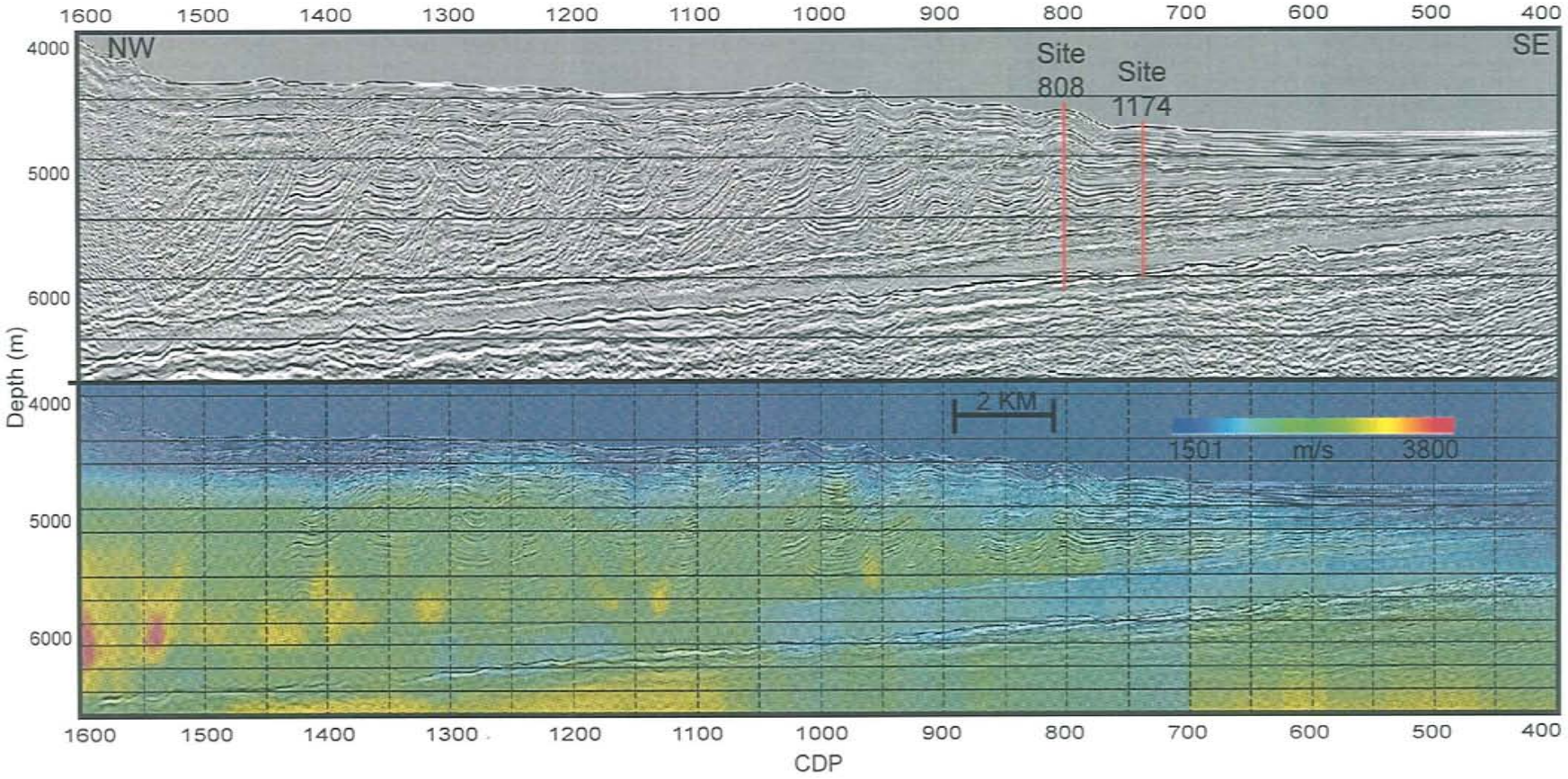

Figure A.7: Inline 220 migrated seismic stack and corresponding velocity model with projected ODP borehole locations

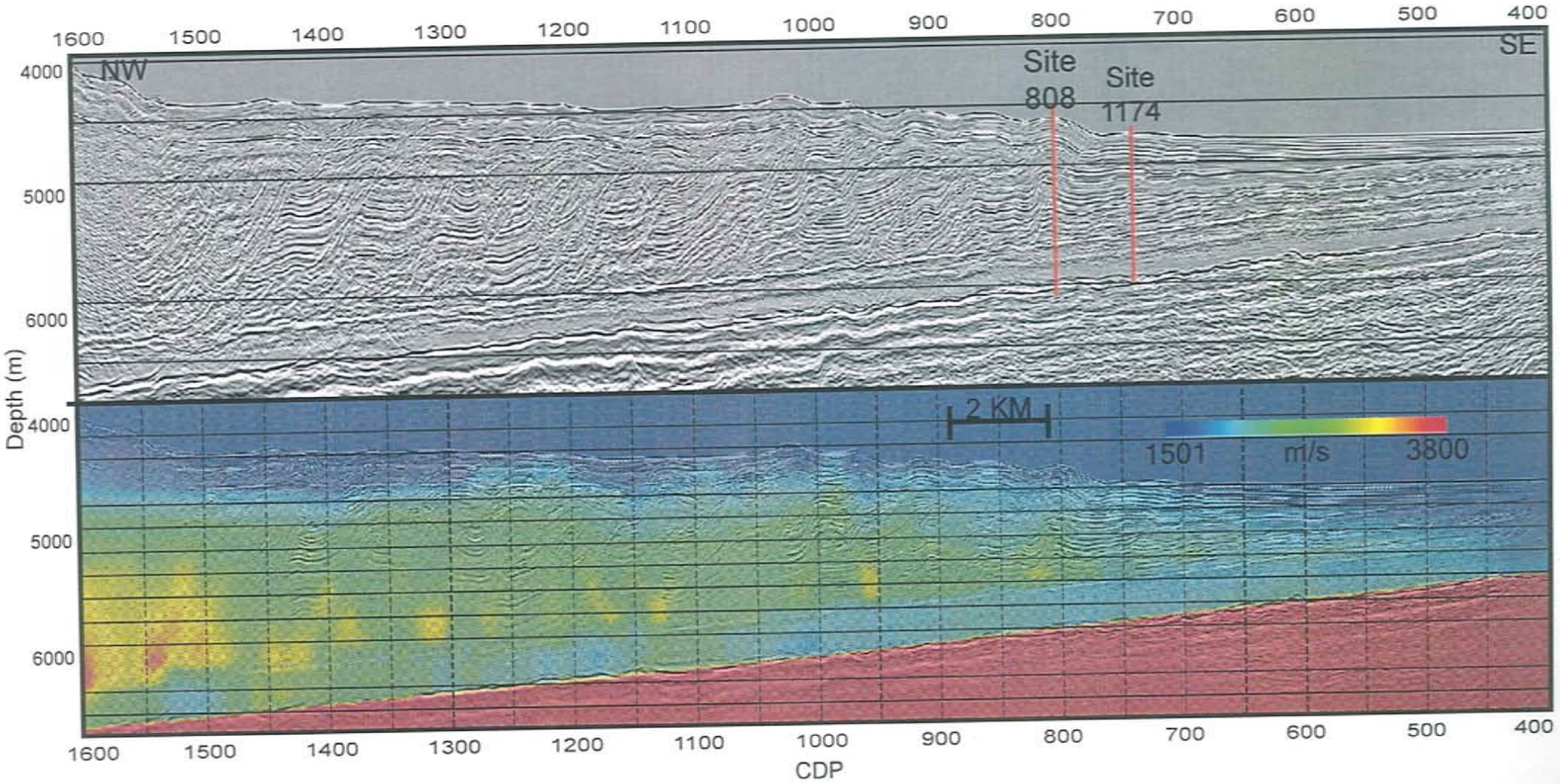

Figure A.8: Inline 225 migrated seismic stack and corresponding velocity model with projected ODP borehole locations

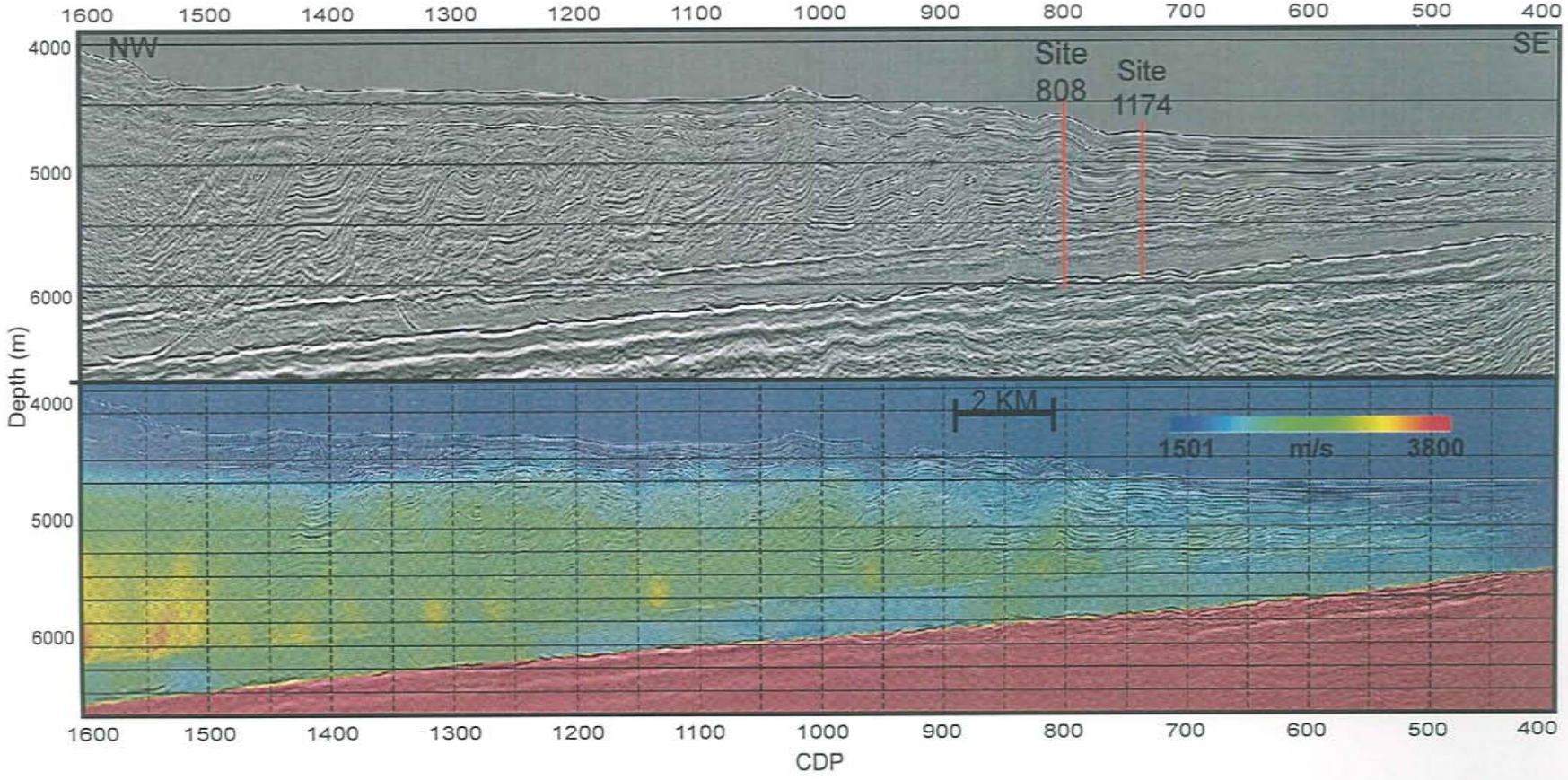

Figure A.9: Inline 230 migrated seismic stack and corresponding velocity model with projected ODP borehole locations

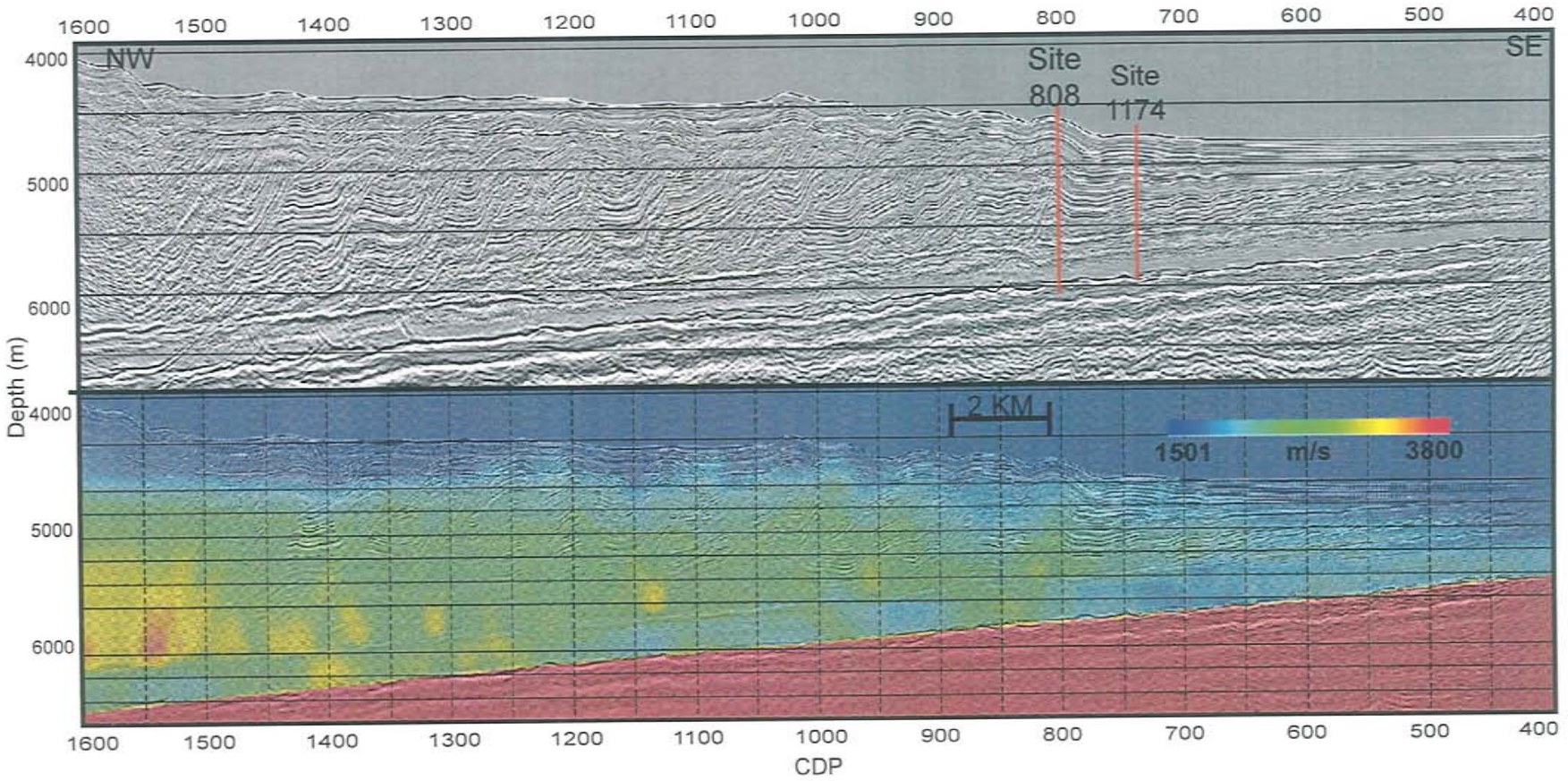

Figure A.10: Inline 235 migrated seismic stack and corresponding velocity model with projected ODP borehole locations

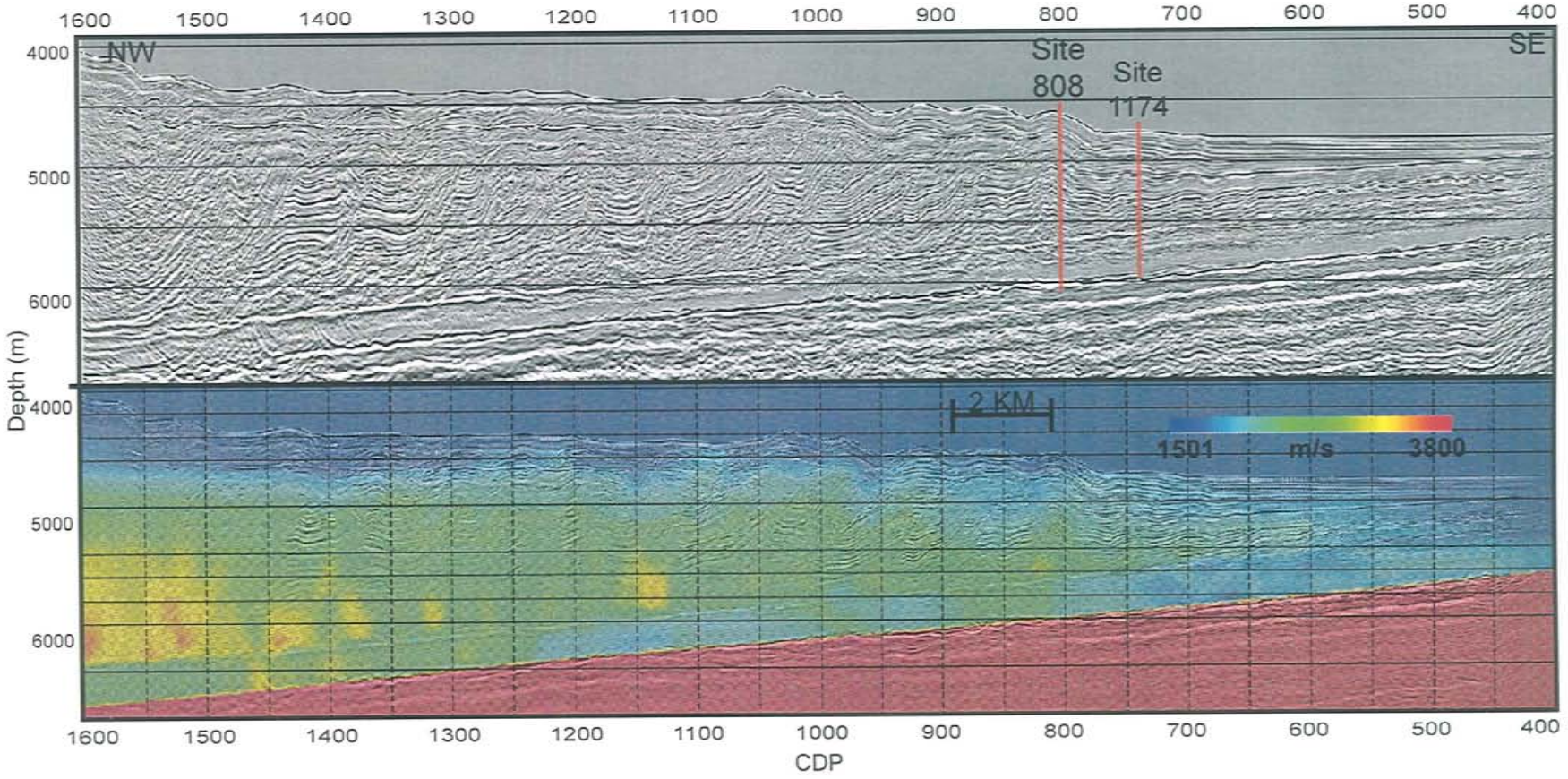

Figure A.11: Inline 240 migrated seismic stack and corresponding velocity model with projected ODP borehole locations

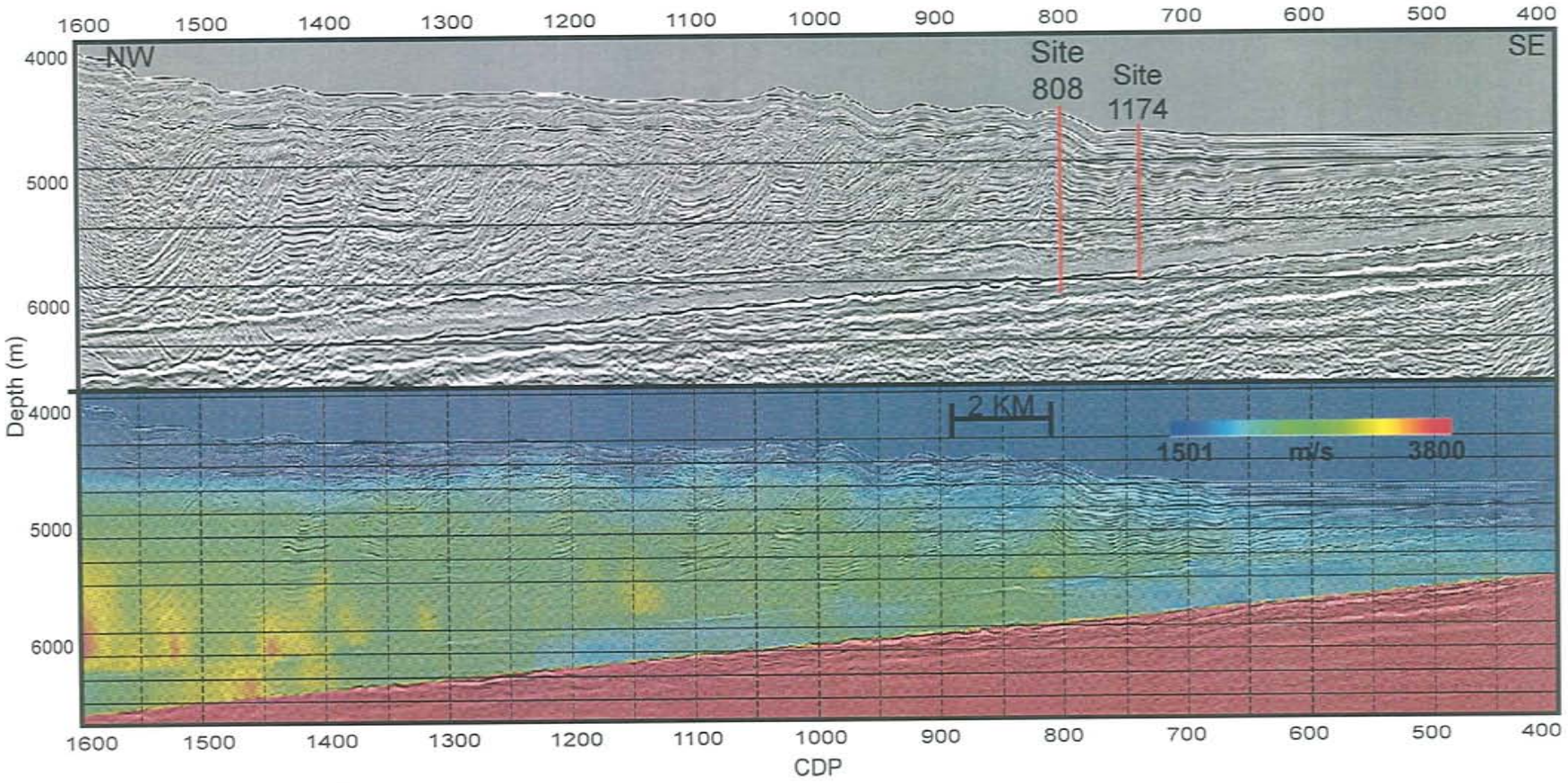

Figure A.12: Inline 245 migrated seismic stack and corresponding velocity model with projected ODP borehole locations

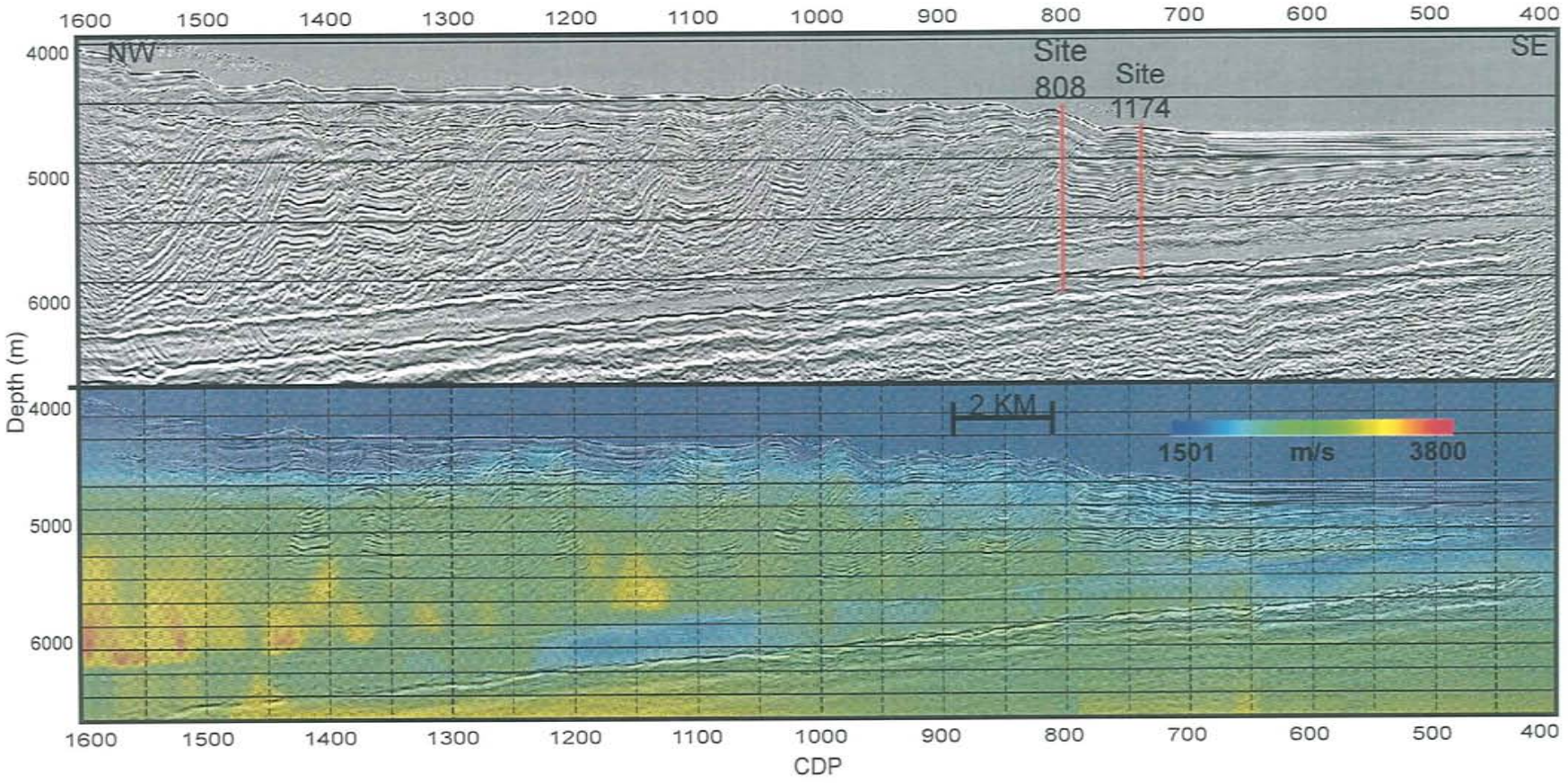

Figure A.13: Inline 250 migrated seismic stack and corresponding velocity model with projected ODP borehole locations

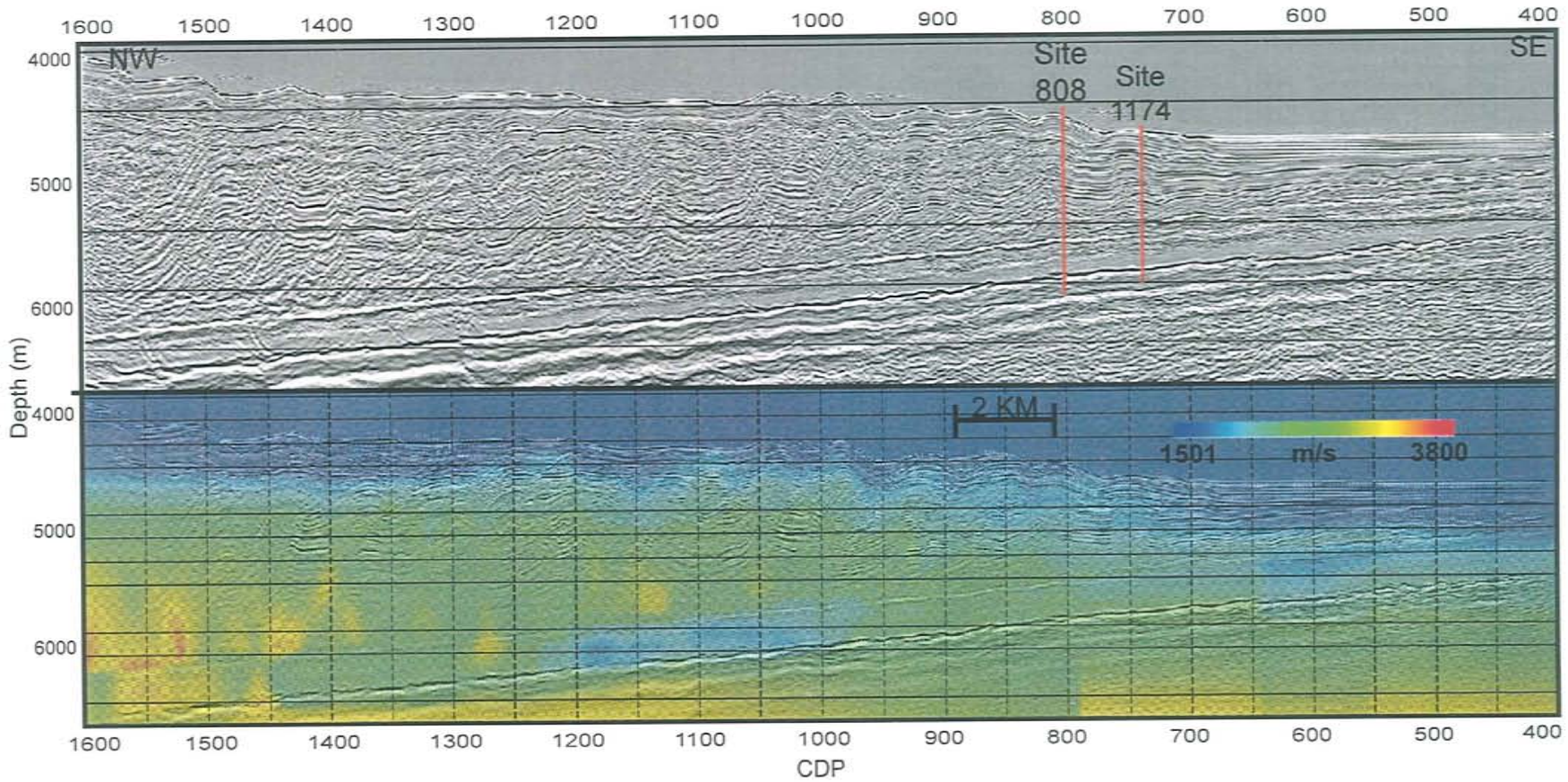

Figure A.14: Inline 255 migrated seismic stack and corresponding velocity model with projected ODP borehole locations

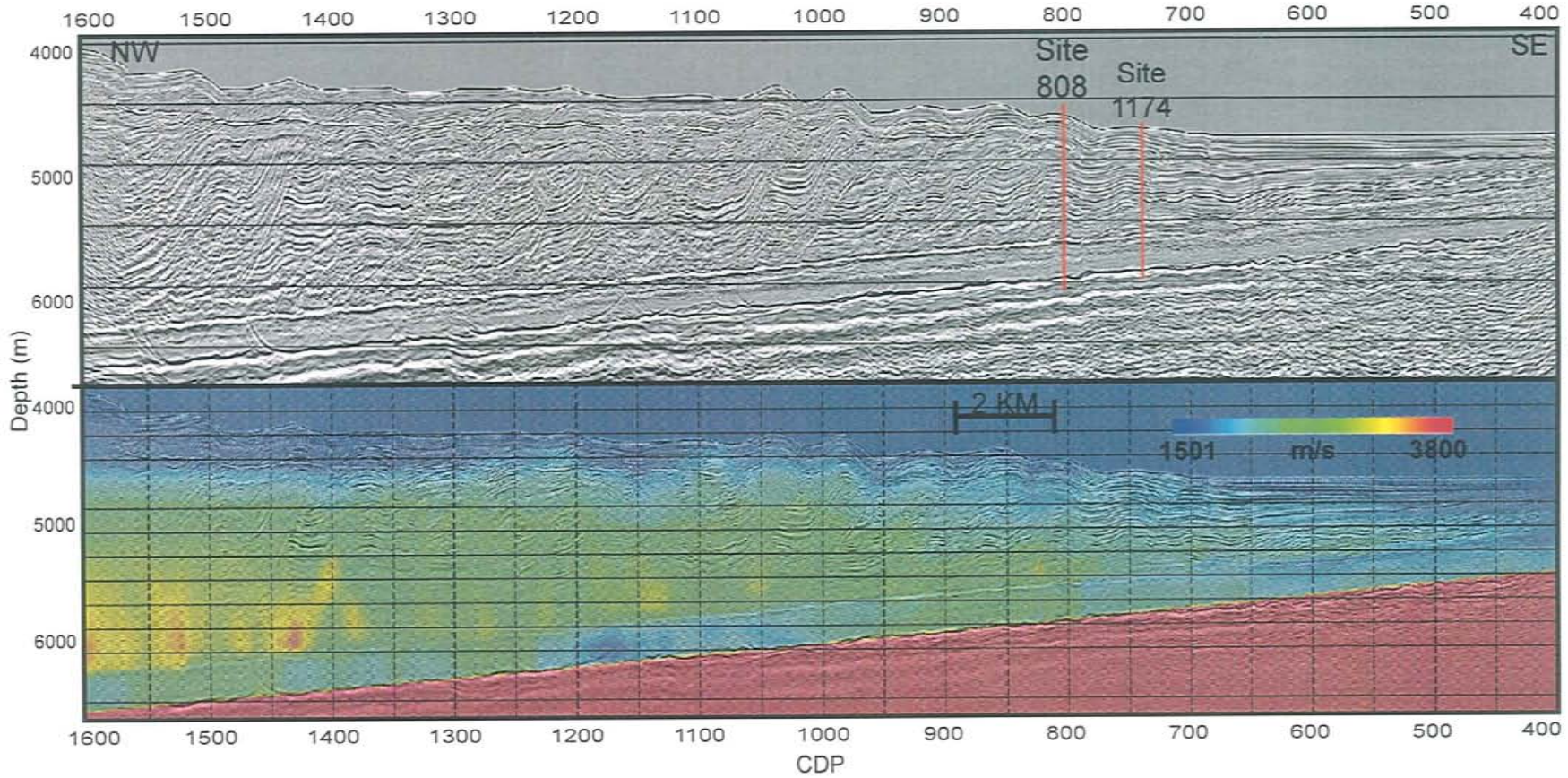

Figure A15: Inline 260 migrated seismic stack and corresponding velocity model with projected ODP borehole locations

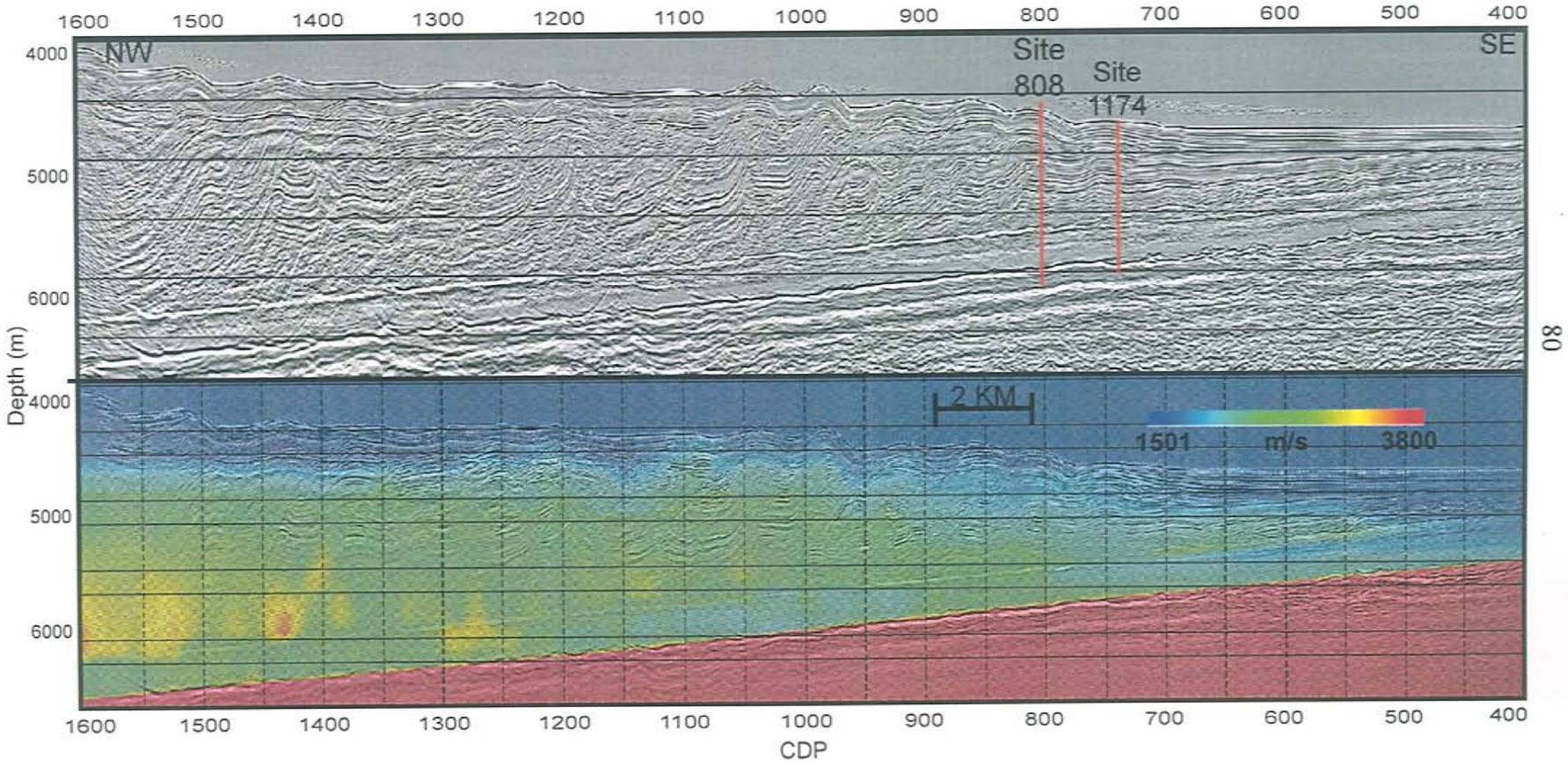

Figure A.16: Inline 265 migrated seismic stack and corresponding velocity model with projected ODP borehole locations

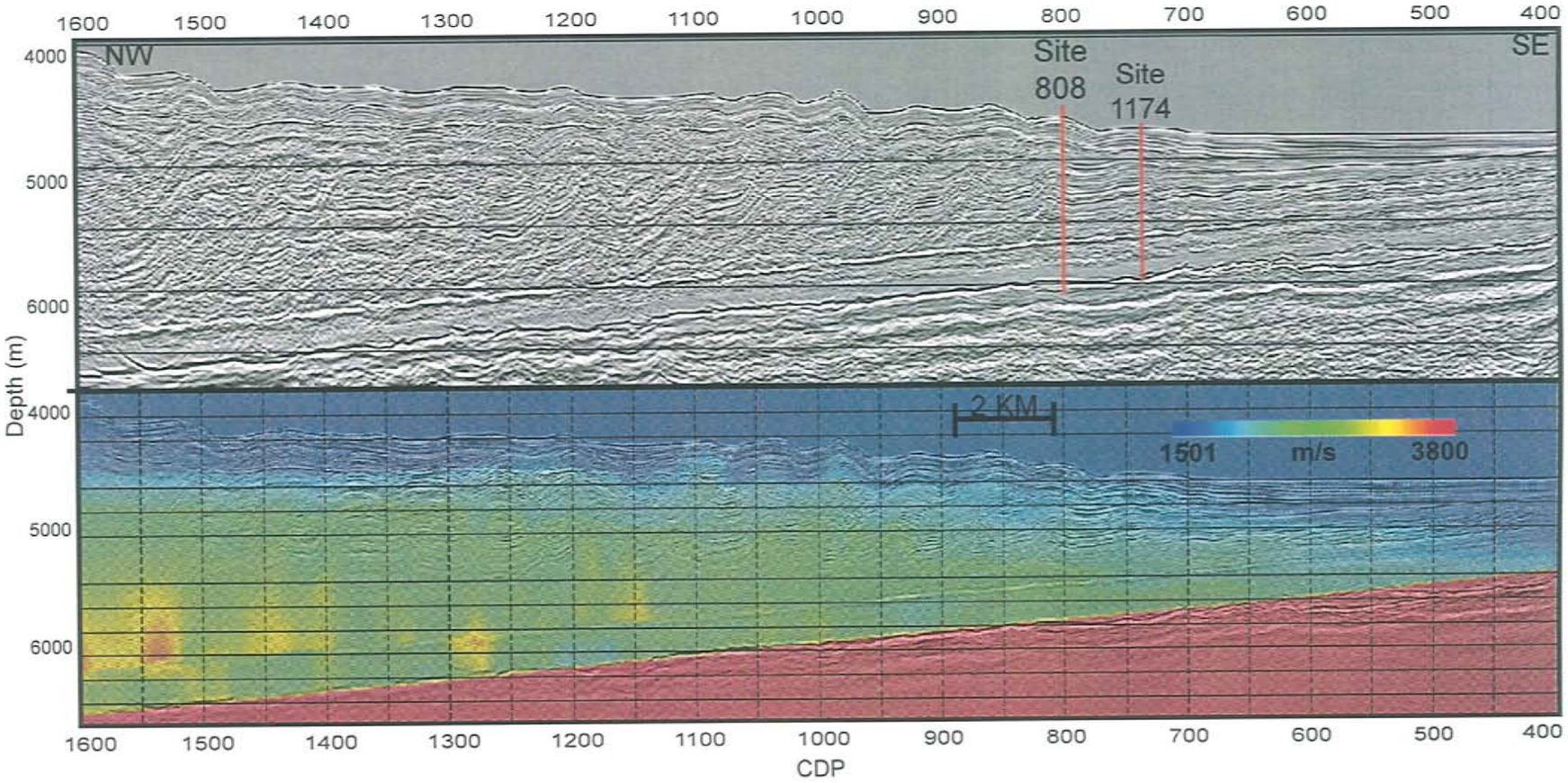

Figure A.17: Inline 270 migrated seismic stack and corresponding velocity model with projected ODP borehole locations

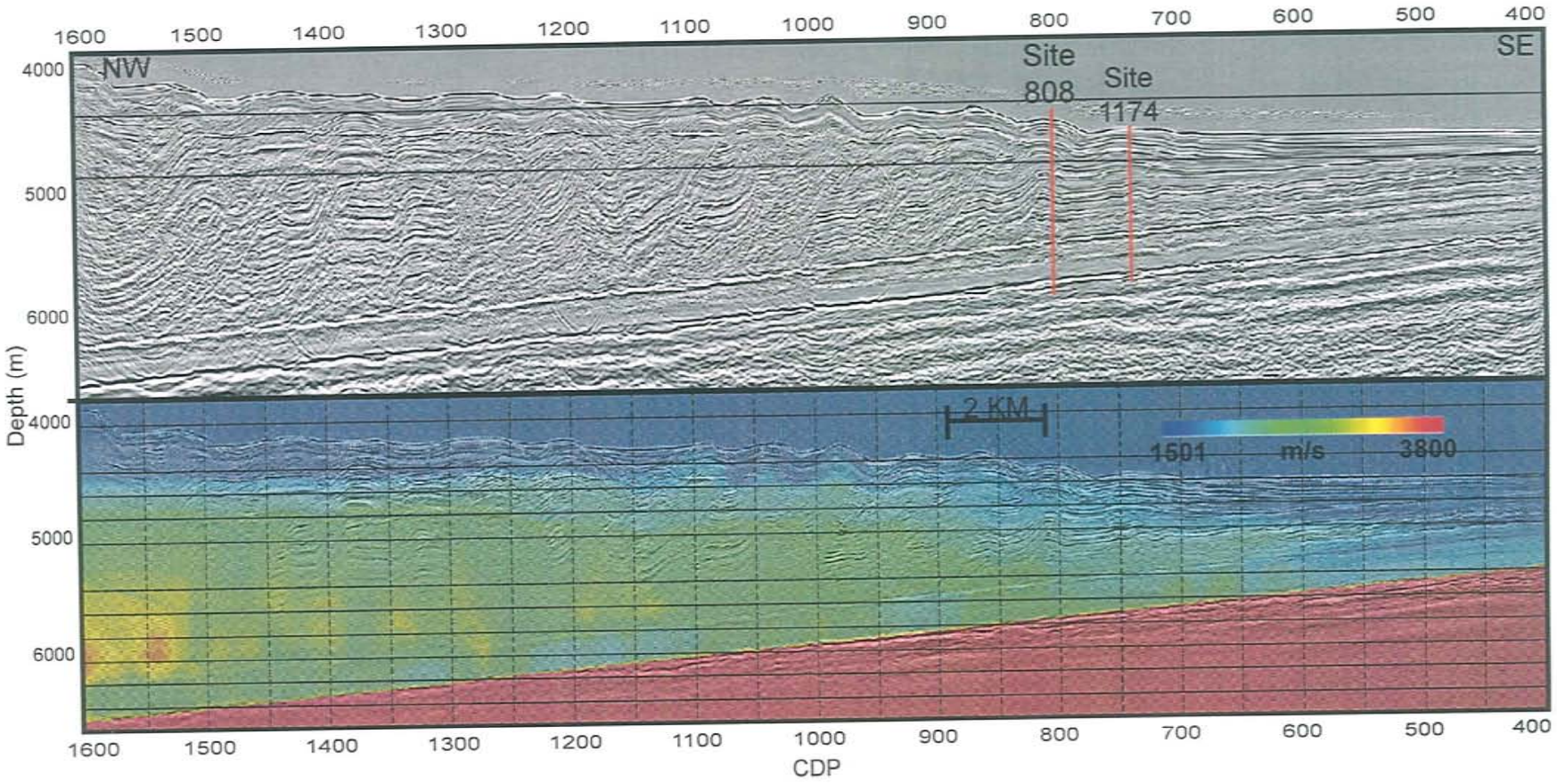

Figure A.18: Inline 275 migrated seismic stack and corresponding velocity model with projected ODP borehole locations

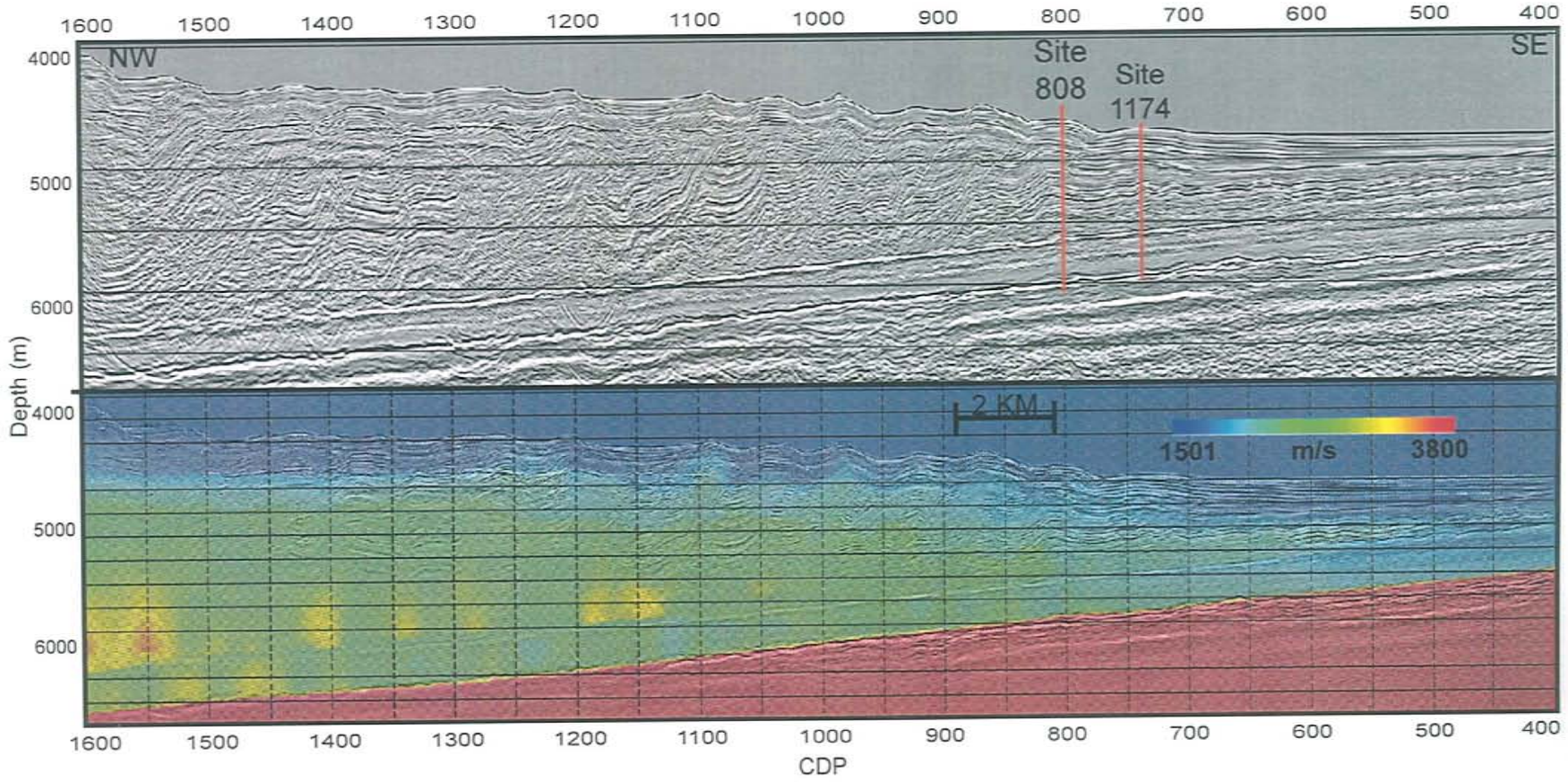

Figure A.19: Inline 280 migrated seismic stack and corresponding velocity model with projected ODP borehole locations

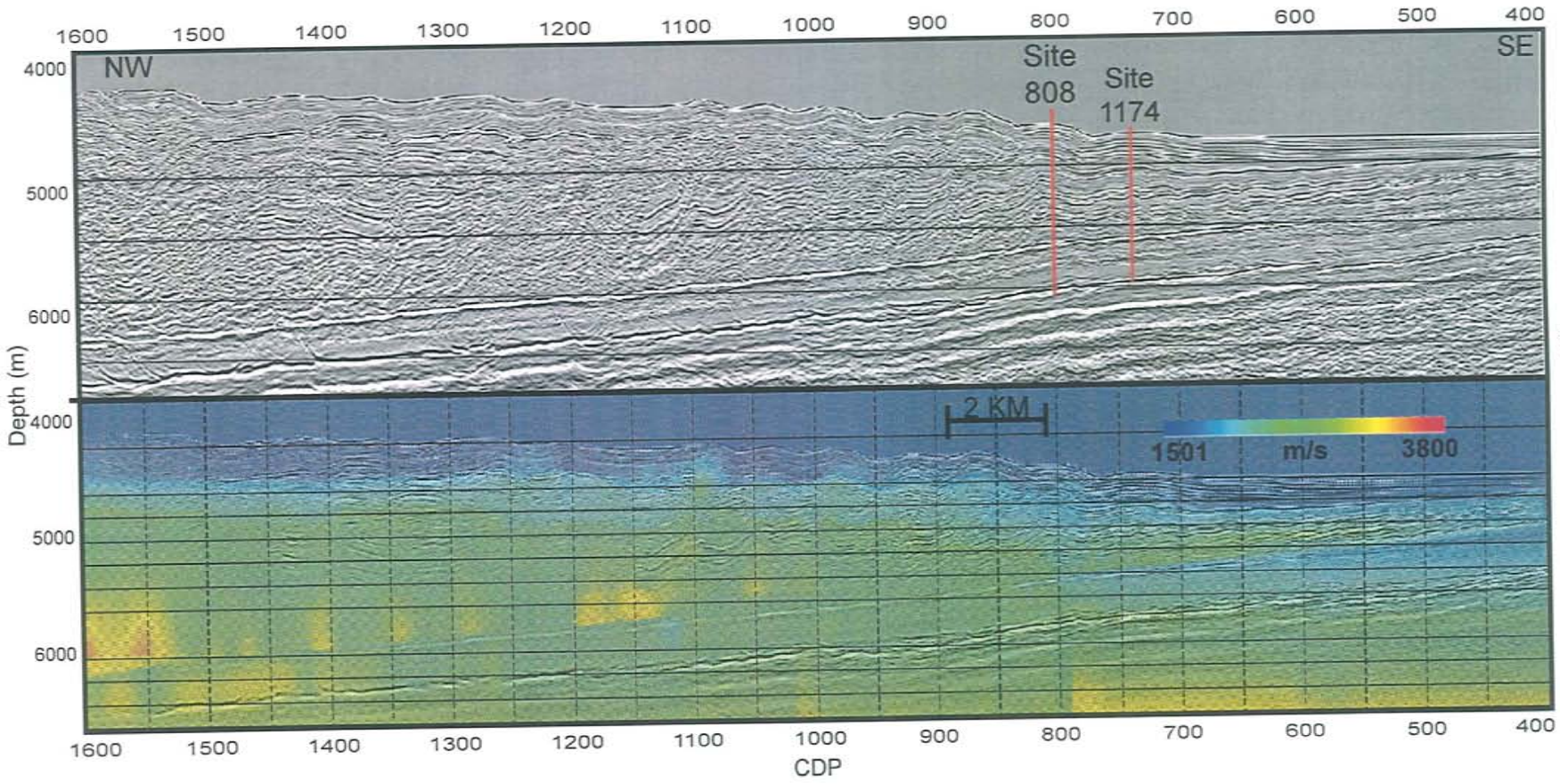

Figure A.20: Inline 284 migrated seismic stack and corresponding velocity model with projected ODP borehole locations

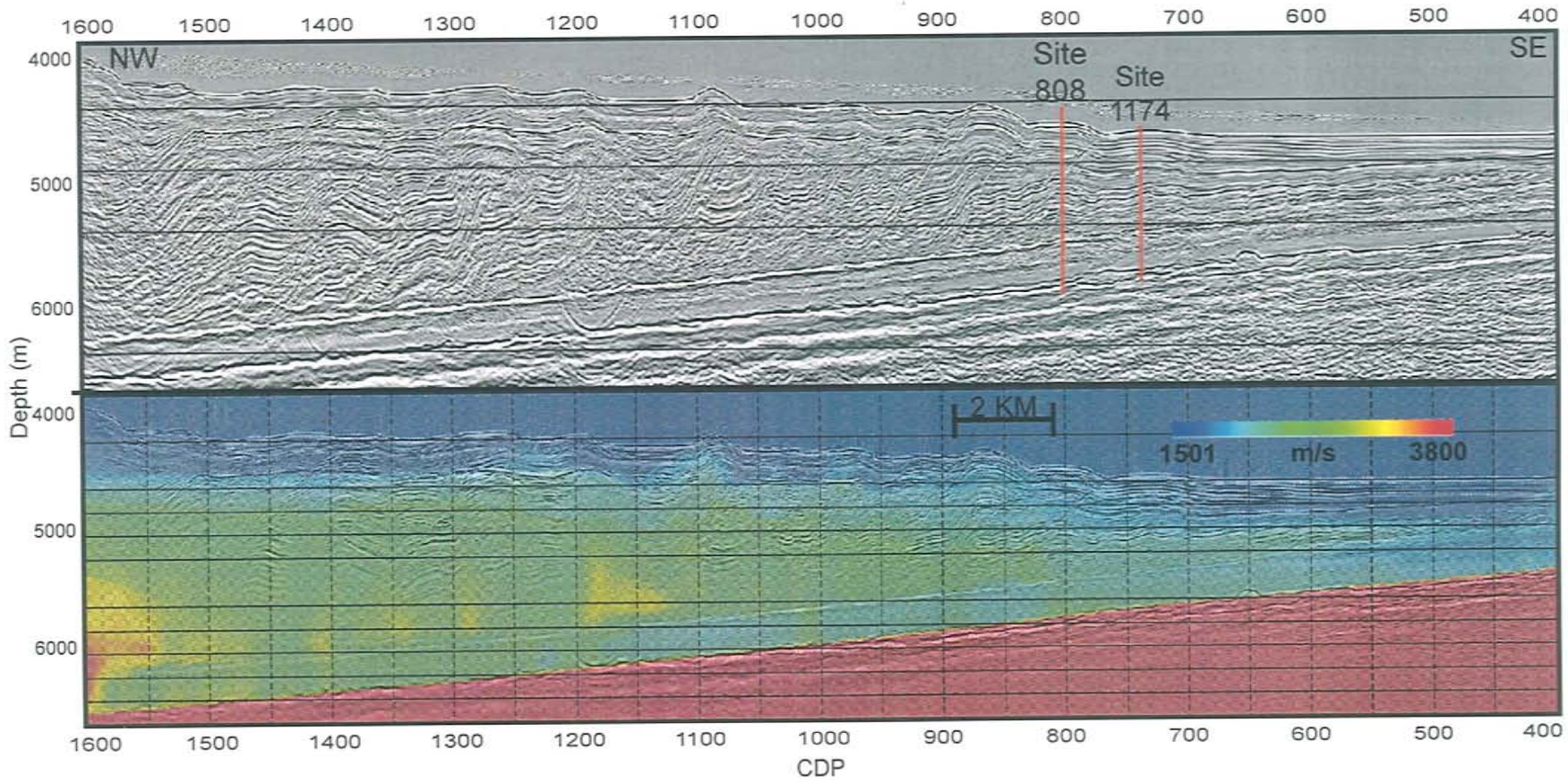

Figure A.21: Inline 294 migrated seismic stack and corresponding velocity model with projected ODP borehole locations

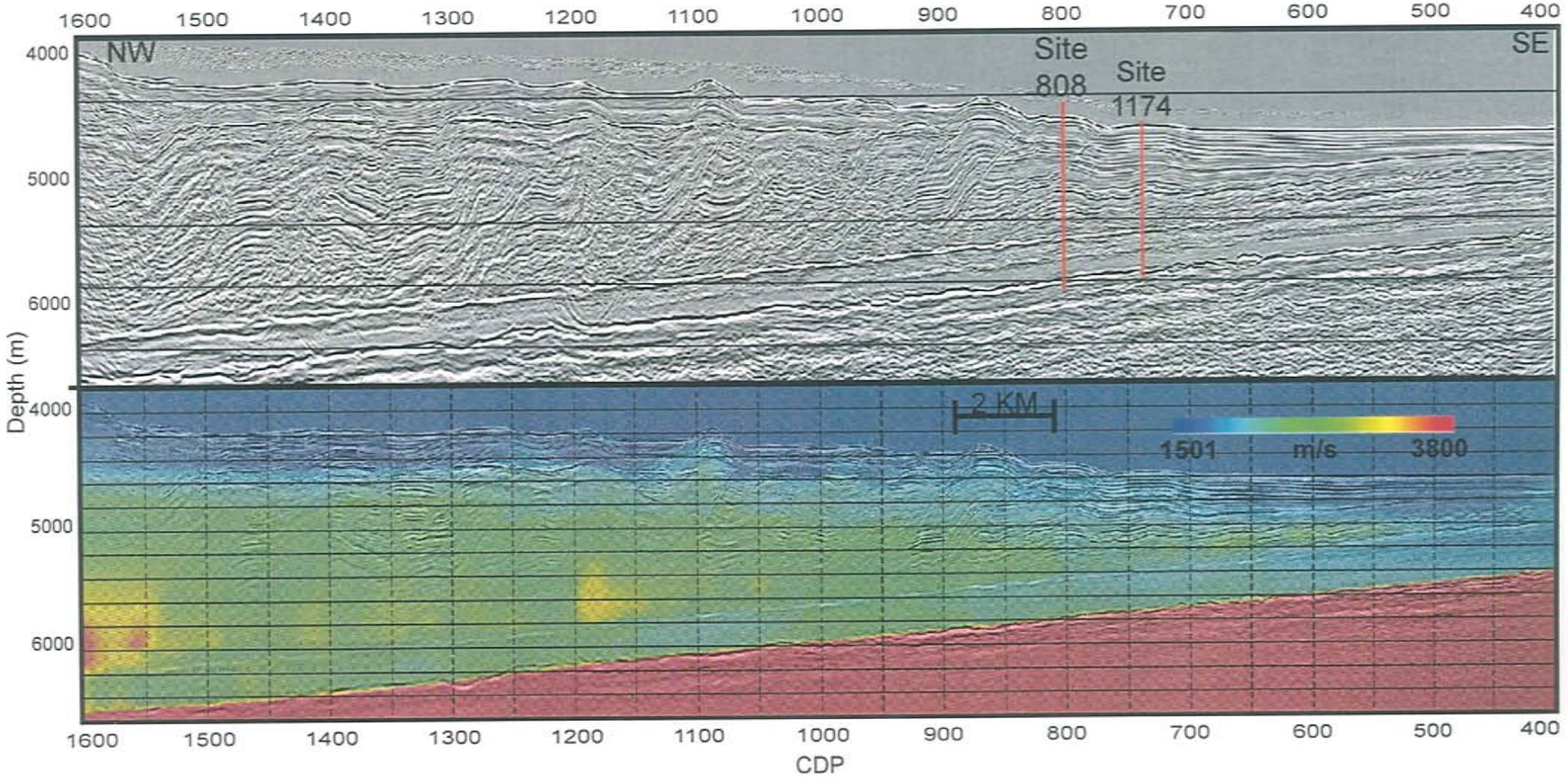

Figure A.22: Inline 300 migrated seismic stack and corresponding velocity model with projected ODP borehole locations

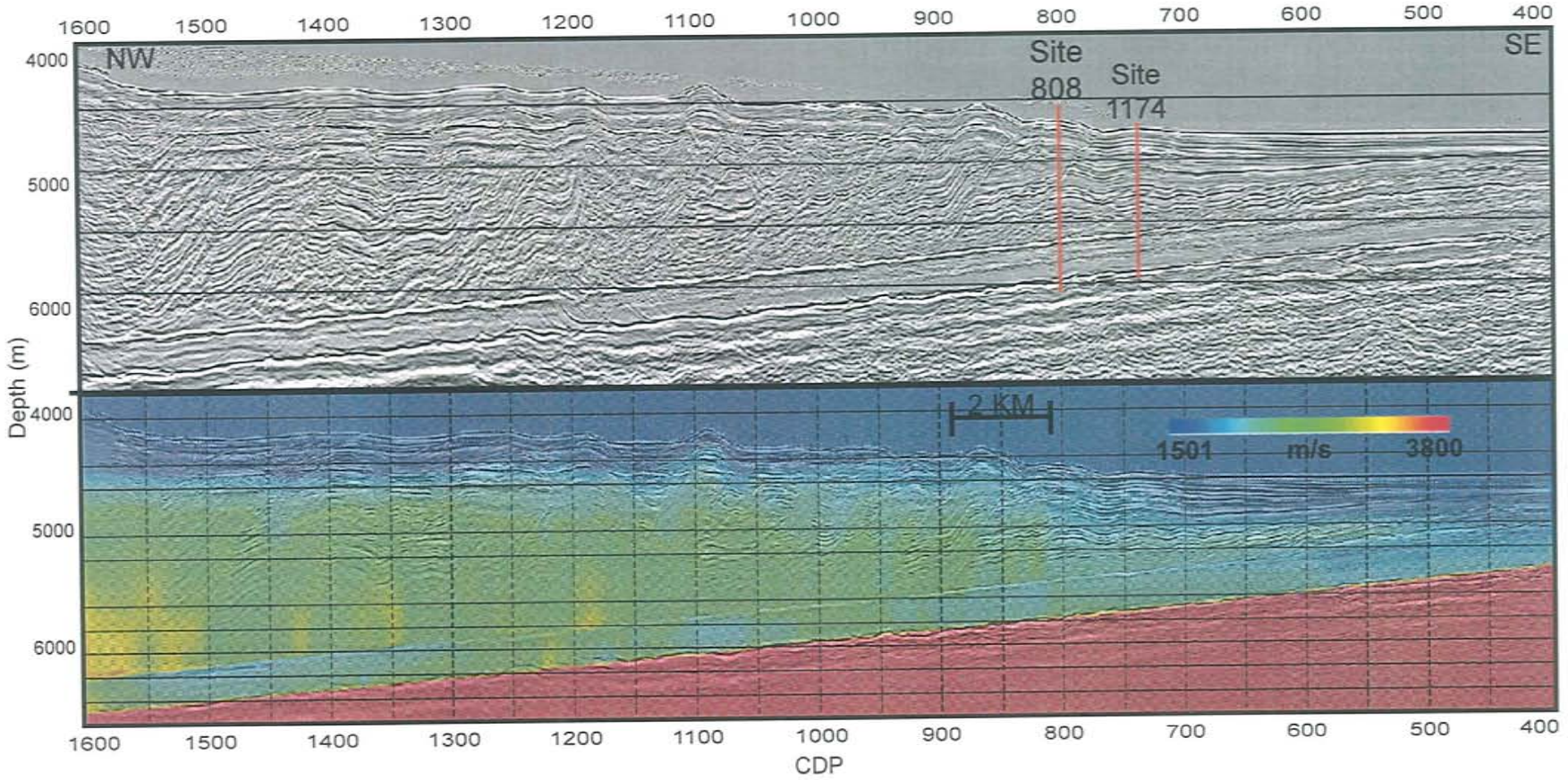

Figure A.23: Inline 305 migrated seismic stack and corresponding velocity model with projected ODP borehole locations

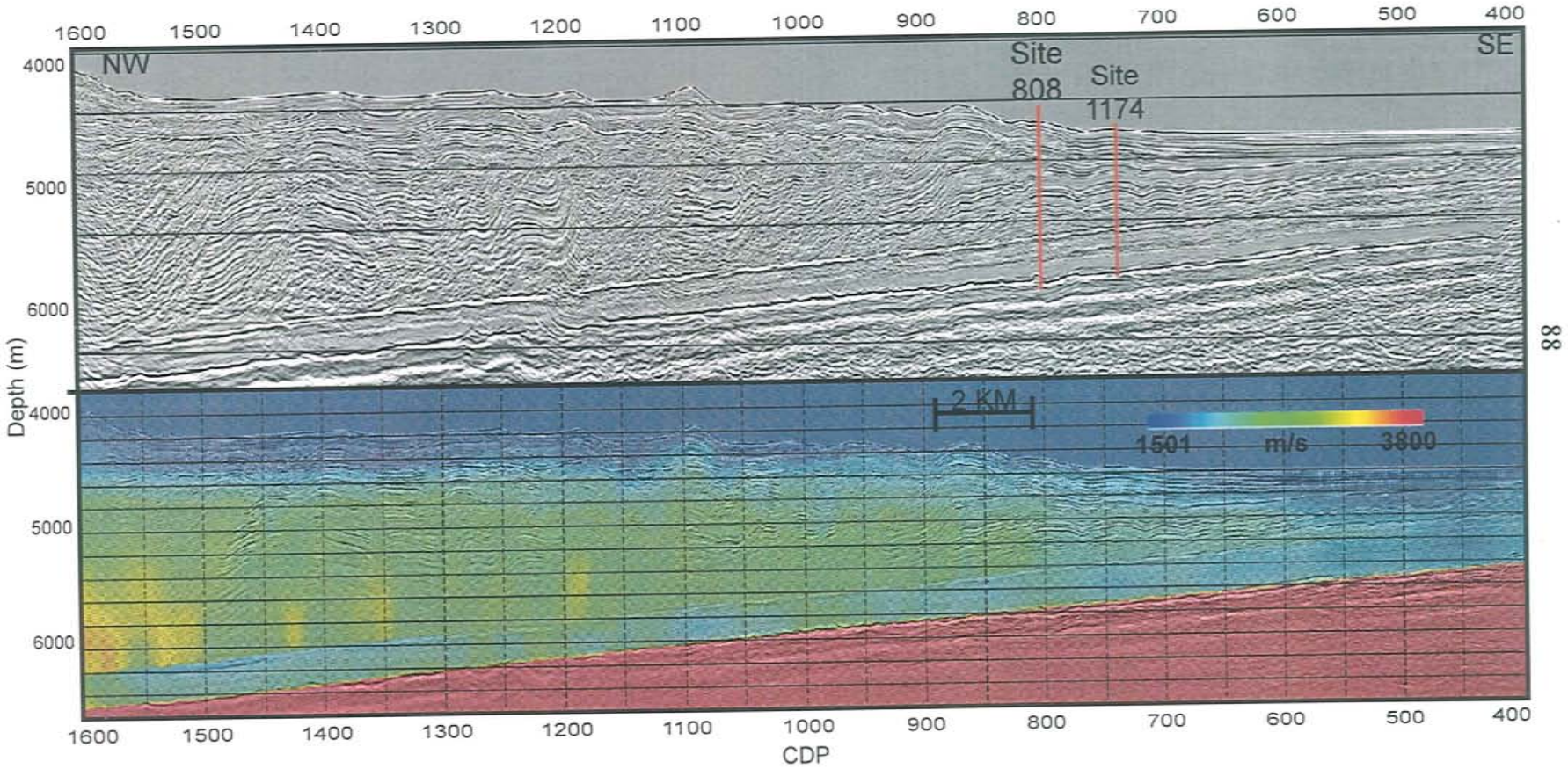

Figure A.24: Inline 310 migrated seismic stack and corresponding velocity model with projected ODP borehole locations

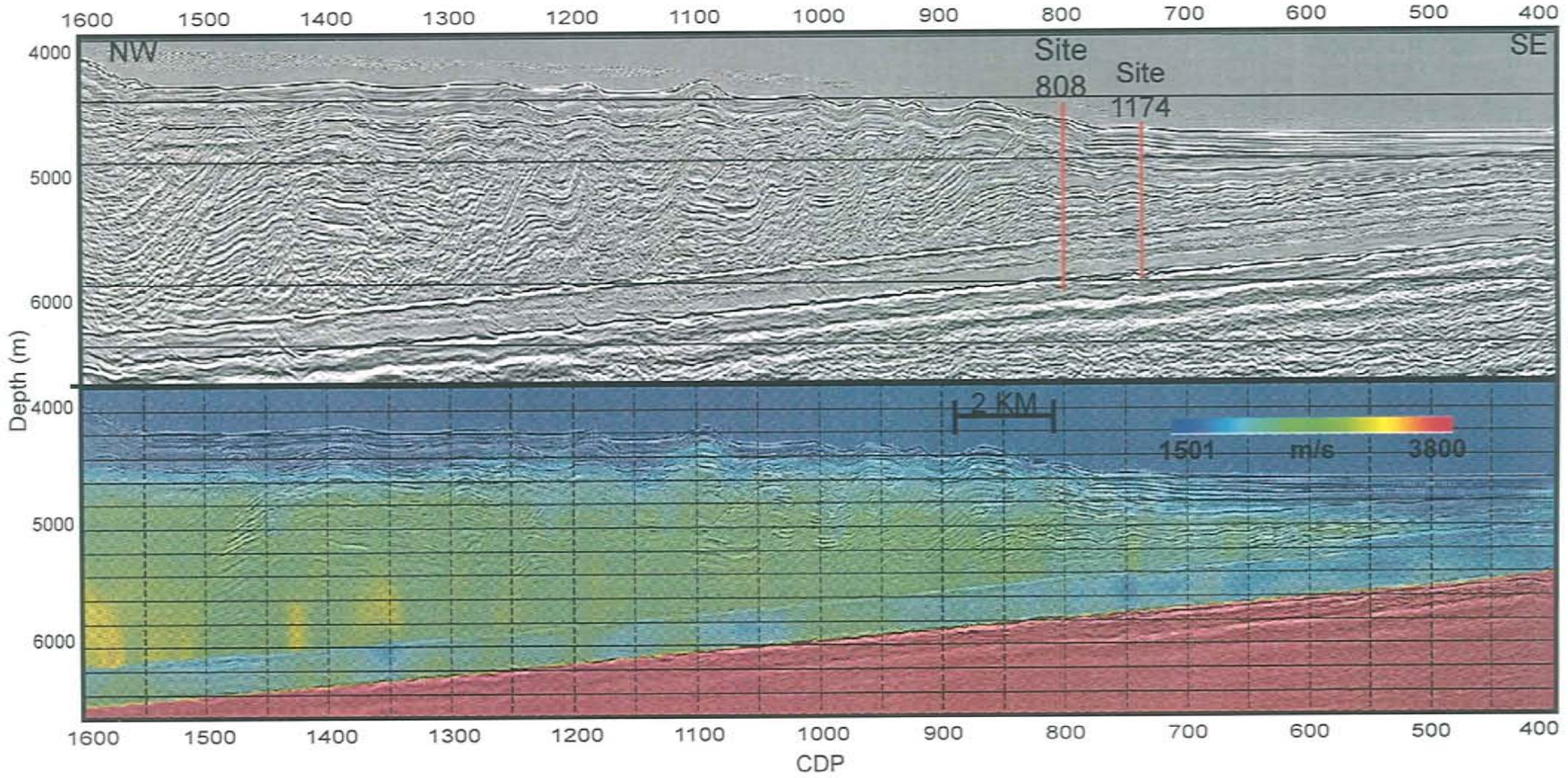

Figure A.25: Inline 315 migrated seismic stack and corresponding velocity model with projected ODP borehole locations

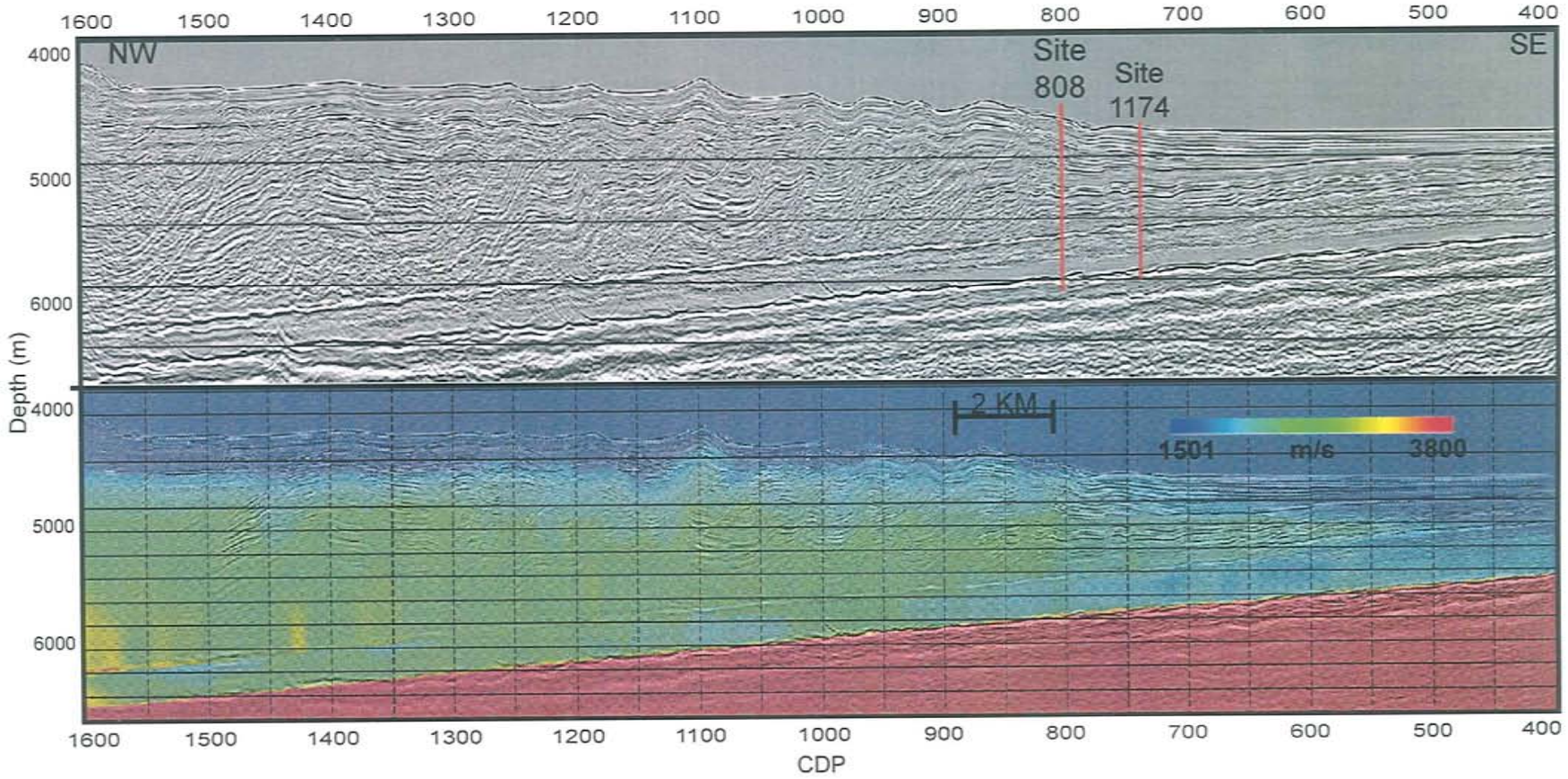

Figure A.26: Inline 320 migrated seismic stack and corresponding velocity model with projected ODP borehole locations

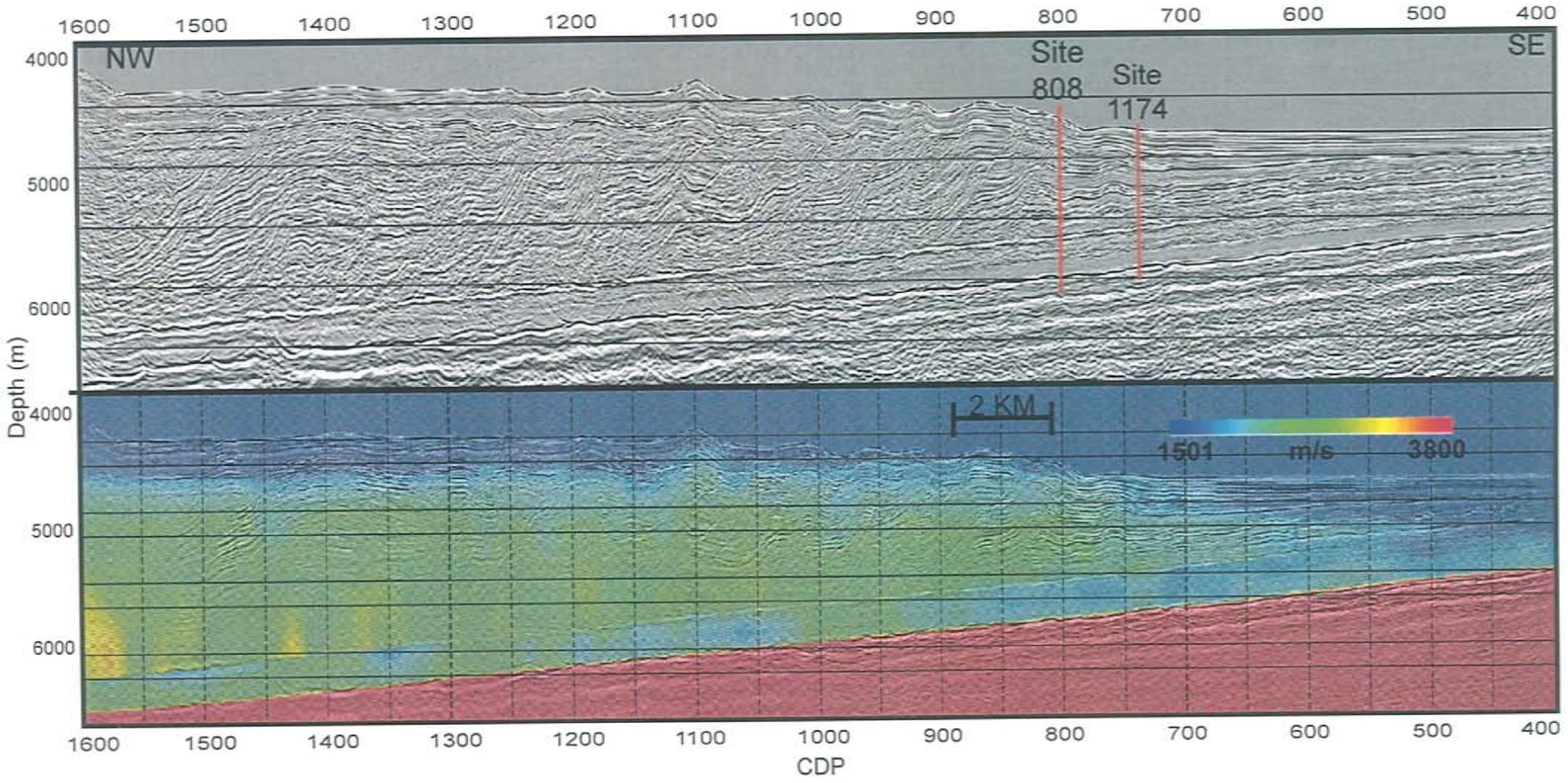

Figure A.27: Inline 325 migrated seismic stack and corresponding velocity model with projected ODP borehole locations

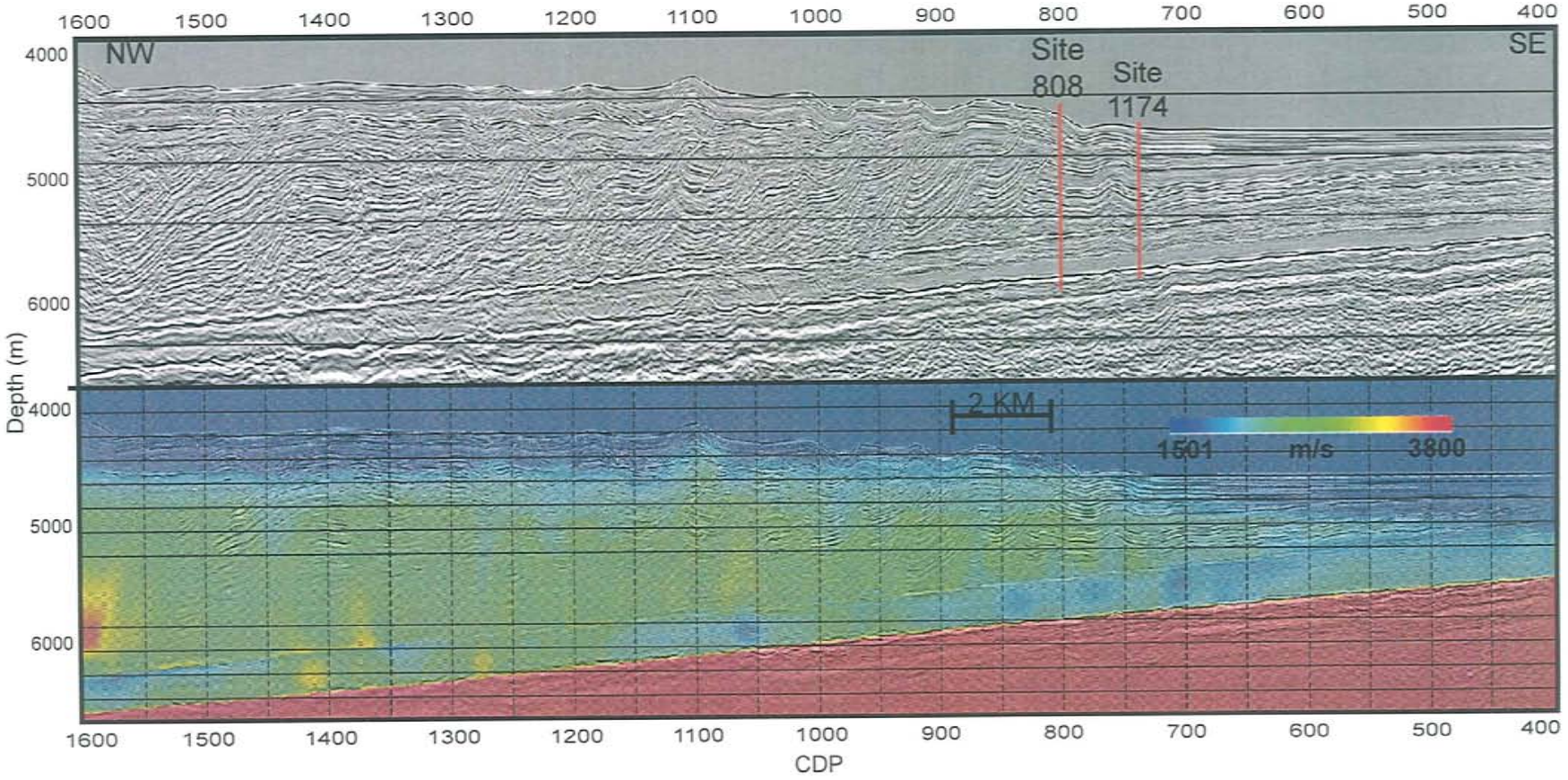

Figure A.28: Inline 330 migrated seismic stack and corresponding velocity model with projected ODP borehole locations

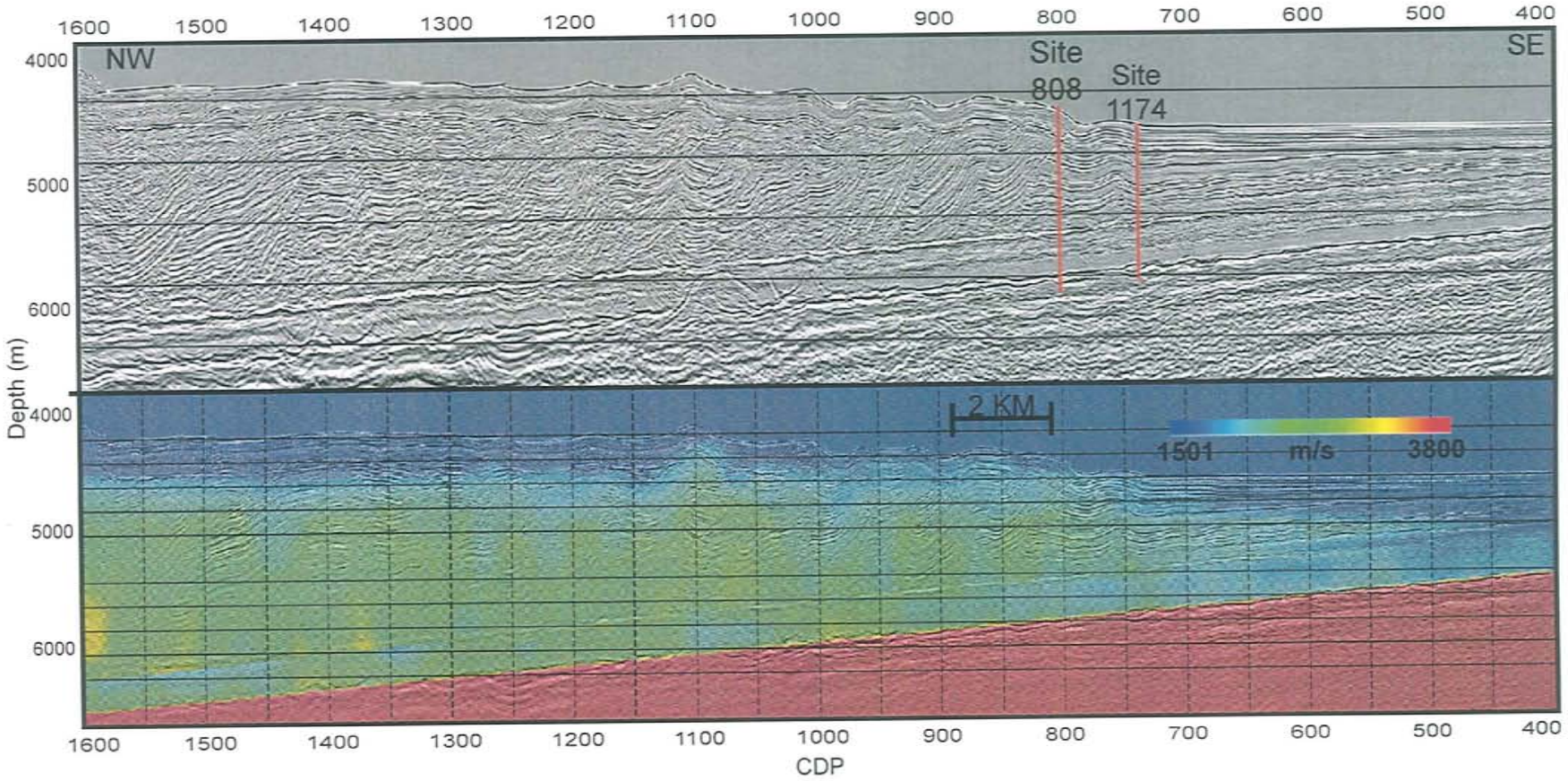

Figure A.29: Inline 335 migrated seismic stack and corresponding velocity model with projected ODP borehole locations

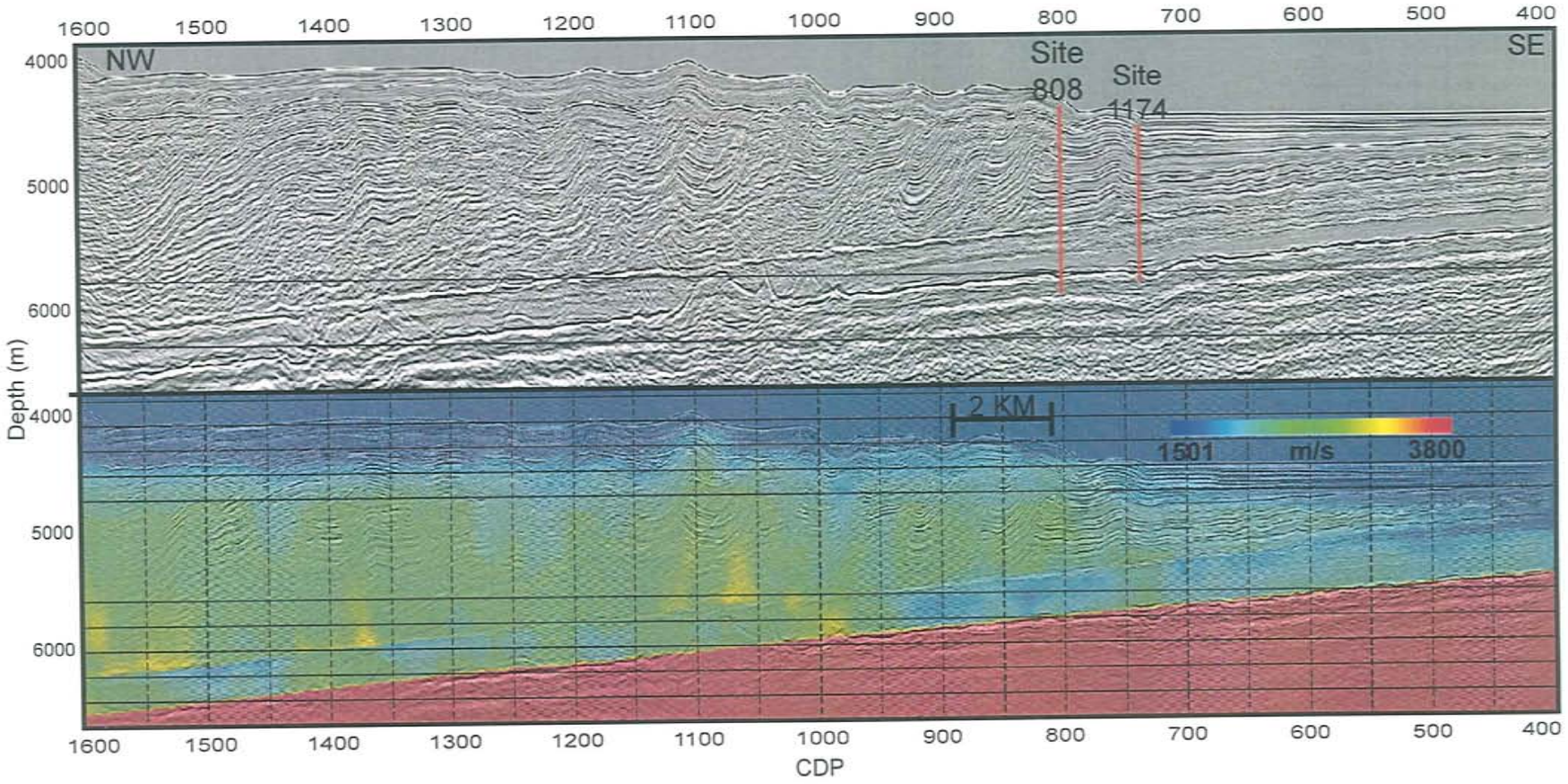

Figure A.30: Inline 340 migrated seismic stack and corresponding velocity model with projected ODP borehole locations

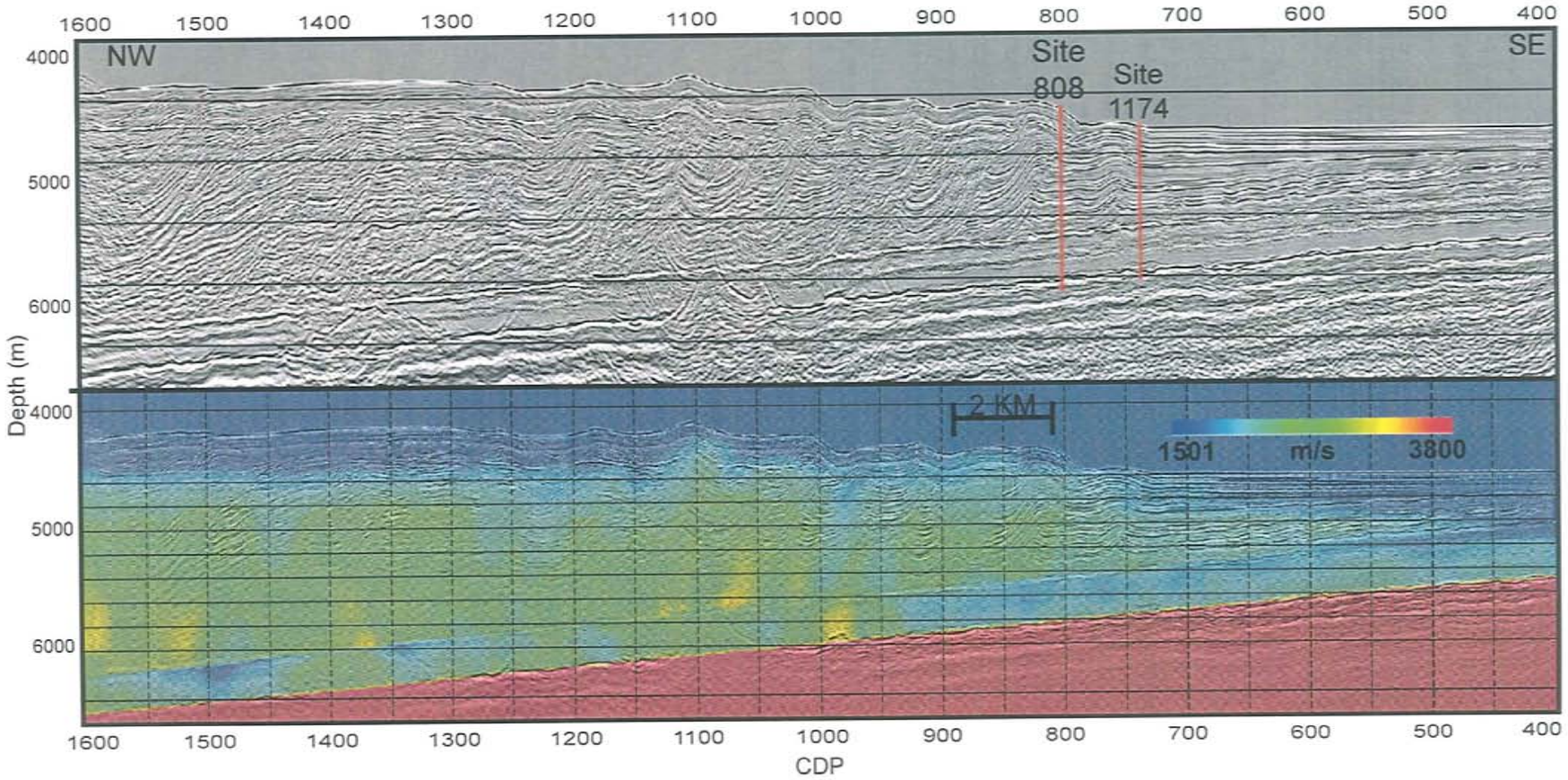

Figure A.31: Inline 345 migrated seismic stack and corresponding velocity model with projected ODP borehole locations

APPENDIX B

MATLAB CODES

```
clear;

% Extract velocity values along depth referenced décollement HORIZON

% Load / Define data/line

load Decollement.txt;
horizon = Decollement;
clear Decollement;
load GK_290_extract_vel.txt;
data = GK_290_extract_vel;
clear GK_290_extract_vel;

% Extract the proper data

for t=1:5
   for b=400:1600;
      Y(b)=290;
      i=b-399;
      j=((i-1)*534)+1;
      k=j+533;
      horizon(i,2) = ((horizon(i,2)) + (25*(t-1)));

      for g=j:k
         if ((data(g,2) - horizon(i,2)) <= 0.0)
            X(b,t)=b;
            Z(b,t)=data(g,2);
            Vel(b,t)=data(g,3);
         end
      end
   end
end
```

% Write extracted data to Excell speadsheets

```
xlswrite('C:\Documents and Settings\gk\Desktop\NANKAI
WORK/Underthrust_Velocity.xls',X((400:1600),1), '290' ,'A4:A1204')
xlswrite('C:\Documents and Settings\gk\Desktop\NANKAI
WORK/Underthrust_Velocity.xls',Z((400:1600),1), '290' ,'B4:B1204')
xlswrite('C:\Documents and Settings\gk\Desktop\NANKAI
WORK/Underthrust_Velocity.xls',Z((400:1600),2), '290' ,'D4:D1204')
xlswrite('C:\Documents and Settings\gk\Desktop\NANKAI
WORK/Underthrust_Velocity.xls',Z((400:1600),3), '290' ,'F4:F1204')
xlswrite('C:\Documents and Settings\gk\Desktop\NANKAI
WORK/Underthrust_Velocity.xls',Z((400:1600),4), '290' ,'H4:H1204')
xlswrite('C:\Documents and Settings\gk\Desktop\NANKAI
WORK/Underthrust_Velocity.xls',Z((400:1600),5), '290' ,'J4:J1204')
xlswrite('C:\Documents and Settings\gk\Desktop\NANKAI
WORK/Underthrust_Velocity.xls',Vel((400:1600),1), '290' ,'C4:C1204')
xlswrite('C:\Documents and Settings\gk\Desktop\NANKAI
WORK/Underthrust_Velocity.xls',Vel((400:1600),2), '290' ,'E4:E1204')
xlswrite('C:\Documents and Settings\gk\Desktop\NANKAI
WORK/Underthrust_Velocity.xls',Vel((400:1600),3), '290' ,'G4:G1204')
xlswrite('C:\Documents and Settings\gk\Desktop\NANKAI
WORK/Underthrust_Velocity.xls',Vel((400:1600),4), '290' ,'I4:I1204')
xlswrite('C:\Documents and Settings\gk\Desktop\NANKAI
WORK/Underthrust_Velocity.xls',Vel((400:1600),5), '290' ,'K4:K1204')
```

% Decollement

```
xlswrite('C:\Documents and Settings\gk\Desktop\NANKAI
WORK/Underthrust_Velocity.xls',(X((400:1600),1)),'Dec','a22821:a24021')
xlswrite('C:\Documents and Settings\gk\Desktop\NANKAI
WORK/Underthrust_Velocity.xls',(Y(400:1600)*-1),'Dec','b22821:b24021')
xlswrite('C:\Documents and Settings\gk\Desktop\NANKAI
WORK/Underthrust_Velocity.xls',(Z((400:1600),1)*-1),'Dec','c22821:c24021')
xlswrite('C:\Documents and Settings\gk\Desktop\NANKAI
WORK/Underthrust_Velocity.xls',Vel((400:1600),1),'Dec','d22821:d24021')
```

% Decollement + 25

```
xlswrite('C:\Documents and Settings\gk\Desktop\NANKAI
WORK/Underthrust_Velocity.xls',(X((400:1600),2)),'Dec+25','a22821:a24021')
xlswrite('C:\Documents and Settings\gk\Desktop\NANKAI
WORK/Underthrust_Velocity.xls',(Y(400:1600)*-1),'Dec+25','b22821:b24021')
```

```
xlswrite('C:\Documents and Settings\gk\Desktop\NANKAI
WORK/Underthrust_Velocity.xls',(Z((400:1600),2)*-1),'Dec+25','c22821:c24021')
xlswrite('C:\Documents and Settings\gk\Desktop\NANKAI
WORK/Underthrust_Velocity.xls',Vel((400:1600),2),'Dec+25','d22821:d24021')

% Decollement + 75
xlswrite('C:\Documents and Settings\gk\Desktop\NANKAI
WORK/Underthrust_Velocity.xls',(X((400:1600),3)),'Dec+75','a22821:a24021')
xlswrite('C:\Documents and Settings\gk\Desktop\NANKAI
WORK/Underthrust_Velocity.xls',(Y(400:1600)*-1),'Dec+75','b22821:b24021')
xlswrite('C:\Documents and Settings\gk\Desktop\NANKAI
WORK/Underthrust_Velocity.xls',(Z((400:1600),3)*-1),'Dec+75','c22821:c24021')
xlswrite('C:\Documents and Settings\gk\Desktop\NANKAI
WORK/Underthrust_Velocity.xls',Vel((400:1600),3),'Dec+75','d22821:d24021')

% Decollement + 150
xlswrite('C:\Documents and Settings\gk\Desktop\NANKAI
WORK/Underthrust_Velocity.xls',(X((400:1600),4)),'Dec+150','a22821:a24021')
xlswrite('C:\Documents and Settings\gk\Desktop\NANKAI
WORK/Underthrust_Velocity.xls',(Y(400:1600)*-1),'Dec+150','b22821:b24021')
xlswrite('C:\Documents and Settings\gk\Desktop\NANKAI
WORK/Underthrust_Velocity.xls',(Z((400:1600),4)*-1),'Dec+150','c22821:c24021')
xlswrite('C:\Documents and Settings\gk\Desktop\NANKAI
WORK/Underthrust_Velocity.xls',Vel((400:1600),4),'Dec+150','d22821:d24021')

% Decollement + 250
xlswrite('C:\Documents and Settings\gk\Desktop\NANKAI
WORK/Underthrust_Velocity.xls',(X((400:1600),5)),'Dec+250','a22821:a24021')
xlswrite('C:\Documents and Settings\gk\Desktop\NANKAI
WORK/Underthrust_Velocity.xls',(Y(400:1600)*-1),'Dec+250','b22821:b24021')
xlswrite('C:\Documents and Settings\gk\Desktop\NANKAI
WORK/Underthrust_Velocity.xls',(Z((400:1600),5)*-1),'Dec+250','c22821:c24021')
xlswrite('C:\Documents and Settings\gk\Desktop\NANKAI
WORK/Underthrust_Velocity.xls',Vel((400:1600),5),'Dec+250','d22821:d24021')


% Calculates values for Nicole's empirical velocity - porosity transform of
Nankai sediments

A=0.746;
```

```
B=0.532;
C=0.124;
Vsh=1.057;
PorCrit=0.295;
por=[0.1:0.00001:0.6];
data1=xlsread('C:\Documents and Settings\gk\Desktop\NANKAI
WORK/Underthrust_Velocity.xls','Dec');
data2=xlsread('C:\Documents and Settings\gk\Desktop\NANKAI
WORK/Underthrust_Velocity.xls','Dec+25');
data3=xlsread('C:\Documents and Settings\gk\Desktop\NANKAI
WORK/Underthrust_Velocity.xls','Dec+75');
data4=xlsread('C:\Documents and Settings\gk\Desktop\NANKAI
WORK/Underthrust_Velocity.xls','Dec+150');
data5=xlsread('C:\Documents and Settings\gk\Desktop\NANKAI
WORK/Underthrust_Velocity.xls','Dec+250');

for i=1:50001
   Xm = tanh(40 * (por(i) - PorCrit)) - abs(tanh(40 * (por(i) - PorCrit)));
   Vel(i)=A + (B * por(i)) + (0.305/((por(i) + C)^2 + (0.305/(1.51 - A - B)) - C^2 - (2
* C) - 1)) + (Xm * (0.61 * (Vsh -1.123)));
   TABLE(i,1)=por(i);
   TABLE(i,2)=Vel(i) * 1000;
end

% finds the porosity of the depth reference velocity values

% Dec
for r=1:36031
   v=1;
   while data1(r,4)>1596.0  &  data1(r,4) < TABLE (v,2)
      v=v+1;
   end
   data1(r,6)=TABLE(v,1);
   data1(r,5)=TABLE(v,2);
end

% Dec + 25
for r=1:36031
   v=1;
   while data2(r,4)>1596.0  &  data2(r,4) < TABLE (v,2)
      v=v+1;
```

```
   end
   data2(r,6)=TABLE(v,1);
   data2(r,5)=TABLE(v,2);
end

%  Dec + 75
for r=1:36031
   v=1;
   while data3(r,4)>1596.0  &  data3(r,4) < TABLE (v,2)
      v=v+1;
   end
   data3(r,6)=TABLE(v,1);
   data3(r,5)=TABLE(v,2);
end

%  Dec + 150
for r=1:36031
   v=1;
   while data4(r,4)>1596.0  &  data4(r,4) < TABLE (v,2)
      v=v+1;
   end
   data4(r,6)=TABLE(v,1);
   data4(r,5)=TABLE(v,2);
end

%  Dec + 250
for r=1:36031
   v=1;
   while data5(r,4)>1596.0  &  data5(r,4) < TABLE (v,2)
      v=v+1;
   end
   data5(r,6)=TABLE(v,1);
   data5(r,5)=TABLE(v,2);
end

 xlswrite('C:\Documents and Settings\gk\Desktop\NANKAI
WORK/Underthrust_Velocity.xls',data1,'DecGrid')
 xlswrite('C:\Documents and Settings\gk\Desktop\NANKAI
WORK/Underthrust_Velocity.xls',data2,'Dec25Grid')
 xlswrite('C:\Documents and Settings\gk\Desktop\NANKAI
WORK/Underthrust_Velocity.xls',data3,'Dec75Grid')
```

```
xlswrite('C:\Documents and Settings\gk\Desktop\NANKAI
WORK/Underthrust_Velocity.xls',data4,'Dec150Grid')
xlswrite('C:\Documents and Settings\gk\Desktop\NANKAI
WORK/Underthrust_Velocity.xls',data5,'Dec250Grid')
```